NANO · MICRO small
www.small-journal.com

Self-Assembly of Precision Noble Metal Nanoclusters: Hierarchical Structural Complexity, Colloidal Superstructures, and Applications

Jose V. Rival, Paloli Mymoona, Kavalloor Murali Lakshmi, Nonappa, Thalappil Pradeep,* and Edakkattuparambil Sidharth Shibu**

Ligand protected noble metal nanoparticles are excellent building blocks for colloidal self-assembly. Metal nanoparticle self-assembly offers routes for a wide range of multifunctional nanomaterials with enhanced optoelectronic properties. The emergence of atomically precise monolayer thiol-protected noble metal nanoclusters has overcome numerous challenges such as uncontrolled aggregation, polydispersity, and directionalities faced in plasmonic nanoparticle self-assemblies. Because of their well-defined molecular compositions, enhanced stability, and diverse surface functionalities, nanoclusters offer an excellent platform for developing colloidal superstructures via the self-assembly driven by surface ligands and metal cores. More importantly, recent reports have also revealed the hierarchical structural complexity of several nanoclusters. In this review, the formulation and periodic self-assembly of different noble metal nanoclusters are focused upon. Further, self-assembly induced amplification of physicochemical properties, and their potential applications in molecular recognition, sensing, gas storage, device fabrication, bioimaging, therapeutics, and catalysis are discussed. The topics covered in this review are extensively associated with state-of-the-art achievements in the field of precision noble metal nanoclusters.

J. V. Rival, P. Mymoona, K. M. Lakshmi, Dr. E. S. Shibu
Smart Materials Lab
Electrochemical Power Sources (ECPS) Division
Council of Scientific and Industrial Research (CSIR)-Central Electrochemical Research Institute (CECRI)
Karaikudi, Tamil Nadu 630003, India
E-mail: shibues@cecri.res.in

J. V. Rival, P. Mymoona, K. M. Lakshmi, Dr. E. S. Shibu
Academy of Scientific and Innovative Research (AcSIR)-CSIR
Ghaziabad, Uttar Pradesh 201002, India

Dr. Nonappa
Faculty of Engineering and Natural Sciences
Tampere University
P.O. Box 541, Tampere FI-33101, Finland
E-mail: nonappa@tuni.fi

Prof. T. Pradeep
Department of Chemistry
DST Unit of Nanoscience (DST UNS)
and Thematic Unit of Excellence (TUE)
Indian Institute of Technology (IIT) Madras
Chennai, Tamil Nadu 600036, India
E-mail: pradeep@iitm.ac.in

The ORCID identification number(s) for the author(s) of this article can be found under https://doi.org/10.1002/smll.202005718.

DOI: 10.1002/smll.202005718

1. Introduction

1.1. Precision Noble Metal Nanoclusters

Atomically precise monolayer thiol-protected noble metal nanoclusters (NCs) emerged as a fascinating area of nanoscience research for the past two decades.[1–10] NCs are distinct pieces of matter, possess ultrasmall metal cores (<2 nm), composed of a few to hundreds of atoms protected with a definite number of ligand shells.[11–19] The electronic stability of NCs was well-explained using the superatom model,[12,20,21] according to which NCs display better stability when the number of free electrons falls in the magic number series.[13,22–24] NCs prepared from gold and silver metals have received substantial attention in recent past due to their size-dependent electronic,[3,9,17] optical absorption,[6,9] photoluminescence (PL),[25–32] and magnetic properties.[33,34] The specific geometry and intrinsic photophysical properties of NCs have been efficiently used to probe catalytic reactions,[35–50] toxic metal ions/molecules,[51–55] biological events,[56–68] solar energy conversion,[69–73] and light-emitting device fabrication.[74,75] A large number of NCs stapled with thiols,[6,7] phosphenes,[76–84] and selenols[85–89] have been synthesized in liquid,[6,7] solid,[90] and interface layers.[91,92] Later on, new and improved protocols were developed to fabricate monodisperse NCs.[93–102] Advanced chromatographic techniques have been employed to separate and purify NCs.[103–108] The molecular composition of several NCs has been determined using mass-spectrometry and single-crystal X-ray diffraction studies.[109–132] Important milestones were the successful characterization of $Au_{18}(SR)_{14}$,[109,110] $Au_{20}(SR)_{16}$,[111] $Au_{23}(SR)_{16}$,[112] $Au_{24}(SR)_{16}$,[113] $Au_{25}(SR)_{18}$,[114,115] $Au_{28}(SR)_{20}$,[116] $Au_{30}(SR)_{18}$,[117] $Au_{36}(SR)_{24}$,[118] $Au_{38}(SR)_{24}$,[119] $Au_{102}(SR)_{44}$,[120] $Au_{144}(SR)_{60}$,[121,122] $Ag_{25}(SR)_{18}$,[123] $Ag_{29}(S_2R)_{12}$,[124] and $Ag_{44}(SR)_{30}$[133] NCs. The chemical reactivity of NCs has been utilized to prepare doped and alloy NCs with altered optical and electrochemical properties.[134–159] Furthermore, the organic synthetic toolbox has allowed the rational design of a variety of NCs with specific functional moieties on their surfaces. Among them, functional thiol-protected NCs have been extensively studied for photoinduced electron or energy

transfer process,[160,161] optical chirality,[162–173] and tagging-pockets to bioconjugate with protein machinery for extracellular labeling and intracellular delivery.[56,66,67] More recently, NCs have been used as attractive nanoscale building blocks to fabricate 3D superstructures via a colloidal self-assembly process. Spontaneous organization of NCs into a highly ordered array of functional nanostructures help to reduce the free energy of the system. One could accomplish the self-assembly by rationally balancing the thermodynamic forces and nanoscale molecular forces.[174–176] In this context, superlattice crystals fabricated from plasmonic nanoparticles (NPs)[174–204] are excellent benchmarks for mimicking the nanoscale-driven self-assembly in NCs. These self-assembled architectures play an important role in harvesting the enhanced and collective optical properties from the neighboring NCs. One could foresee that such enhanced photophysical properties are important for future precision devices. NCs offer several advantages compared to plasmonic NPs, i) NCs are strictly monodisperse, i.e., structures with an exact number of metal atoms and ligand molecules; ii) the covalently bound ligands with functional groups allow facile chemical transformation without affecting the metal core; iii) their patchy ligand distribution offer better control over the directional assembly; and iv) their dispersion behavior is similar to supramolecular complexes allowing self-assembly in solution. Therefore, atomically precise NCs are often considered as colloidal molecules. However, there are also certain challenges to achieve NC self-assembly; for example, due to their small size, the thermal fluctuation energy of the surroundings is close to the inter-NC interactions. Moreover, the traditional Derjaguin–Landau–Vervey–Overbeek (DLVO) theory of colloidal stability,[205–207] interactions between colloidal particles, and their aggregation behavior are not applicable to NCs.[208–210] Nevertheless, successful attempts have been made on NC self-assembly in recent years. Herein, we mainly focus on the significant contributions and recent advances on NC self-assembly. Particularly, we will review some of the selected examples for the self-assemblies driven by inter-NC interactions and NC-plasmonic NP interactions facilitated by surface ligands. Further, we discuss the hierarchical structural complexity within a NC driven by specific packing patterns of the metal atoms. Finally, an overview of potential applications of self-assembled NCs, in molecular and metal ion sensing, gas sensing and storage, bioimaging and therapeutics, catalysis, and device fabrications are presented.

1.2. Self-Assembly of Precision NCs

Self-assembly of plasmonic noble metal NPs has been extensively studied, ranging from noble metal NP supercrystals,[195] supraparticles,[211–214] capsids[215] to protein-NP superlattices.[216] Driving forces such as hydrogen bonding, electrostatic interactions, van der Waals interactions, dipolar interactions, C—H$\cdots\pi/\pi\cdots\pi$ interactions, amphiphilicity, metal chelation, metal–metal interactions, light-triggered dipole-induced attractions, and external templates have been implemented to achieve the self-assembly in noble metal NPs. These constitute the basis for studying the self-assembly of NCs in solution and interface. For the clarity of discussion, self-assembly of NCs via such interactions are categorized into four sections, viz i) template-free self-assembly, ii) template-directed self-assembly, iii) directed self-assembly using external stimuli (e.g., temperature, light, or metal ions), and iv) miscellaneous examples such as covalently linked NC oligomers and atom transfer reaction facilitated alloy NP assemblies. In the case of template-free self-assembly, the inter-NCs connections are driven by hydrogen bonding, electrostatic interactions, van der Waals interactions (including dipolar, C—H$\cdots\pi$, and $\pi\cdots\pi$ interactions) facilitated by the surface ligands between neighboring NCs, and in some cases, the metallophilic and amphiphilic interactions. The template-directed assembly of NCs is facilitated using molecules such as polymers, DNA, and macrocycles. Externally directed assembly of NCs includes the addition of metal-ions or external stimuli such as photons or temperature to achieve the higher-order structures. Different interactions used to accomplish the self-assembly of NCs are summarized in **Scheme 1**.

2. Molecular Interactions in NC Self-Assembly

2.1. Template-Free Assembly of NCs

In this section, we will focus on the role of nanoscale surface forces such as hydrogen bonding, electrostatic, van der Waals, C—H$\cdots\pi/\pi\cdots\pi$, metallophilic, and amphiphilic interactions on the self-assembly of NCs in their colloidal as well as the crystalline state.

2.1.1. Hydrogen Bonding Interactions

Hydrogen bonding-induced crystallization of NCs was first reported by Jadzinsky et al. in water-soluble $[Au_{102}(p\text{-MBA})_{44}]$

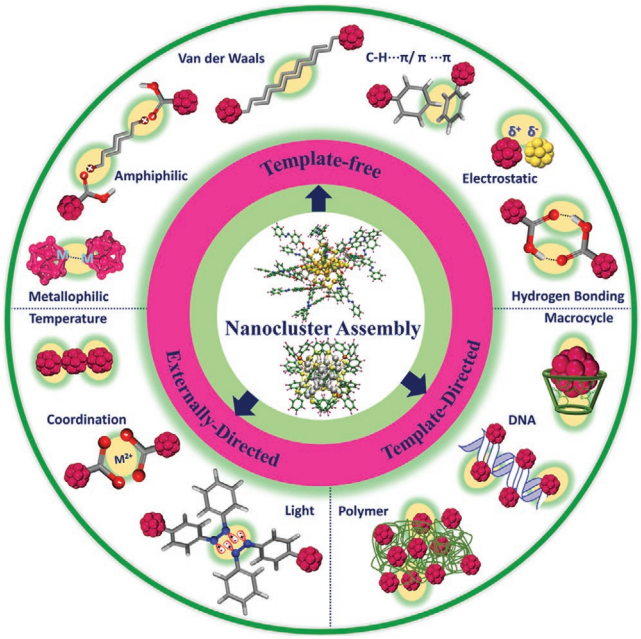

Scheme 1. Schematic showing an overview of different nanoscale driving forces behind the assembly of NCs.

NCs (*p*-MBA = *p*-mercaptobenzoic acid).[120] In another study, Yoon et al. investigated the large-scale synthesis and superlattice formation of ultrastable $[Na_4Ag_{44}(p\text{-MBA})_{30}]$ NCs and their quantum-mechanical simulation studies.[217] To demonstrate the hydrogen bonding-mediated self-assembly, $[Na_4Ag_{44}(p\text{-MBA})_{30}]$ NCs were initially synthesized in semi-aqueous solution protected with *p*-MBA ligand shells. Storage of NCs in *N*, *N*-dimethylformamide (DMF) solution produced superlattice crystals. Here, every carboxylic acid groups of the ligands were completely protonated to dissolve NCs in DMF. The free carboxylic acid group tends to form dimers or trimers through hydrogen bonding, which resulted in the formation of rhombus-shaped superlattice crystals. Single crystal X-ray crystallography revealed that the superlattice crystal possesses a triclinic unit cell containing two NCs in the asymmetric unit of the crystal lattice. Intriguingly, *p*-MBA ligands were aligned parallelly to form two types of molecular bundles. The hydrogen bonding bundles viz, double (L2) and triple (L3) bundles facilitate the intralayer and interlayer hydrogen bonding, respectively. The 30 interfacing pairs of ligands from a NC and its nearest neighbors in the superlattice crystal could form 60 hydrogen bonds, including 24 intralayer and 36 interlayer bonds (**Figure 1**A–D). Such sophisticated networks of hydrogen bonds with flexible and structure-directing properties provided chiral rotation to NC and their superstructures. Furthermore, the anisotropic distribution of hydrogen bonding in NCs helps to activate the pressure softening behavior of superlattice structures under hydrostatic compression. Subsequently, Yao et al. demonstrated the formation of superstructures from $[Ag_{44}(p\text{-MBA})_{30}]^{4-}$ NCs under highly alkaline conditions.[218] The complete deprotonation of *p*-MBA followed by the addition of counterions in dimethylsulfoxide (DMSO)/water crystallization system, NCs resulted in the formation of engineered superstructures with controllable shapes. The addition of cesium (Cs^+) counterions perturbed the directional hydrogen bonds, which resulted in the packing of deprotonated $[Ag_{44}(p\text{-MBA})_{30}]^{4-}$ NCs into polymorphic octahedral single crystals via electrostatic interactions. Further supplement of Cs^+ ions created a charge screening environment in $[Ag_{44}(p\text{-MBA})_{30}]^{4-}$ NCs to induce a concavity in octahedral crystal faces, and therefore contributed concave octahedral shaped crystals.

Highly monodisperse self-assembly of $[Au_{102}(p\text{-MBA})_{44}]$ NCs into 2D colloidal crystals and spherical capsids were reported by Nonappa et al.[219,220] To demonstrate the self-assembly via partial hydrogen bonding, $[Au_{102}(p\text{-MBA})_{44}]$ NCs were synthesized by chemical reduction method in the presence of *p*-MBA. The dispersion of NCs in sodium hydroxide (NaOH) solution resulted in the formation of partially deprotonated NCs. Subsequent solvent exchange from water to methanol using dialysis triggered the inter-NC hydrogen bonding and furnished 2D colloidal crystals (Figure 1E,F). Using a spherical coordination system, the authors hypothesized that the anisotropic and patchy distribution of the ligands drives the 2D colloidal crystal formation. More interestingly, by changing the crystallization kinetics via electrostatic interactions, they were able to tune the shapes of

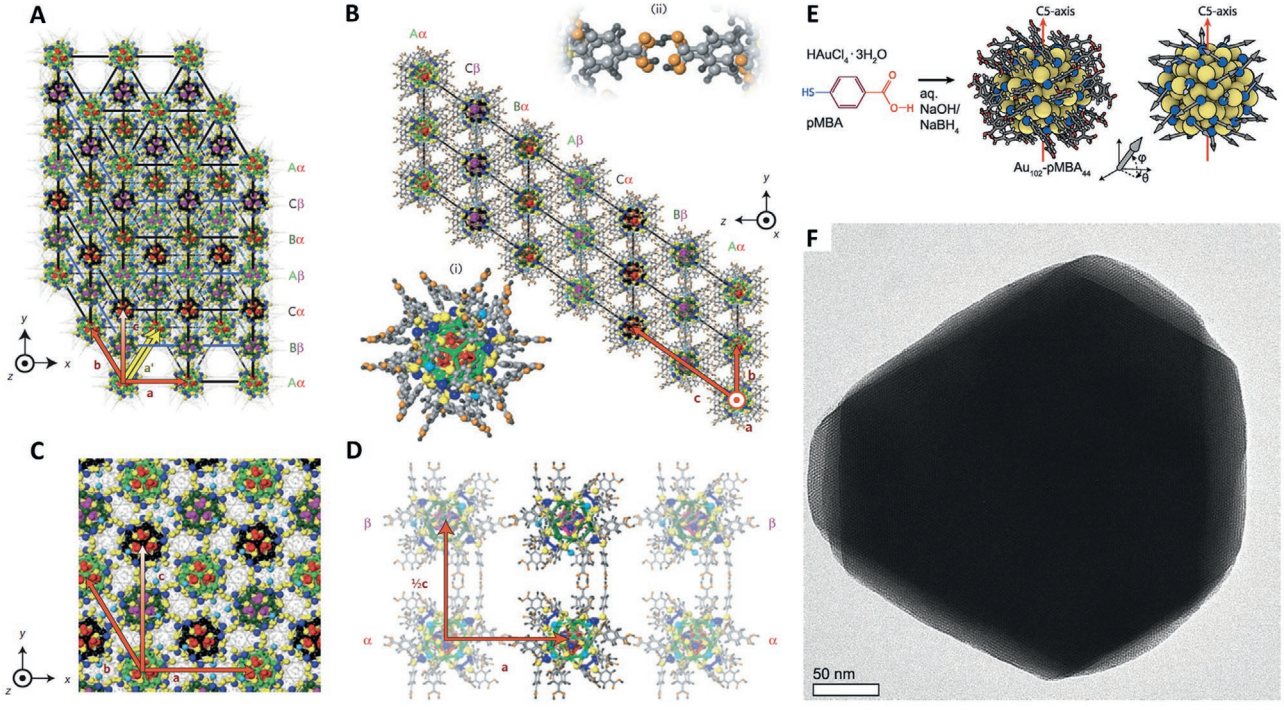

Figure 1. A) 3D and B) 2D views of $[Na_4Ag_{44}(p\text{-MBA})_{30}]$ NC superlattice structures. A view of a single NC is provided in the inset (i). C) The stacking of NC layers in the assembly is depicted in the *XY* three-layer projection. D) The interlayer hydrogen bonding between neighboring NCs, involving triply bundled ligands are shown. An enlargement of the hydrogen-bonded region is given in inset (ii), showing two hydrogen bonds between each pair of interfacing ligands. Reproduced with permission.[217] Copyright 2014, Springer Nature. E) Synthetic route for $[Au_{102}(p\text{-MBA})_{44}]$ NCs and their internal structure extracted from the solid-state structure. F) HR-TEM image of 2D colloidal crystal fabricated from $[Au_{102}(p\text{-MBA})_{44}]$ NCs with facetted edges showing the stacked NC layers. Reproduced with permission.[219] Copyright 2016, Wiley-VCH.

assembled superstructures. For example, instead of dialysis, the direct addition of an aqueous dispersion of NCs into methanol resulted in the formation of spherical superstructures with monolayer shells. The electron tomographic (ET) 3D reconstruction studies demonstrated the formation of spherical capsids. Later, Zhang et al. established the spherical self-assembly from glutathione (GSH)-protected Au_{22} NCs to mimic the capsid protein self-assembly.[221] $[Au_{22}(SG)_{18}]$ NCs were synthesized by the pH-mediated reduction of a mixture of gold precursor ($HAuCl_4 \cdot 3H_2O$) and GSH in the presence of tetrabutylammonium borohydride (TBAB) at low temperature.[222] To demonstrate the self-assembly of NCs, the hydrogen bonding network between water molecules and NCs was initially interrupted by introducing DMSO. Subsequently, hydrogen bonding between SG ligands from the adjacent NCs was achieved by displacing the hydrated water molecules around the NCs via evaporation (50 °C) method. The pH-dependent studies showed the formation of larger self-assembled spheres at lower pH. In parallel, dialysis of NCs using water–DMSO or water–DMF binary solvent systems were also implemented to engage hydrogen bonding between SG ligands. The higher dielectric constant of water–DMSO cosolvents resulted in larger assemblies than water–DMF cosolvents due to the efficient screening of the repulsive electrostatic forces between negatively charged NCs. Such self-assembly processes could be useful to understand the protein self-assembly mechanism, as it follows the capsid-like assembly. More recently, Xie et al.[223] and Sun et al.[224] investigated the significance of the position (*ortho* or *para*) of −COOH group on the bound ligands during the self-assembly of NCs via hydrogen bonding. To address this, $(NH_4)_9[Ag_9(o\text{-MBA})_9]$ and $(NH_4)_9[Ag_9(p\text{-MBA})_9]$ NCs were prepared in water by the pH-mediated reduction of silver nitrate ($AgNO_3$) in the presence of *o*-MBA or *p*-MBA. The addition of ethanol (anti-solvent) into $(NH_4)_9[Ag_9(o\text{-MBA})_9]$ NCs resulted in the gelation of NCs by forming self-assembled nanofibers.[223] Though such gelation was not observed in $(NH_4)_9[Ag_9(p\text{-MBA})_9]$ NCs, they could self-assemble into nanorods by carefully adjusting the pH of the solution.[224] The self-assembled nanofibers fabricated from $(NH_4)_9[Ag_9(o\text{-MBA})_9]$ NCs showed fluorescence to phosphorescence (delayed fluorescence) switching. Chakraborty et al. demonstrated the hydrogen bonding mediated self-assembly of NCs on the surface of plasmonic gold nanorods (GNRs) to achieve a composite nanocage.[8,225] To accomplish such NC-GNR nanocages, GNRs synthesized in cetyltrimethylammonium bromide (CTAB) template were initially surface-functionalized with *p*-MBA via ligand exchange process. Upon mixing a dispersion of *p*-MBA functionalized GNRs with $[Na_4Ag_{44}(p\text{-MBA})_{30}]$ NCs in DMF, systemic assembly of NCs on the GNR surface was found through the hydrogen bonding via carboxylic acid dimerization of *p*-MBA ligands. Scanning transmission electron micrograph (STEM) and high-resolution transmission electron micrographs (HR-TEMs) showed that composite structures consisted of a single GNR in each superstructure. ET reconstructions revealed the formation of octahedral nanocages, where the length of GNRs controlled the size of the cages. 3D reconstructions of GNRs suggest that the geometry of the GNR surface is accountable for directing the assembly of $[Na_4Ag_{44}(p\text{-MBA})_{30}]$ NCs leading to octahedral symmetry (**Figure 2**). However, the addition of water-soluble Au NCs such as $[Au_{250}(p\text{-MBA})_n]$ or $[Au_{102}(p\text{-MBA})_{44}]$ into *p*-MBA functionalized GNR resulted in the formation of monolayered shells encapsulating GNRs due to the less packing density of partially deprotonated NCs in water. In another study, Som et al. examined the self-assembly of tellurium nanowires (TeNWs) into crossed-bilayered structures with precise geometry.[226] To achieve these 2D structures, the tellurium nanowires were initially decorated with $[Na_4Ag_{44}(p\text{-MBA})_{30}]$ NCs. Here, the carboxylate group of *p*-MBA ligands on the NC surface allows tellurium–oxygen bonding, resulting in the formation of stable TeNW–NC complexes at the air–liquid interface. Interestingly, Ag_{44} NC wrapped-tellurium nanowires were self-assembled to form a crossed-bilayer structure during the solvent evaporation process. TEM analysis has shown a woven-fabric-like structure, in which nanowires in the same layer were parallel, but nearby layers were arranged at an unusual angle of 81°. The above-discussed science can be further extended to develop multifunctional nanoprobes for the fabrication of advanced devices.

2.1.2. Electrostatic Interactions

Electrostatic interactions are generally strong attractions or repulsions between two oppositely charged ions, mostly positive and negative charges. To demonstrate the self-assembly of NCs via electrostatic interactions, it is necessary to introduce charge separations between the neighboring units either by selecting the oppositely charged NCs or by adding the counterions in monocharged NCs. For example, $[Na_4Ag_{44}(p\text{-MBA})_{30}]$ NCs were initially self-assembled using hydrogen bonding as a significant driving force.[217] However, the adequate supplement of counterions in $[Ag_{44}(p\text{-MBA})_{30}]^{4-}$,[218] or $[Au_{102}(p\text{-MBA})_{44}]$,[219] NCs allow electrostatic interactions apart from their inherent hydrogen bonding. The balanced control over these two interactions offered customized morphologies during the self-assembly. Later, a combination of oppositely charged NPs and NCs were used to demonstrate the formation of hybrid superstructures. For example, the electrostatic interactions between negatively charged [Au@SG] NCs and positively charged amino sugar-modified silicon NPs have been shown to form spherical superstructures.[227] Using a similar strategy, Jia et al. developed a dual emitting hybrid system composed of positively charged carbon dots and negatively charged [Au@SG] NCs.[228] More recently, He et al. attempted the self-assembly of two counter-charged NCs, by mixing the cationic and anionic Au_{25} NCs. Although the protocol was not feasible, owing to the instability of cationic NCs, the authors were able to successfully demonstrate the self-assembly of cationic and anionic Au–Ag bimetallic NCs in a one-pot method.[229] NCs were synthesized by a two-step method, in which the multisized Ag-thiolates were initially prepared by the chemical reduction of $AgNO_3$ in the presence of thiol (2-ethylbenzenethiol; 2-EBT) and triphenylphosphine (TPP). Subsequent reaction of Ag-thiolates with a mixture of [Au(TPP)Cl] complex and TPP molecule resulted in the formation of $[Ag_{26}Au(2\text{-EBT})_{18}(TPP)_6]^+[Ag_{24}Au(2\text{-EBT})_{18}]^-$ NCs with a molar ratio 1:1. This NC is an example of an ionic

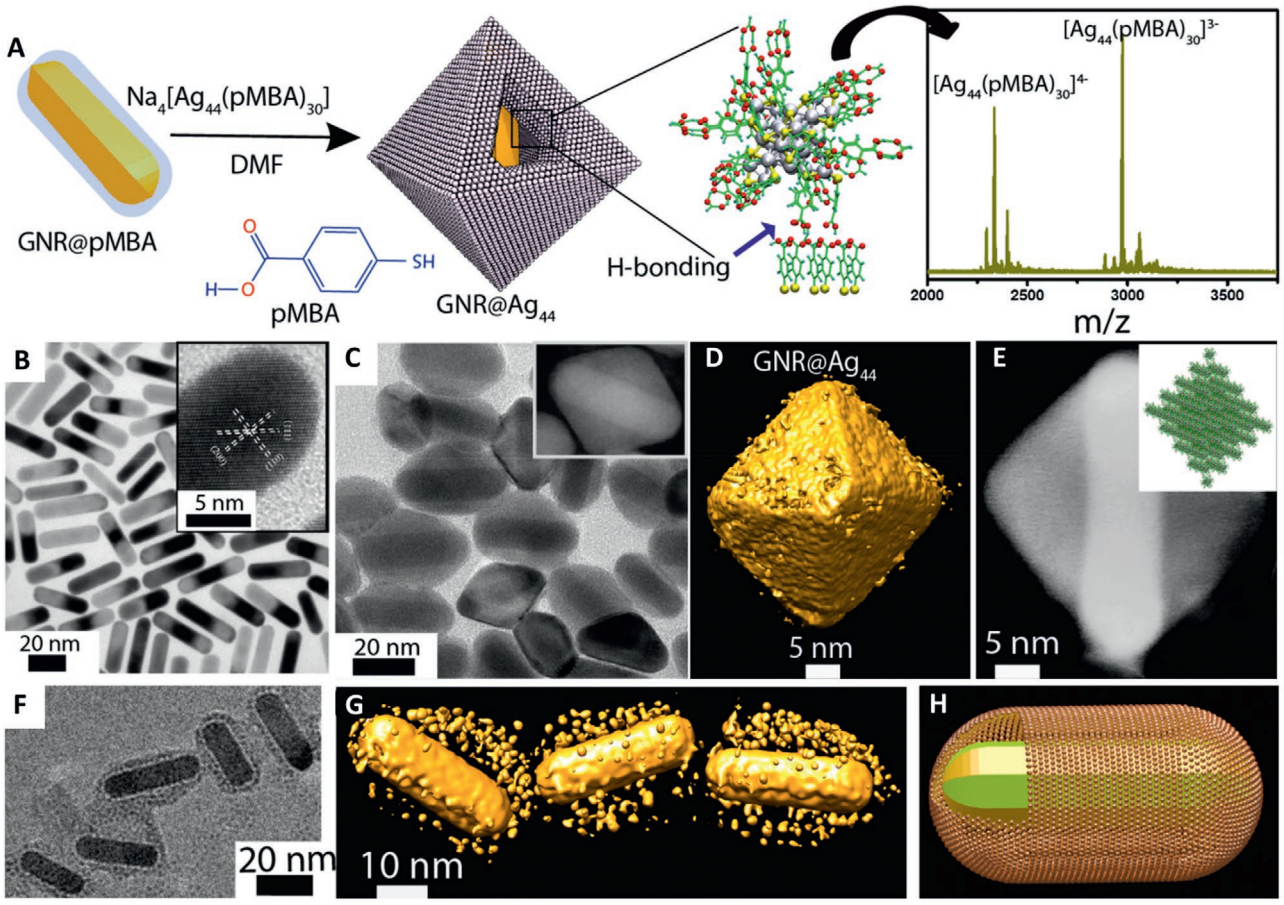

Figure 2. A) Assembly of Ag_{44} NCs on the GNR@*p*-MBA surface. The ESI-MS of Ag_{44} is shown. B) TEM image of GNR@*p*-MBA. HR-TEM image of the tip of a GNR is shown in the inset. C) TEM image of $GNR@Ag_{44}$. A dark-field STEM image is shown in the inset. D,E) ET and dark-field STEM images of $GNR@Ag_{44}$. The image shows that NCs make a nanocage and encapsulate the GNR. A theoretical model of the assembly of Ag_{44} clusters forming an octahedral shape is presented in the inset. F) TEM image of $GNR@Au_{250}$. G,H) 3D reconstructed structures and 3D graphical representation of $GNR@Au_{250}$, respectively. Reproduced with permission.[8] Copyright 2019, American Chemical Society. Originally published images: Reproduced with permission.[225] Copyright 2018, Wiley-VCH.

compound originated from NC ions, which is called as a double NC ion compound (DNIC). The authors exclusively synthesized $[PPh_4]^+[Ag_{24}Au(2\text{-}EBT)_{18}]^-$ NCs, an example of a single NC ion compound (SNIC). Interestingly, the cationic $[Ag_{26}Au(2\text{-}EBT)_{18}(TPP)_6]^+$ and anionic $[Ag_{24}Au(2\text{-}EBT)_{18}]^-$ NCs in DNIC was found to gather and assemble in an unusual alternating array of cationic and anionic stacking structure via strong electrostatic interactions and weak C—H$\cdots\pi/\pi\cdots\pi$ interactions. SNIC displayed a *k*-vector-differential crystallographic arrangement (**Figure 3**A–C). Such a significant difference in the crystallographic arrangement was governed by the exciting influence of ligands and counterions. Wei et al. demonstrated the electrostatic self-assembly of $[Ag_{29}(BDT)_{12}(TPP)_4]^{3-}$ NCs by simply mixing with Cs^+ ions.[230] To address such assembly, Ag_{29} NCs were initially prepared by the chemical reduction of Ag–S complexes presynthesized by mixing 1,3-benzenedithiol (BDT) and TPP in $AgNO_3$ solution.[124] The replacement of TPP ligands by Cs^+ cations produces $[Cs_3Ag_{29}(BDT)_{12}(DMF)_x]^0$ NCs ($x = 5$ or 6), which leads to the formation of the 1D assembly via different surface forces including electrostatic attraction, Cs—S bond formation, and Cs–π interactions.

2.1.3. Van der Waals Interactions

The van der Waals forces are distance-dependent weak electrostatic attraction or repulsion that arise due to the fluctuating electromagnetic polarization of nearby atoms, molecules, or particles. Based on the origin of interactions, three subcategories of van der Waals attractions viz Keesom, Debye, and London dispersion forces are known.[231] Keesom forces develop when two polarized molecules interact owing to their inherent difference in the charge distribution. In the case of Debye force, a polarized molecule induces the charge redistribution to adjacent units with null dipole moments. However, the London force arises in molecules that hold no permanent dipole moments. Here, the fluctuating electron clouds on a molecule induce the charge redistribution to similar neighboring units. Such van der Waals attractions are expected to initiate the long-range periodic self-assembly in NCs. For example, Wu et al. demonstrated the self-assembly of 1-dodecane thiol (DT)-tethered Au NCs at high temperature.[232] Initially, Au_{15} NCs were synthesized using room-temperature reduction of $HAuCl_4$ in the presence of DT. When the temperature

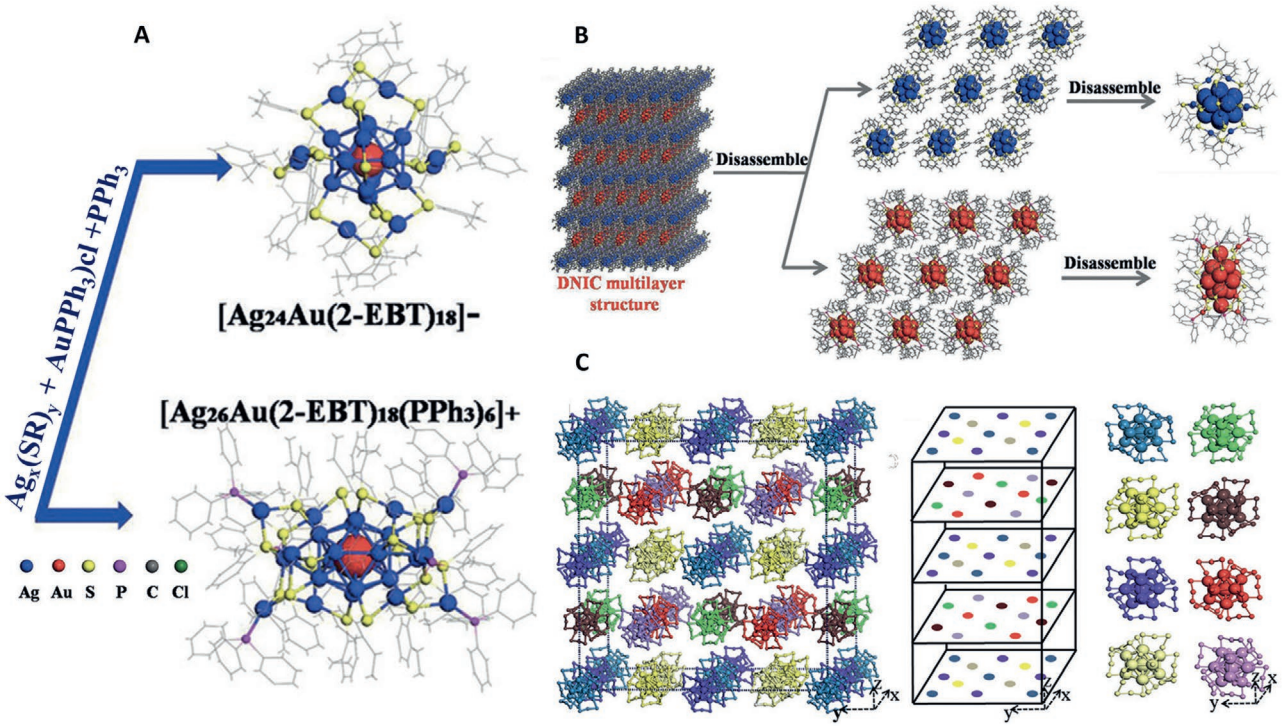

Figure 3. A) X-ray crystal structure of $[Ag_{26}Au(2\text{-}EBT)_{18}(TPP)_6]^+[Ag_{24}Au(2\text{-}EBT)_{18}]^-$ NC-based DNIC. B) Illustration of the self-assembly of $[Ag_{26}Au(2\text{-}EBT)_{18}(TPP)_6]^+[Ag_{24}Au(2\text{-}EBT)_{18}]^-$ NCs. C) Crystallographic arrangement of $[PPh_4]^+[Ag_{24}Au(2\text{-}EBT)_{18}]^-$ NCs. Reproduced with permission.[229] Copyright 2019, Wiley-VCH.

of colloidal dispersion (liquid paraffin/dibenzyl ether) was increased above 140 °C in vacuum, NCs self-assembled into nanosheets. At high temperatures, NCs hold together by the attractive hydrophobic interactions between the long alkyl chains of ligands. Here, the lamellar interface offered by the solvent microphase separation has been acted as a soft template to trigger the assembly. The calculated hydrophobic attractions between the ligands around the neighboring NCs were found to be 7 k_BT, where k_B is the Boltzmann constant and T is the absolute temperature. The attractive hydrophobic interaction technique has been further extended to study the self-assembly of Cu NCs.[233] $[Cu_{12}(DT)_8Ac_4]$ NCs synthesized by the reduction of copper (II) acetylacetonate ($CuAc_2$; Ac-acetylacetonate) in the presence of DT was used to demonstrate the assembly. The permanent dipole moment of NC core helped to induce a robust dipolar attraction apart from the expected van der Waals attraction of ligands. Such combined dipolar and van der Waals attractions resulted in the self-assembly of NCs into long nanowires. However, at high temperature, $[Cu_{12}(DT)_8Ac_4]$ NCs could be converted into $[Cu_8(DT)_8]$ by removing the Ac-ligands, which eventually reduced the overall dipole moment of NC core. Hence, when the temperature increased, nanowires were switched into nanoribbons owing to the prominent van der Waals attractions (**Figure 4**). Later, the combined dipolar and van der Waals attractions have been employed to self-assemble $[Au_{15}(DT)_{15}]$[234] and $[Co_{14}(DT)_9]$[235] NCs. The advantage of such self-assembled NCs is discussed in Section 4.[236–241]

Zeng et al. reported the hierarchical structural complexity of $[Au_{246}(p\text{-MBT})_{80}]$ NCs (*p*-MBT = *p*-methylbenzenethiolate) in its single-crystal X-ray structure and superlattice crystals with translational, rotational, and orientational orders.[242] Interestingly, *p*-MBT ligands were self-organized into α-rotational (pole site) and β-parallel (waist) patterns on the NC surface via intermolecular C—H···π interaction. The α-rotation pattern forms four pentagonal circles at the pole site by using 25 *p*-MBT ligands having the same latitude and rotational direction. The top and bottom of NCs were covered by two of such α-rotation patterns. But the waist is wrapped with five β-parallel patterns with each pattern includes three alternating parallel pairs of six *p*-MBT ligands. Such symmetry and packing density of *p*-MBT surface patterns helped to achieve the directional packing of $[Au_{246}(p\text{-MBT})_{80}]$ NCs via the maximum van der Waals interactions between nearby ligands (**Figure 5**).

2.1.4. C—H···π/π···π Interactions

The weak attraction between the C—H bond and the delocalized π electron system is known as C—H···π interaction.[243] The similar kind of attraction between the delocalized π electrons is called π···π interaction. The C—H···π attraction is often considered as the weakest hydrogen bonding interaction occurring between the soft acids and bases. Though the dispersion interaction is the primary source of attraction in C—H···π interactions, a small percentage of electrostatic interaction is also accompanied. Remarkably, C—H···π interactions play an important role in the nanoscale assemblies and crystal packing of NCs. For example, AbdulHalim et al. demonstrated the C—H···π interaction driven crystallization of $[Ag_{29}(BDT)_{12}(TPP)_4]^{3-}$ NCs using the solvent evaporation technique.[124] Room temperature

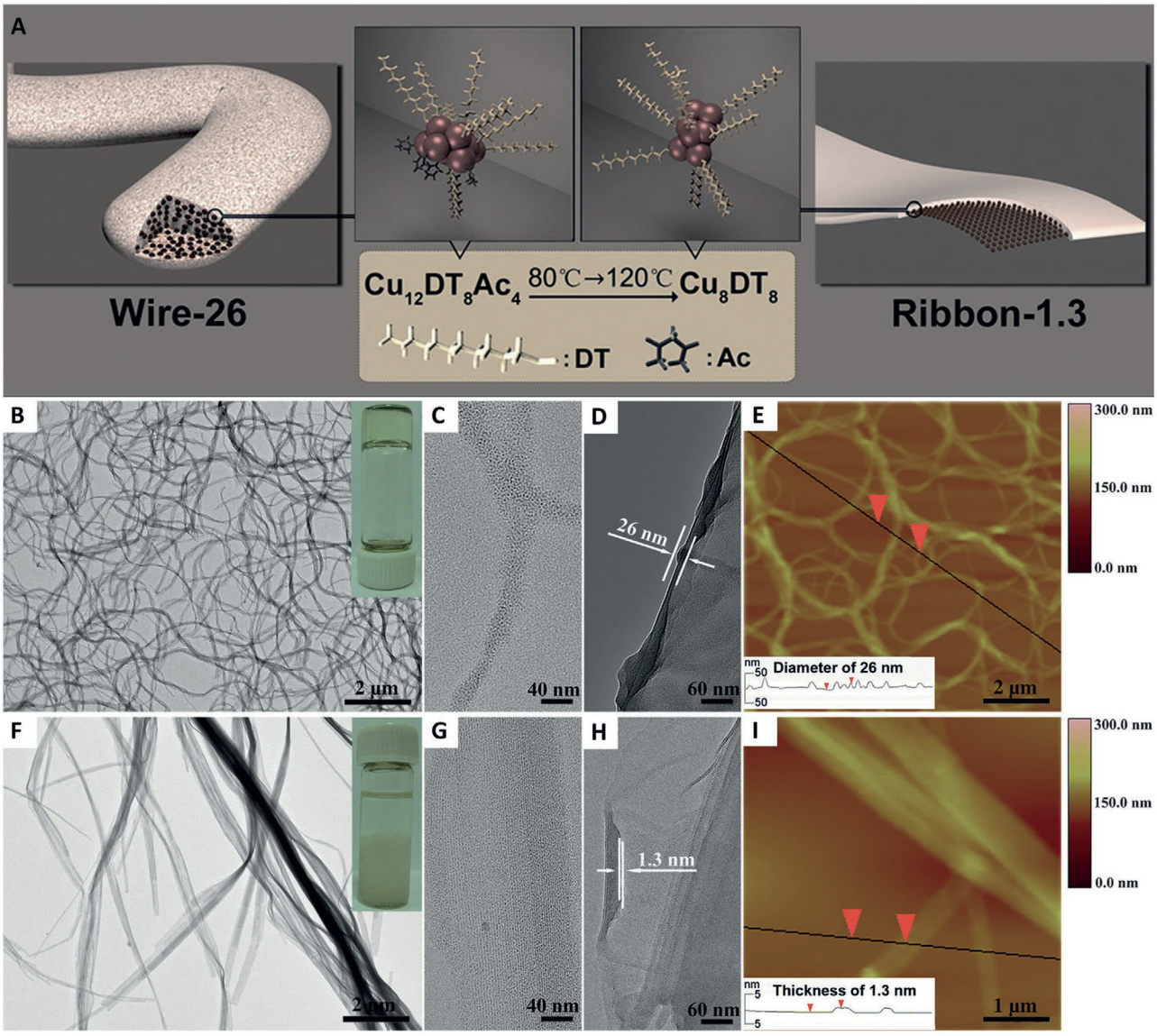

Figure 4. A) Schematic illustration showing the evolution of $[Cu_{12}(DT)_8Ac_4]$ NC self-assembly architectures from nanowire to nanoribbon. B–D,F–H) TEM and E,I) tapping-mode AFM images of B–E) nanowire and F–I) nanoribbon. TEM images of a small region captured from nanowire and nanoribbon oriented C,G) parallel to, and D,H) vertical on the TEM grid are indicated. Photographs of nanowire and nanoribbon dispersions are shown in the inset in (B) and (F), respectively. Reproduced with permission.[233] Copyright 2014, Wiley-VCH.

evaporation of NC solution (DMF) drop-casted on a glass slide resulted in the formation of self-assembled macroscopic cubic lattice crystals. Later, Nag et al. reported polymorphism in the self-assembled $[Ag_{29}(BDT)_{12}(TPP)_4]^{3-}$ NC crystals owing to the solvent-dependent C—H···π interaction of TPP molecules.[244] Interestingly, they could tune the crystal packing of $[Ag_{29}(BDT)_{12}(TPP)_4]^{3-}$ NCs into two different polymorphic forms, trigonal (T) and cubic (C) lattices by using different crystallization methods (**Figure 6**). Though solvent evaporation of $[Ag_{29}(BDT)_{12}(TPP)_4]^{3-}$ NCs resulted in the formation of C crystals, vapor-diffusion of methanol into DMF solution of NCs produced T crystals. Here, the intra- and intermolecular interactions between BDT and TPP molecules bound on the NC surface drive the self-assembly. In the intra-NC interactions, the C—H bond of TPP molecules interacts with the benzene ring of BDT molecules bound on the same NCs. However, in the inter-NC interactions, the C—H bond of BDT interacts with the phenyl ring of TPP ligands connected in the nearby NCs. The dominating C—H···π interaction of TPP molecules during the solvent evaporation resulted in the formation of C crystals. The C lattice crystal has shown enhanced PL owing to the restricted molecular rotations and vibrations. The electronic coupling between nearby NCs in the C crystals resulted in a bathochromic shift in their PL spectrum. A similar strategy has been further extended to crystalize $[Ag_{46}(2,5\text{-DMBT})_{24}(TPP)_8]$ (DMBT = dimethylbenzenethiol), and cocrystals of $[Ag_{40/46}(2,4\text{-DMBT})_{24}(TPP)_8]$ NCs.[245] The exceptional mechanical properties of assembled crystals are discussed in Section 3.

Another important NC assembly triggered by the C—H···π interaction was reported by Shi et al. in chiral Au NCs.[246]

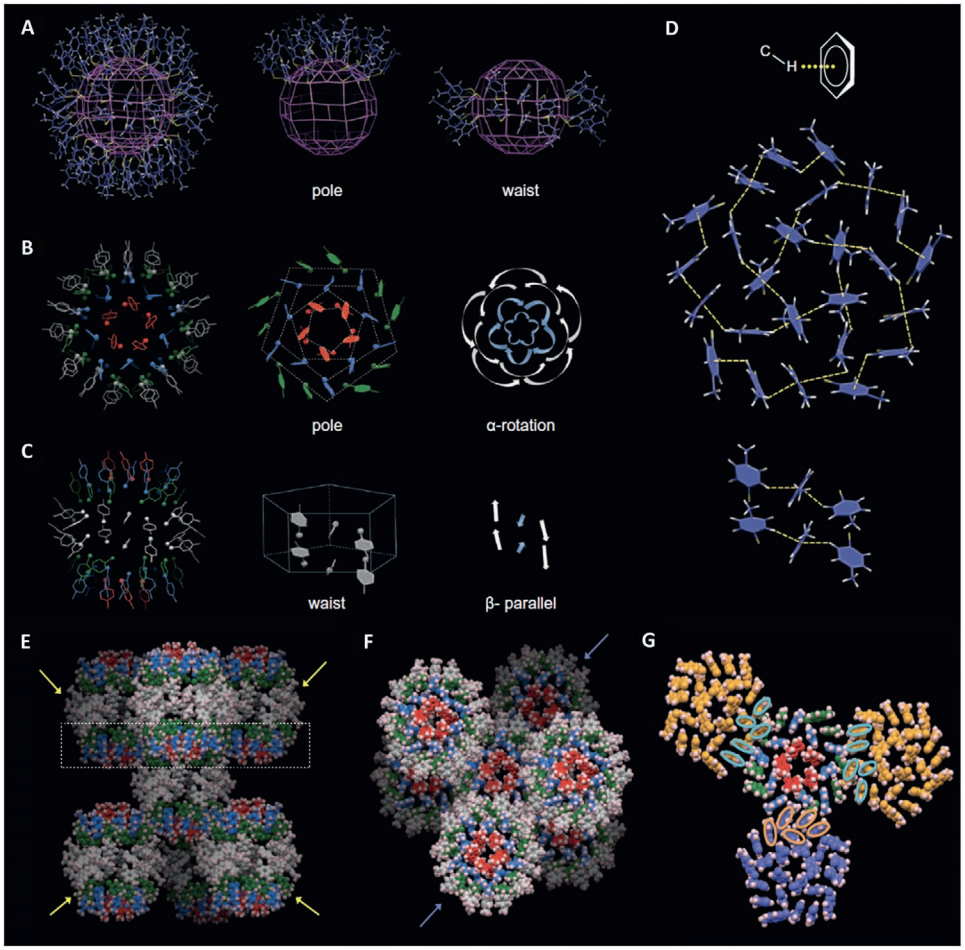

Figure 5. A) Overall structure of ligands on the surface of $[Au_{246}(p\text{-MBT})_{80}]$ NCs. B) Rotational and C) parallel packing of ligands at the pole site and waist of NC, respectively. D) The C—H···π interactions for stabilizing the large-scale rotational patterns and parallel patterns are shown. E,F) The coordination geometry of NCs in the crystal lattice: E) side view and F) top view. G) Contacting environment among the interparticle ligands. The outside pentagons are located at the bottom of the top three NCs in (E), and the central pentagon is located at the top of the central NC. Reproduced with permission.[242] Copyright 2016, AAAS.

The smallest chiral $[Au_3\{(R)\text{-Tol-BINAP}\}_3Cl]$ and $[Au_3\{(S)\text{-Tol-BINAP}\}_3Cl]$ NCs (BINAP = 2,2′-bis(di-*p*-tolylphosphino)-1,1′-binaphthyl) were initially synthesized by the chemical reduction method.[247] The drop-wise addition of *n*-hexane (antisolvent) into the NC solution prepared in dichloromethane (DCM) helped to induce a strong intermolecular interaction among the ligands. When the concentration of *n*-hexane reaches 40%, an orange emission was observed from the NC solution, indicates the formation of assembled body-centered cubic (BCC) nanocubes via strong C—H···π interactions (**Figure 7**). The intermolecular interactions amplified the circularly polarized luminescence (CPL) and chiral responses from the assembled superstructures owing to the restricted movements of ligands (detailed discussion is provided in Section 3).

Recently, Huang et al. reported the synthesis and structural characterization of racemic anisotropic $[Ag_{30}(C_2B_{10}H_9S_3)_8(DPPM)_6]$ NCs, (Ag_{30}-*rac*) protected with a mixture of achiral carboranetrithiolate and phosphine ligands ($C_2B_{10}H_9S_3$ = 8,9,12-trimercapto-1,2-*closo*-carborane and DPPM = bis(diphenylphosphino)methane) via one-pot reduction method using hydrazine.[248] The spiral arrangement of the ligands directed by unusual B—H···π and C—H···π bonding interactions between the carborane cages and benzene rings could induce chirality for Ag_{30}-*rac*. During the crystallization of Ag_{30}-*rac* in dimethylacetamide, the racemates (*R*-Ag_{30} and *L*-Ag_{30}) were self-resolved into the racemic conglomerates and the enantiomeric NCs self-assembled into helical structures. The noncovalent interactions, including B—H···π, C—H···π, π···π, and van der Waals interactions direct such helical superstructures.

The C—H···π interactions have been further extended to explain the crystallization of larger NCs. For example, Higaki et al. demonstrated the synthesis and crystal structure determination of $[Au_{103}S_2(S\text{-NAP})_{41}]$ NCs (S-NAP = 2-naphthalenethiol) via C—H···π and π···π interactions.[249] Ligand exchange-induced size/structure transformation of $[Au_{99}(SPH)_{42}]$ (SPH = thiophenol)[250] NCs with a mixture of 4-*tert*-butyltoluene and S-NAP at 80 °C resulted in the formation of $[Au_{103}S_2(S\text{-NAP})_{41}]$ NCs. The crystallization of NCs via the vapor diffusion method shows that the ligands bound on NC surface form

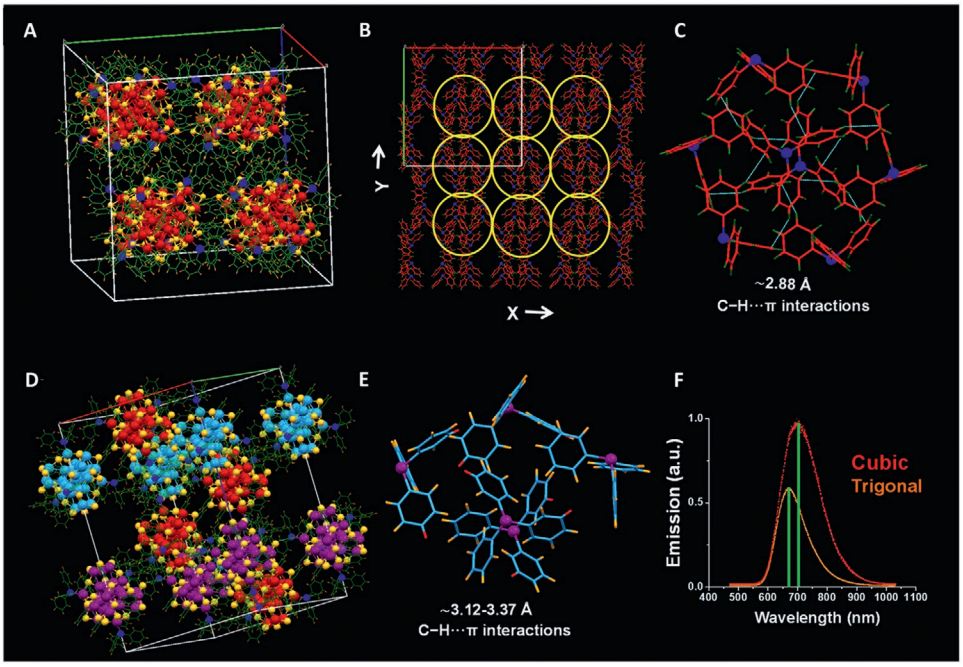

Figure 6. A) Cubic unit cell of $[Ag_{29}(BDT)_{12}(TPP)_4]^{3-}$ NCs. B) Packing of TPP subunits viewed from the *Z*-axis in the C system. C) Strong C—H···π interactions (T-shaped) between the eight TPP subunits forming a hexagonal shape in the C system. D) The trigonal unit cell of NCs. E) C—H···π interactions between the TPP subunits in the T system. F) Emission spectra obtained from single crystals of the C and T lattices. The C structure exhibits stronger and slightly red-shifted (≈30 nm) PL compared with the T structure. Reproduced with permission.[8] Copyright 2019, American Chemical Society. Originally published images: Reproduced with permission.[244] Copyright 2018, The Royal Society of Chemistry.

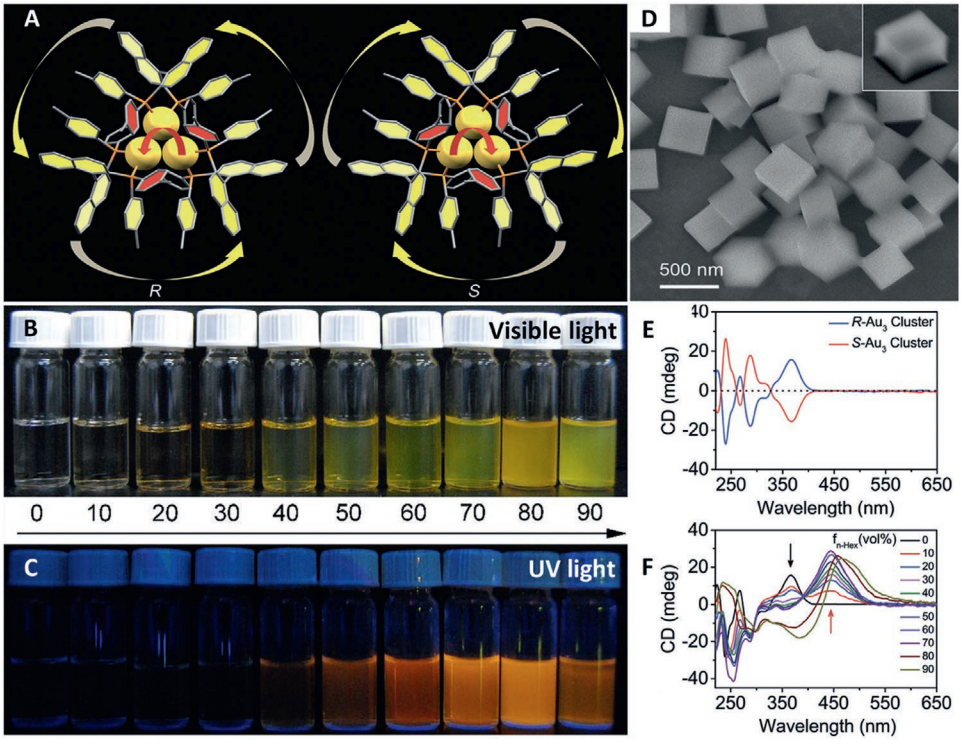

Figure 7. A) Chiral $[Au_3\{(R)\text{-Tol-BINAP}\}_3Cl]$ and $[Au_3\{(S)\text{-Tol-BINAP}\}_3Cl]$ NCs. Photographs of $[Au_3\{(R)\text{-Tol-BINAP}\}_3Cl]$ NCs in DCM with a different fraction of *n*-hexane under B) visible light and C) UV light. D) SEM image of $[Au_3\{(R)\text{-Tol- BINAP}\}_3Cl]$ NC assembly fabricated in DCM with 70% *n*-hexane. E) CD spectra of $[Au_3\{(R)\text{-Tol-BINAP}\}_3Cl]$ and $[Au_3\{(S)\text{-Tol-BINAP}\}_3Cl]$ NCs in DCM. F) CD spectra of $[Au_3\{(R)\text{-Tol-BINAP}\}_3Cl]$ NCs in DCM with various *n*-hexane contents. Arrows show the direction of change with increasing *n*-hexane content. Reproduced with permission.[246] Copyright 2017, Wiley-VCH.

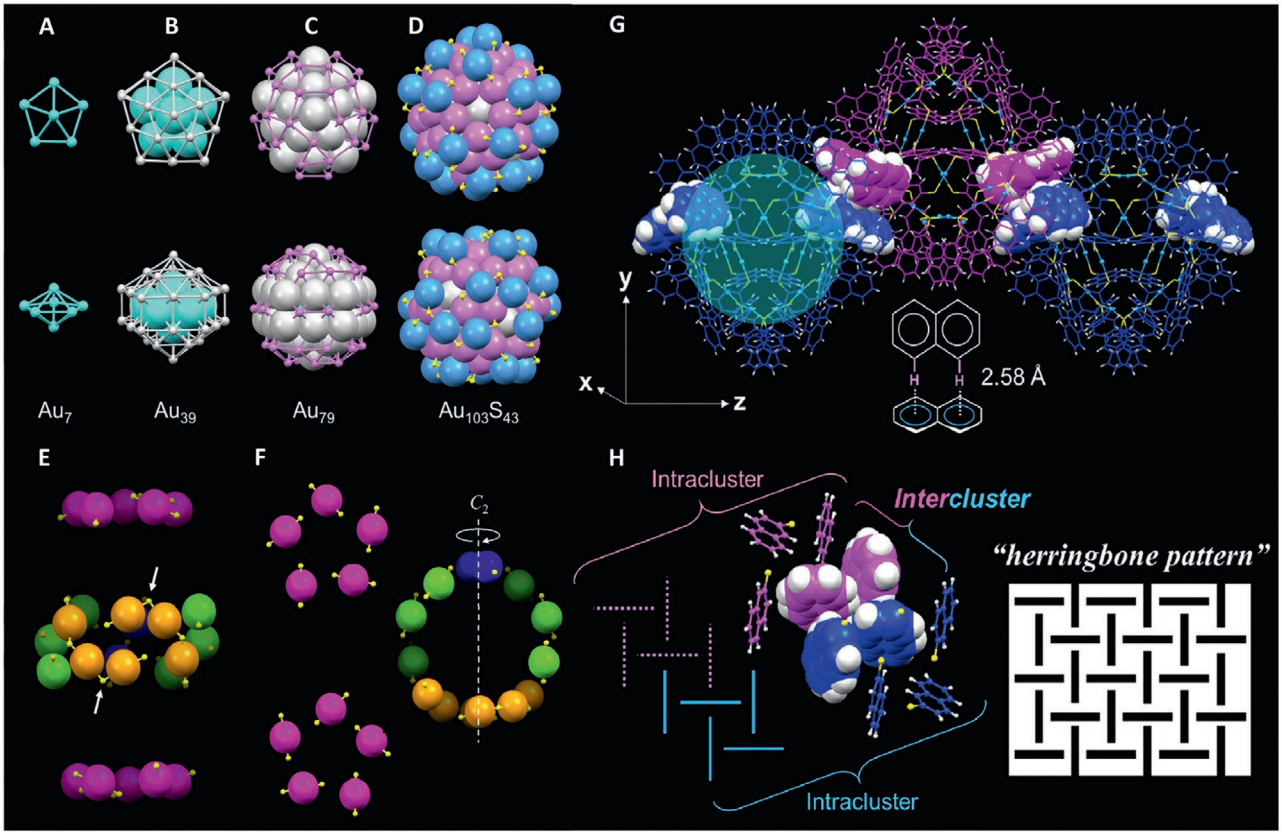

Figure 8. Kernel and surface structure of $[Au_{103}S_2(S\text{-}NAP)_{41}]$ NC: A) the first shell Au_7; B) the second shell Au_{32}; C) the third shell Au_{40}; D) the fourth shell Au_{24} and S_{43}; and E,F) side and top views of surface staple motifs. G) Inter-NC ligand–ligand interactions via C—H···π in the crystal packing structure of NC. H) Combination of inter-NC and intra-NC ligand–ligand interactions to form a herringbone pattern. Reproduced with permission.[249] Copyright 2017, American Chemical Society.

local tetramers (herringbone pattern) by C—H···π and π···π stacking (**Figure 8**). The kernel of $[Au_{103}S_2(S\text{-}NAP)_{41}]$ NC is decahedron with Au_{79} atoms, similar to $[Au_{102}(p\text{-}MBA)_{44}]$ NCs. The weak intra- and inter-NC interactions between the ligands are the key reason behind the assembly and crystallization of NCs. Such C—H···π interactions have been further used to demonstrate the crystal structure of $[Au_{144}(PMT)_{60}]$ (PMT = phenyl methanethiol)[121] and $[Au_4Ag_{13}(DPPM)_3(2,5\text{-}DMBT)_9]$[251] and self-assembly of $[Au_{11}(TPP)_7Cl_3]$ (Au_{11}-H), $[Au_{11}(p\text{-}Cl\text{-}TPP)_7Cl_3]$ (Au_{11}–Cl),[252] and $[Au_{52}Cu_{72}(p\text{-}MBT)_{55}]^+Cl^-$ NCs.[253] In the case of Au_{11} NCs, Au_{11}-H assembled through C—H···π interaction between TPP ligands and Au_{11}–Cl interacts via C–H/Cl–C van der Waals interaction of *p*-Cl-TPP ligands, resulted in monoclinic (M) and trigonal (T) unit cell systems. In another example, Li et al. have shown the formation of 1D assemblies by pairing the cationic $[Au_{21}(S\text{-}C_6H_{11})_{12}(DPPM)_2]^+$ NCs (HS-C_6H_{11} = cyclohexanethiol) with the different counteranions.[254] The counteranions, $[AgCl_2]^-$ and $[Cl]^-$ interacted with NC surface ligands or acted as "surface hooks" to yield self-assembly. The synthesized $[Au_{21}(S\text{-}C_6H_{11})_{12}(DPPM)_2]^+[AgCl_2]^-$ and $[Au_{21}(S\text{-}C_6H_{11})_{12}(DPPM)_2]^+[Cl]^-$ NCs subjected to form single crystals owing to π···π, anion···π, and aryl C—H···Cl interactions of counterion and phenyl ring of the ligands. $[Au_{21}(S\text{-}C_6H_{11})_{12}(DPPM)_2]^+[Cl]^-$ assembly showed better electron transport properties compared to $[Au_{21}(S\text{-}C_6H_{11})_{12}(DPPM)_2]^+[AgCl_2]^-$ owing to their parallel-displaced π-stacking arrangement and smaller interparticle spacing.

2.1.5. Metallophilic Interactions

The noncovalent attractions between the closed-shells (d^{10}, s^2) or pseudoclosed-shell (d^8) of metal cations can hold NPs together to form self-assembled superstructures. Such interactions are known as metallophilic interactions.[255] Transition metals such as Pt, Pd, Au, Ag, and Cu have been reported to display metallophilic interactions, especially at nanoscale assemblies. Though such interactions are weak, it will be very prominent in the presence of particular solvents. Gold–gold (Au–Au) interactions (aurophilic interactions) and their possible structure-directing assemblies are known in the literature.[256] Au NCs are emerging candidates to examine the chemistry of such self-assemblies. For example, Nardi et al. demonstrated the formation of 1D linear crystalline self-assembly from $[Au_{25}(SBu)_{18}]^0$ NCs (HSBu = *n*-butanethiol) via the aurophilic interaction.[257] To address such $[Au_{25}(SBu)_{18}]^0{}_n$ polymer assembly, initially, the neutral $[Au_{25}(SBu)_{18}]^0$ NCs were prepared by passing the anionic $[Au_{25}(SBu)_{18}]^-$ through a silica gel column under aerobic conditions. The slow crystallization (4 °C) of $[Au_{25}(SBu)_{18}]^0$ NC solution in DCM in the presence of acetonitrile (CH_3CN; NC

insoluble solvent) resulted in $[Au_{25}(SBu)_{18}]^0_n$ assembly, in which the $[Au_{25}(SBu)_{18}]^0$ units were interconnected by Au—Au bonds. A twist-and-lock mechanism between neighboring NCs and bound ligands also played an important role in the formation of polymer assembly. However, such assembly was not observed in the case of $[Au_{25}(SET)_{18}]^0$ (HSET = ethylthiol) under similar experimental conditions due to less steric hindrance offered by the bound ligands. Later, the aurophilic-induced 1D self-assembly of $[Au_{25}(S\text{-}C_nH_{2n+1})_{18}]^0$ NCs (n = 3, 4, and 5) and $[Au_{25}(PET)_{18}]^0$ (PET = 2-phenylethanethiol) into millimeter-long polymers using the electrocrystallization approach has been introduced.[258] Various bimetallic NCs including $[Au_{24}Hg(SBu)_{18}]^0$, $[Au_{24}Cd(SBu)_{18}]^0$, $[Au_4Pt_2(SR)_8]^0$, and $[(AuAg)_{34}]$ NCs were successfully self-assembled into 1D polymers via the metallophilic interactions.[259–261] Among these, the single crystal polymer fabricated from $[(AuAg)_{34}]$ NCs showed anisotropic p-type semiconducting properties.[261] Recently, Wu et al. investigated the aurophilic interaction-induced colloidal (3D) self-assembly in Au NCs.[262] In their study, $[Au_{25}(p\text{-}MBA)_{18}]^-$ NC has taken as a model system to understand the structure-directional assembly and their enhanced PL. To address such nanoscale assembly, $[Au_{25}(p\text{-}MBA)_{18}]^-$ NCs were initially synthesized by the pH-adjusted chemical reduction of Au-thiolates in the presence of $NaBH_4$.[263] The cyclic dialysis process has been used to decrease the pH of NC solution, which eventually transformed the parent $[Au_{25}(p\text{-}MBA)_{18}]^-$ NCs to surface-motif reconstructed NCs having Au^1 centers with d^{10} electronic configuration. These surface-reconstructed NCs consist of long SR-$[Au^1\text{-}SR]_x$ motifs ($x > 2$) and small Au^0 core. The overnight incubation of the above NC solution resulted in the formation of self-assembled nanoribbons. Self-assembly is triggered by surface-motif reconstruction of NCs from the short SR-$[Au^1\text{-}SR]_2$ units into long SR-$[Au^1\text{-}SR]_x$ ($x > 2$) staples followed by the structural change of intrinsic Au_{13} kernel. The Fourier transform extended X-ray absorption fine-structure (FT-EXAFS) revealed an enhancement in the Au–S and Au_{staple}–Au_{staple} character, which confirms the formation of long SR-$[Au^1\text{-}SR]_x$. The rich Au^1 content and short aurophilic $Au^1\cdots Au^1$ interactions in the primary stage of assembly have driven NCs into 1D nanowires. Successive formation of nanoribbons from nanowires has been attributed to the $\pi\cdots\pi$ stacking between p-MBA ligands from the adjacent nanowires, which is evident from the reduced inter-nanowire spacing (**Figure 9**). Interestingly, nanoribbons displayed two independent emission bands (at 77 K) and temperature-responsive luminescence. In contrast to the lower quantum yield (QY) of $[Au_{25}(p\text{-}MBA)_{18}]^-$, nanoribbons have shown enhanced PL with a 6.2% quantum yield (at 77 K). The authors adopted a similar strategy to fabricate the self-assembled nanoribbons from $[Au_{38}(p\text{-}MBA)_{24}]$ and $[Au_{44}(p\text{-}MBA)_{26}]^{2-}$ NCs too. In another study, Wu et al. reported the self-assembly of $[Cu_{14}(DT)_{10}]$ NCs via cuprophilic interactions.[236] NCs were synthesized by the chemical reduction of copper chloride ($CuCl_2\cdot 2H_2O$) in the presence of DT. The detailed structural investigations revealed that individual NC is composed of $Cu^0_4Cu^1_{10}DT_{10}$. The high-temperature (128 °C) annealing of the above NC solution in dibenzyl ether in the

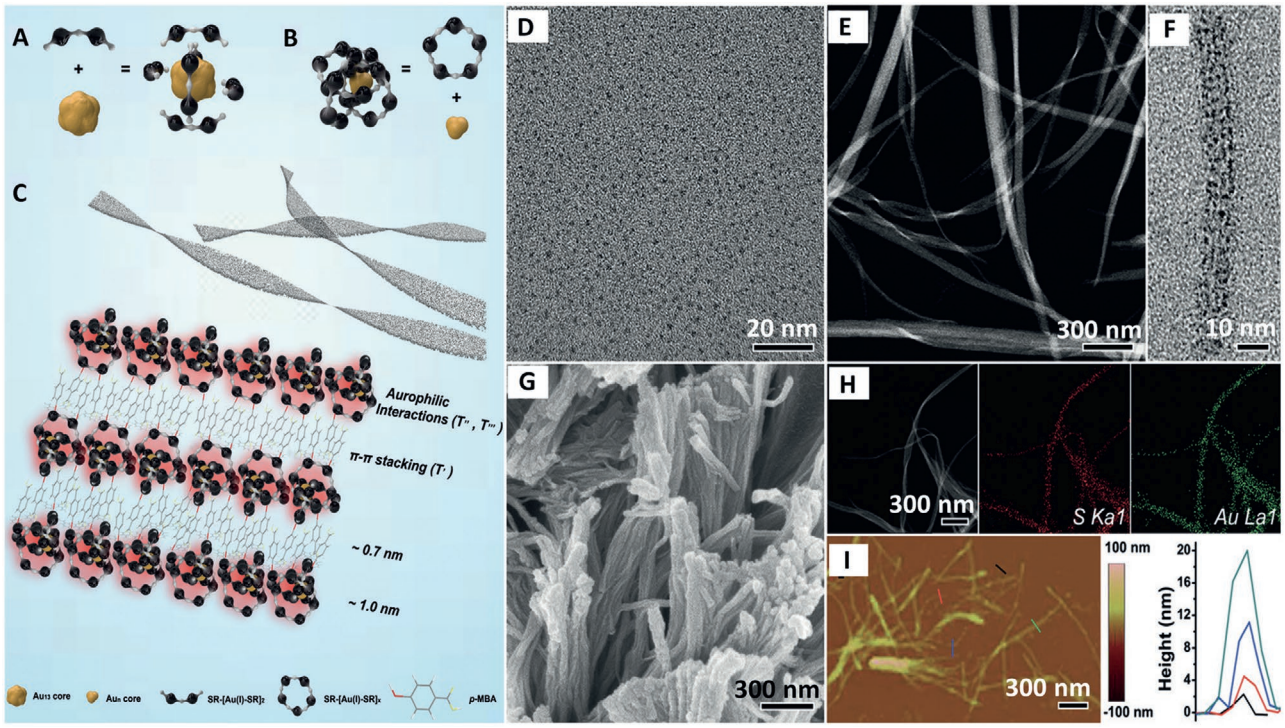

Figure 9. Schematic shows the evolution of $[Au_{25}(p\text{-}MBA)_{18}]^-$ NCs into well-defined self-assembled nanoribbons. The schematic pictures illustrate the structure of A) $[Au_{25}(p\text{-}MBA)_{18}]^-$ NCs and B) the as evoked smaller NCs, and C) their spatial arrangement within nanoribbons. D) TEM image of $[Au_{25}(p\text{-}MBA)_{18}]^-$ NCs, E) high-angle dark-field scanning TEM, F) high-resolution TEM, and G) SEM images of the nanoribbons. H) High-angle dark-field scanning TEM (left), corresponding energy-dispersive X-ray (EDX) element maps (middle and right), and I) AFM image of the representative nanoribbons are shown. Reproduced with permission.[262] Copyright 2019, Wiley-VCH.

presence of excess DT triggered the formation of self-assembled nanoribbons. The PL properties of assembled NCs were found to depend on DT ligands and cuprophilic $Cu^1\cdots Cu^1$ interactions. Such NC assembly shows reversible thermochromic PL, details provided in Section 3. Further, Sun et al. reported the similar chemistry behind the argentophilic interactions in Ag NCs.[264] The interaction of water-soluble $[Ag_9(o\text{-MBA})_9]$ NCs with succinic acid resulted in the conversion of NCs into well-ordered phosphorescent hydrogels. The acid interaction helped to induce a topography reconstruction of NCs into Ag^1 species on the surface. The subsequent argentophilic ($Ag^1\cdots Ag^1$) interactions triggered a long-range self-assembly of NCs into nanofibers. The interligand interactions such as hydrophobic interactions, hydrogen bonding, and $\pi\cdots\pi$ stacking were also played an important role in the hydrogel formation. The assembled NCs have shown temperature-sensitive phosphorescence.

2.1.6. Self-Assembly Driven by Amphiphilicity of NCs

Self-assembly of NCs has been further demonstrated by introducing the amphiphilicity. Amphiphilic molecular level surfactants, as well as block-copolymers, undergo self-assembly into a wide range of nanostructures. Morphologically diverse structures such as micelles, vesicles, or bilayers can be achieved by tuning the hydrophilic–hydrophobic balances.[265] However, the functionalization of colloidal metal NPs with specific patterns of hydrophobic and hydrophilic surface coverage is challenging. This issue was addressed by preparing the amphiphilic NPs via the ligand replacement reaction with a suitable combination of hydrophobic and hydrophilic molecules.[266–269] Yao et al. adopted the "surfactant-mimicking" strategy to self-assemble the hydrophilic $[Au_{25}(MHA)_{18}]$ (MHA = 6-mercaptohexanoic acid) NCs.[270] $[Au_{25}(MHA)_{18}]$ were synthesized by the NaOH-mediated $NaBH_4$ reduction method.[95] A careful exchange of nearly half of the monolayer ligands (MHA) with hydrophobic cations (cetyltrimethylammonium, CTA^+) using the phase-transfer driven ion-pairing reaction resulted in amphiphilic Au_{25} NCs. The electrostatic interaction between the negatively charged carboxylate group of MHA and positively charged CTA^+ ions resulted in the formation of amphiphilic $[Au_{25}(MHA)_{18}@xCTA]$ (x = 6–9) NCs, in which the flexible hydrophilic MHA and hydrophobic MHA$\cdots$CTA ligands can coexist on the NC surface. The subsequent slow evaporation of amphiphilic Au_{25} NCs from the DMSO–ethanol mixture leads to the formation of a self-assembled film at the air–liquid interface with exactly stacked bilayers, imitating the structure of lyotropic liquid crystalline phases by molecular surfactants.

2.2. Template-Directed Assembly of NCs

Apart from the surface ligands induced-assembly discussed above, the soft templates created by molecules such as polymers, DNA, and macrocycles could also play an important role in organizing NCs. Templates can be considered as substrates that consist of many active sites to bind NCs selectively. Such molecular organization is a dynamic platform that can induce the assembly in NCs accompanied by the morphology of templates. In the recent past, the diverse synthetic protocols and new properties of NCs have been probed to demonstrate a variety of hybrid assemblies. However, the ability to form such hybrid assemblies largely depends on the stability of NCs and template-NC interactions.[271,272] This section will discuss the assembly of NCs directed by molecular templates.

2.2.1. Polymer-Templated Assembly

Polymers can act as an active scaffold to induce the anisotropic ordering of NCs. Though the polymers and NCs are entirely different functional moieties, mutually compatible NCs can be well dispersed in a polymer matrix, resulting in homogeneous assemblies. By introducing the interactive functional groups into polymers and NCs, one could control such assemblies. For example, Yahia-Ammar et al. demonstrated the pH-dependent and size controllable self-assembly of [Au@SG] NCs in aqueous medium by introducing a cationic polymer.[273] The electrostatic interaction between the positively charged amine group of poly(allylamine hydrochloride) (PAH) and a negatively charged carboxylate moiety of NC ligand resulted in the self-assembled [Au@SG-PAH] spheres. Such self-assembled superstructures showed an aggregation-induced emission (AIE). Shen et al. extended a similar protocol for the fabrication of self-assembled nanospheres and nanovesicles from $(NH_4)_6[Ag_6(MNA)_6]$ NCs (MNA = 2-mercaptonicotinic acid) via multiple electrostatic interactions with polyethyleneimine (PEI).[274] Later, Yin et al. modified the polyamine-based assembly by introducing a salt of polyvalent anions.[275] Here, the polymer-salt aggregates helped to entrap charged NCs to produce Au NC containing microcapsules. The multilayered and semipermeable matrix of microcapsules was further stabilized with SiO_2 NPs. The assembled composite has shown PL enhancement about five times greater than parent NCs. Hembury et al. synthesized Au NCs protected with thermosensitive diblock copolymers of poly(*N*-isopropylacrylamide) (PNIPAm) and poly(ethylene glycol) (PEG) to demonstrate micellar assembly of NCs.[276] The polymers were prepared using reversible addition-fragmentation chain-transfer (RAFT) polymerization approach, followed by functional group conversion to produce the thiol-terminated PEG-PNIPAm-SH polymers. The in situ preparation of thiolated-polymer-capped NCs was carried out using the chemical reduction method. Interestingly, when the temperature was above lower critical solution temperature (LCST) of the polymers, [Au@S-PNIPAm-PEG] NCs formed the hydrophobic cores of micellar assemblies. Further, Yang et al. demonstrated the self-assembly of Au NCs inside the poly(amidoamine) dendrimer (PAMAM) by mixing the presynthesized [Au@SG] NCs with aqueous PAMAM.[277] The electrostatic interaction between negatively charged carboxylic groups in [Au@SG] NCs and positively charged amine groups in PAMAM resulted in self-assembled structures with enhanced PL. More recently, Benavides et al. successfully self-assembled Cu NCs inside the multithiolated thermo- and pH-responsive copolymer, p(MEO_2MA-*co*-AcSEMA) [(poly-2-(2-methoxyethoxy) ethyl methacrylate and poly-2-(acetylthio) ethyl methacrylate)].[278] The one-pot reduction of copper sulfate ($CuSO_4\cdot 5H_2O$) using hydrazine in the presence of

p(MEO_2MA-*co*-AcSEMA) resulted in the formation of greenish-yellow emitting assembled [Cu@S-p(MEO_2MA-*co*-AcSEMA) NCs inside the polymer matrix with better photostability and oxidation resistance. The biopolymers (peptides, proteins, lipids, etc.) have been used to demonstrate the self-organization of NCs. For example, Ju et al. demonstrated the pH-dependent assembly and disassembly of [Au@SG] NCs via electrostatic interactions with *Streptococcus pyogenes* bacterial protein (SpCas9).[279] The controlled addition of positively charged SpCas9 to the negatively charged [Au@SG] NC in phosphate buffer resulted in a self-assembled NC-protein composite ([Au@SG]-SpCas9). Such biopolymer mediated NC-assembly was further used for cancer cell imaging, protein delivery, and phototherapy (detailed discussion provided in Section 4).[279–282] The assembly of NCs demonstrated via the polymer templates discussed above are often unsuccessful due to the uncontrolled aggregation.

2.2.2. DNA-Templated Assembly

A combination of DNA and metallic NPs were successfully self-assembled to form a wide variety of hybrid materials.[283,284] Replacing metallic NPs with precision NCs could bring more exciting monodisperse assemblies. The quantum confinement and PL properties of NCs would be added advantages for such template-based assemblies. Recently, Ouyang et al. demonstrated DNA-nanoribbon-templated self-assembly of Cu NCs.[285] The DNA-nanoribbon templates (C-DNR) composed of multiple units of single-strand DNA were prepared by a simple and effective thermal annealing method.[286] Based on the position of DNA sequences, six types of C-DNR assemblies were prepared. Subsequently, NCs were prepared in situ on the C-DNRs, by mixing $CuSO_4$ with C-DNR solution in a mixture of MOPS (3-(*N*-morpholino)propane sulfonic acid) buffer and NaCl. Chemical reduction of metal ions with sodium ascorbate followed by keeping the solution at room temperature for 30 min resulted in the periodic self-assembly of NCs on C-DNR (**Figure 10**). The incubation period of the metal salt and C-DNR is crucial for the formation of NCs. The control experiments with single-stranded DNA could not produce NCs, which confirm that NCs were formed only in the presence of C-DNRs. The self-assembled NCs protected with C-DNRs have shown better photostability and temperature-dependent PL compared to the luminescent Cu NPs stabilized on the double-stranded DNA reported earlier.[287,288] Later, Wang et al. fabricated the self-assembled Au NCs–DNA (GNC–DNA) complexes in situ by introducing the Au precursor and double-stranded DNA

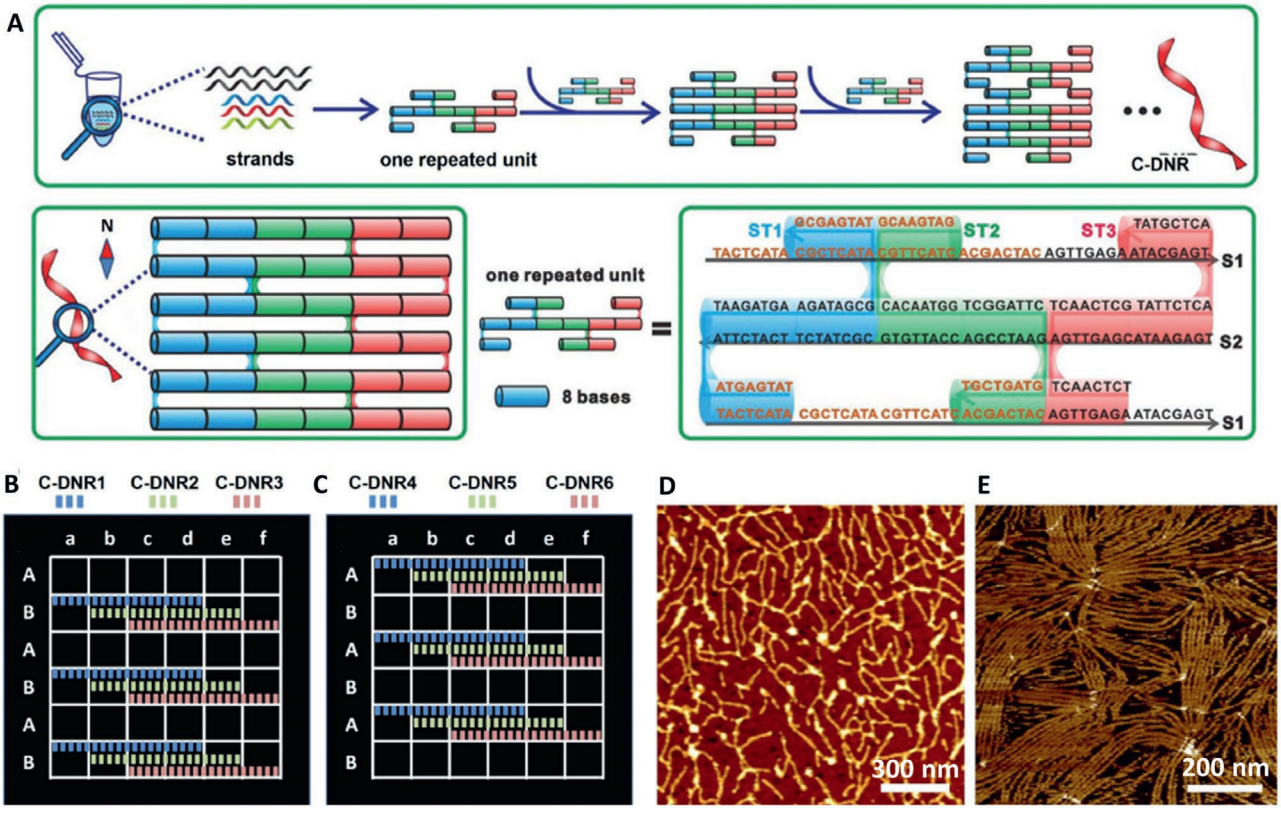

Figure 10. A) Top: Formation scheme of C-DNRs. Bottom: Schematic diagram of C-DNR, the double helix structure is represented by a cylinder, and each small cylinder contains eight complementary base pairs. A repeating unit consists of five short chains of scaffold strand 1 (S1), scaffold strand 2 (S2), staple strand 1 (ST1), staple strand 2 (ST2), and staple strand 3 (ST3). Schematic diagram of B) C-DNR1, C-DNR2, and C-DNR3, and C) C-DNR4, C-DNR5, and C-DNR6 are shown. Sequence A is indicated by a square bar; each square lattice represents eight base pairs, row A represents the DNA helix containing S2 strand, row B represents the DNA helix containing S1 strand. AFM images of C-DNR1 under D) tapping mode in air and E) in liquid. Reproduced with permission.[285] Copyright 2020, Wiley-VCH.

solution into the cancer cells.[289] To confirm the self-assembly inside the cell, GNC–DNA complexes were isolated and analyzed with different microscopic techniques. Assembled NCs were used for cancer diagnosis and theranostics, details of which are provided in Section 4.

2.2.3. Macrocycle-Templated Assembly

The molecular recognition between the host and guest molecules through the noncovalent bonding resulted in the evolution of supramolecular assemblies.[290] A proper combination of host–guest interactions could also produce assembled NCs with improved photophysical properties. For example, the noncovalent interactions between the macrocyclic host and ligand protected NCs (guest) created a rigid-NC framework with enhanced optical features and stability.[8] Though, some of those assemblies were restricted to host single NCs.[291–294] Later, the long-range NC assembly has been achieved by the careful selection of the host and guest molecules. For example, Jiang et al. demonstrated the self-assembly of Au_{22} NCs by utilizing the noncovalent ligand interaction of NCs with cucurbituril host cavities.[295] $[Au_{22}(FGGC)_{18}]$ NCs were initially synthesized by the pH adjusted reduction of $HAuCl_4$ in the presence of N-terminal Phe-Gly-Gly-Cys peptide (FGGC). NCs purified by the preparative thin-layer chromatography (PTLC) techniques were allowed to interact with cucurbiturils 7 and 8 (CB[7] and CB[8]), separately. Though CB[7] accommodates only one peptide moiety, the large cavity of CB[8] could accommodate two peptides from two adjacent NCs. Such interactions resulted in the formation of self-assembled spheres with an improved PL quantum yield (CB[8]-39%). Further, Chakraborty et al. demonstrated the supramolecular host–guest interaction-based coassembly of $[Ag_{29}(BDT)_{12}(TPP)_4]^{3-}$ NCs with crown ether (dibenzo-18-crown-6; DB18C6).[296] Vapor-diffusion of methanol into the DMF solution of NCs and DB18C6 resulted in the formation of DB18C6 coassembled NC crystals. The electrostatic interaction between the cationic $DB18C6Na^+$ units and anionic $[Ag_{29}(BDT)_{12}(TPP)_4]^{3-}$ NCs helped to trigger the assembly. The source of Na^+ in the crystallization medium could be the previously used $NaBH_4$ during NC synthesis. Further intra- and intermolecular C—H$\cdots\pi$ interactions between the crown ether and TPP/BDT resulted in long-range assembled NC crystals composed of hexameric $DB18C6Na^+$ units (**Figure 11**). The assembled $[Ag_{29}(BDT)_{12}(TPP)_4][(DB18C6Na)_3]$ crystals showed enhanced PL (3.5-fold) compared to the parent NCs. The authors also demonstrated the interaction of 25 atom Au and Ag NCs with fullerene (C_{60} and C_{70}).[297] The ion–dipole interactions between fullerene and NC resulted in the formation of higher-order self-assembly. Further, Muhammed et al. demonstrated the host–guest interaction-based self-assembly in Ag_{29} NCs stabilized with dithiol lipoic acid terminated copillar[5]arene (LA-P5).[298] To address such interactions, $[Ag_{29}(LA\text{-}P5)_{12}(TPP)_2]$ NCs were initially synthesized by the chemical reduction of $AgNO_3$ in the presence of TPP and LA-P5. In this particular case, host molecules are chemically bound on the NC surface via Au—S bond. Addition of cationic quaternary ammonium salts (guest molecules) into above NCs resulted in the formation of assembled spheres owing to cation–π interactions. Such assembled structures showed ≈2000-fold enhancement in their PL due to AIE. More interestingly, injection of methanol (polar solvents) into the assembled NCs could demolish them into well-separated individual NCs. Recently, Huang et al. demonstrated the self-assembly of cyclodextrin functionalized Cu NCs via host–guest interactions with di(adamantan-1-yl)phosphine molecule (AD-AD).[299] To address such assembly, water-soluble NCs were initially synthesized by reducing the copper nitrate in the presence of mono-(6-mercapto-6-deoxy)-β-cyclodextrin

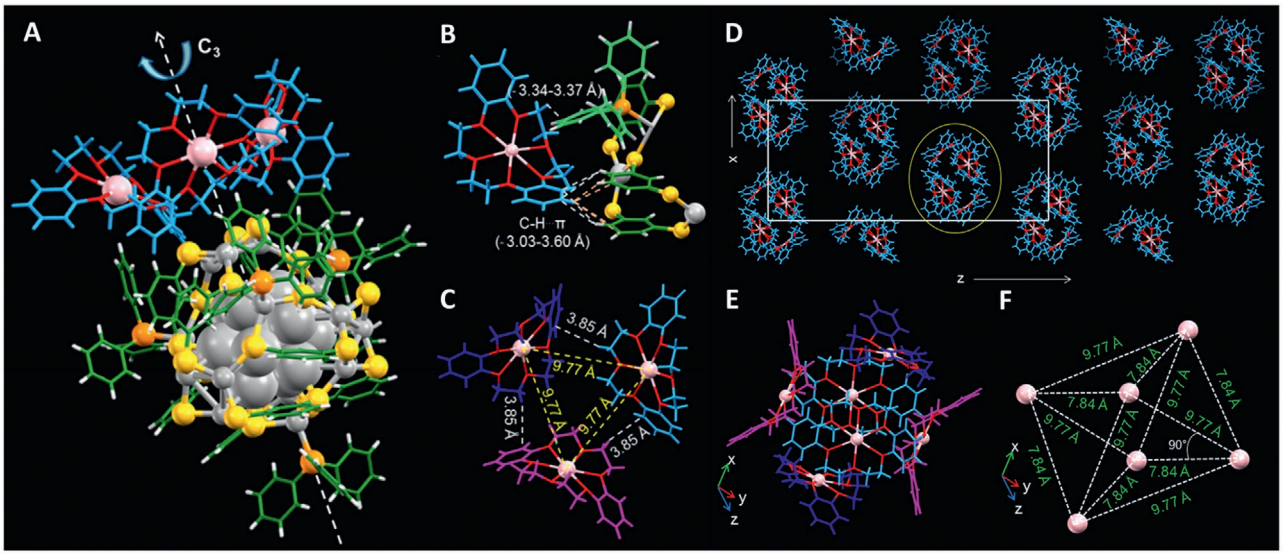

Figure 11. A) Structure of $[Ag_{29}(BDT)_{12}(TPP)_4][(DB18C6Na)_3]$. B) Expanded view showing the interaction between one of the $DB18C6Na^+$ molecules and BDT/TPP ligands of the NC, and C) expanded view of the three $DB18C6Na^+$ molecules attached on the NC surface. D) Packing of $DB18C6Na^+$ molecules into hexameric units throughout the crystal lattice view from the *y*-axis. E) Expanded view of one of the hexameric units showing the formation of cage-like structures. Opposite crown ethers, shown in similar colors, are related by a center of inversion. F) The orientation of Na^+ of the crown ether hexamer in a rectangular bipyramidal geometry. Reproduced with permission.[296] Copyright 2019, American Chemical Society.

(SH-β-CD) as both reducing and stabilizing agents. The addition of AD-AD into the β-CD-tethered NCs showed enhanced PL due to AIE resulting from the supramolecular assembly triggered by host–guest interactions. The membrane-associated glycoprotein (Mucin 1 protein; MuC1) has been successfully imaged using the enhanced PL from ad-aptamer conjugated NC assembly.

2.3. Externally Directed Assembly of NCs

The externally directed assembly of NCs can be performed by either adding external reagents such as metal ions and bridging ligands or other physical stimuli such as light and temperature. In this section, light-triggered, coordination-assisted, and temperature-controlled assemblies will be discussed with selected examples.

2.3.1. Light-Triggered Assembly

Long-range reversible assembly of nanomaterials using light as an external stimulus can be achieved using well-tailored ligands that undergo reversible photoisomerization.[190,300] Azobenzene[185,190,301–303] and spiropyran[304–308] molecules are extensively studied photoswitchable systems to initiate the self-assembly of plasmonic NPs,[185,190,304,309] magnetic NPs,[302,303,308,309] silica NPs,[301,307] and polymer NPs.[306] These molecules can change their conformation when irradiated with a particular wavelength of light. Importantly, photoisomerization can also results in altered solubility in a given solvent promoting light triggered reversible assembly–disassembly. For example, in azobenzene, the *trans* isomer usually has a dipole moment close to zero compared to its *cis* isomer (≈3.0 D). When such molecular-dipoles arrange on the NC surface, the increment in their dipole moment results in a dipole–dipole attraction, promoting the self-assembly of nanosystems. Klajn et al. demonstrated the light-stimulated self-assembly in plasmonic Au NPs.[190,310] Udayabhaskararao et al. extended the concept of switchable self-assembly into NCs.[311] To address the light-induced self-assembly in NCs, they have synthesized PET-tethered Au_{25} NCs ($[Au_{25}(PET)_{18}]^-$), followed by stapling thiolated spiropyran (SP) molecules by a ligand exchange reaction at low temperature. The spiropyran tethered-Au_{25} ($[Au_{25}(PET)_{18-x}(SP)_x]^-$) NCs showed light-induced assembly under UV light (345 nm) due to the dipolar interactions created by the ring-opening isomerization. The self-assembly was proved by the visible changes in the optical contrast of NCs and the subsequent dynamic light scattering (DLS) measurements. Though thiolated azobenzene-tethered Au_{25} NCs ($[Au_{25}(C_4\text{-}AMT)_{18}]^-$; AMT = azobenzene monothiol) are known,[312] their light-mediated self-assembly was not systematically investigated. Recently, Rival et al. investigated the photon-assisted switchable self-assembly in $[Au_{25}(C_3\text{-}AMT)_{18}]^-$ NCs using two different wavelengths of light.[313] The modified Brust–Schiffrin method[96] was used to synthesize the kinetically controlled Au_{25} NCs using C_3-AMT as the protecting ligand. Photoisomerization of $[Au_{25}(C_3\text{-}AMT)_{18}]^-$ NCs under visible (435 nm) and ultraviolet (345 nm) lights has shown systematic changes in the optical absorption bands and chemical shifts in NMR spectra. The attractive dipole–dipole interactions between nearby NCs in the *cis* arrangement helped to organize NCs into superstructures. Light-mediated temporal evolution of NCs into disc-like superstructures and their disassembly were studied using atomic force microscopy (AFM), DLS, TEM, and subsequent ET reconstruction (**Figure 12**). Remarkably, such assembly was not observed during the photoactivation of $[Au_{25}(PET)_{18}]^-$ NCs. The controlled assembly and disassembly of $[Au_{25}(C_3\text{-}AMT)_{18}]^-$ NCs under UV and visible light show the significance of AMT in the light-triggered self-assembly.

In a similar way, Ai et al. demonstrated the light-induced self-assembly in thiolated azobenzene-protected Cu NCs.[314] $[Cu_{13}(C_nAMT)_{10}Ac_2]$ NCs (n = 4, 6, and 8) were synthesized using a method similar to $[Cu_{12}(DT)_8Ac_4]$ NC preparation.[233] NCs were initially shown to form self-assembled nanoribbons at high temperatures due to their dipole-induced asymmetric van der Waals attraction between the DT ligands. Interestingly, such nanoribbons were reinforced into spherical superstructures under UV illumination (365 nm) due to photoisomerization-induced dipole–dipole attractions. However, the process was irreversible due to the difficulty of improving the inter-NCs van der Waals attraction.

2.3.2. Coordination-Assisted Assembly

Coordination of NCs with suitable metal ions and subsequent formation of metal–organic frameworks (MOFs) is another exciting possibility to self-assemble NCs. Metal coordination-assisted assembly could be achieved either by incorporating NCs into the presynthesized MOFs or by the in situ formation of MOF while coordinating the metal ions with organic moieties on the NC surface. For example, Luo et al. incorporated water-soluble $[Au_{25}(SG)_{18}]$ NCs into zeolitic imidazolate framework-8 (ZIF-8) prepared by the room temperature mixing of 2-methylimidazole (MeIm) and Zn^{2+} ions.[315] In this case, the coordination-assisted self-assembly is accomplished by impregnating NCs in aqueous ZIF-8 ($[Au_{25}(SG)_{18}]$/ZIF-8). On the other hand, the addition of $[Au_{25}(SG)_{18}]$ before the formation of ZIF-8 resulted in NC-encapsulated ZIF-8 ($[Au_{25}(SG)_{18}]$@ZIF-8) (**Figure 13**). NCs in the encapsulated framework were arranged by the coordination of metal ions with the carboxylate group of SG and nitrogen atom of 2-MeIm linkers. Though impregnated NCs were arranged outside the framework owing to the larger size of NCs compared to ZIF-8, the efficient zinc-carboxylate linkage helped to hold NCs and ZIF-8 together at the interface. An increment in the size of the nanocomposites and the presence of bright spots in STEM confirm the outside-decorated impregnated- and inside-incorporated encapsulated-NC assembly. Enhanced catalytic efficiency and PL were observed from the impregnated NCs and encapsulated NCs, respectively. Further, Zhu et al. employed the coordination-assisted self-assembly approach in combination with electrostatic interactions to sandwich the captopril tethered water-soluble Au_{25} NCs between an inner core and an outer shell made of zirconium-based MOF (UiO-66).[316] The nanocomposite was fabricated by a two-step method, in which the initial mixing of UiO-66 and Au_{25} NCs helps to form the inner core by a wet

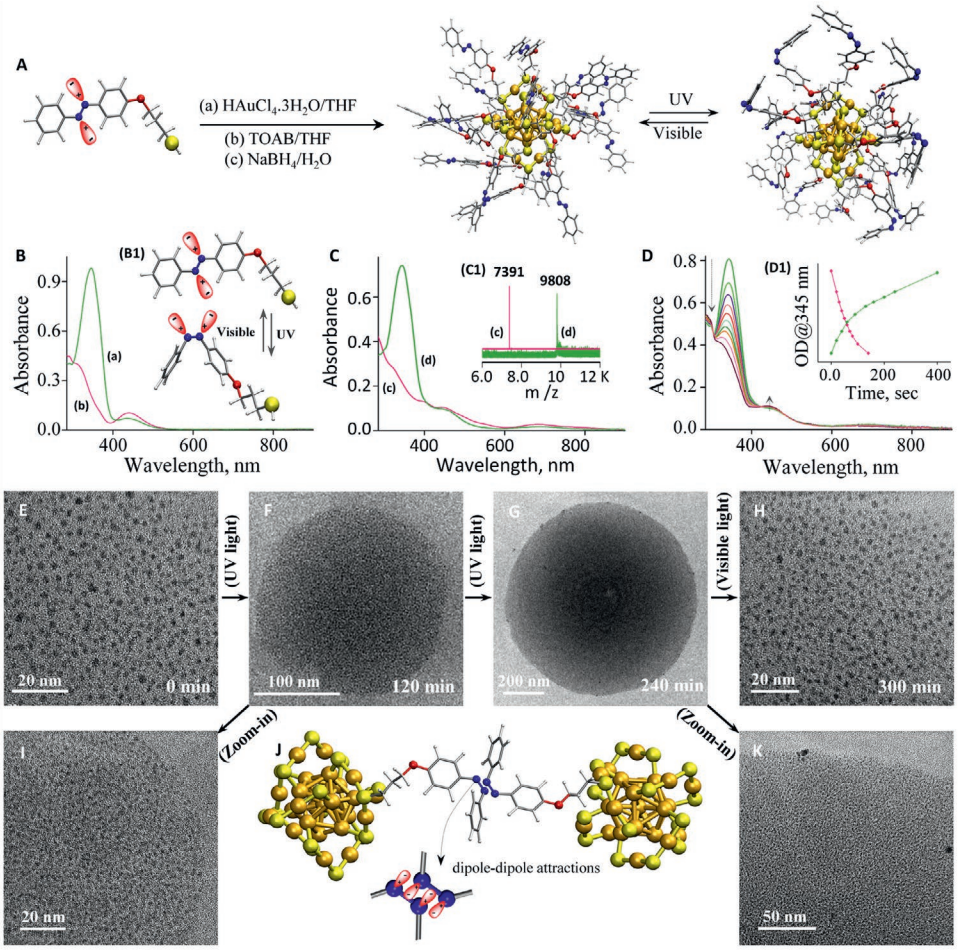

Figure 12. A) Schematic representation showing the synthesis, energy-minimized structures, and photoisomerization of $[Au_{25}(C_3\text{-AMT})_{18}]^-$ NCs. B) Absorption spectra of C_3-AMT under a) visible light and b) UV light. Energy-minimized structures of the two geometrical isomers of C_3-AMT are shown in the inset (B1). C) Absorption spectra of d) $[Au_{25}(C_3\text{-AMT})_{18}]^-$ and c) $[Au_{25}(PET)_{18}]^-$ NCs. ESI-MS of both NCs are shown in the inset (C1). D) Temporal absorption spectra of $[Au_{25}(C_3\text{-AMT})_{18}]^-$ at 345 nm illumination. A plot of OD (≈345 nm) versus illumination time under ultraviolet and visible light is shown in the inset (D1). TEM images of E) *trans* $[Au_{25}(C_3\text{-AMT})_{18}]^-$ NCs and F,G) *cis* $[Au_{25}(C_3\text{-AMT})_{18}]^-$ NC assembly captured during F) 120 min and G) 240 min of light illumination (345 nm). The TEM image of $[Au_{25}(C_3\text{-AMT})_{18}]^-$ NC self-assembled superstructures after 435 nm illumination is shown in (H), exhibiting their disassembly. Zoom-in and focused HR-TEM images taken from the edges are shown in (I) and (K), respectively. Schematic representation of dipole-induced self-assembly in $[Au_{25}(C_3\text{-AMT})_{18}]^-$ NCs is shown in (J). Reproduced with permission.[313] Copyright 2020, American Chemical Society.

impregnation protocol. Subsequently, the additional metal precursors and ligands were coassembled to form the outer core. The coordination-assisted self-assembly, together with the electrostatic interactions between the carboxylate anion of captopril and metal nodes of MOFs, helped to sandwich Au_{25} NCs between the inner and outer core of UiO-66. The sandwiched [UiO-66@Au_{25}@UiO-66] has shown excellent stability with enhanced catalytic efficiency. Details are provided in Section 4.

The electrostatic interaction between negatively charged NCs and polyvalent cations under ambient conditions could produce NC-based coordination complexes. Yao et al. first introduced such a strategy, in which the [Au@SG] NCs were coordinated with Zn^{2+} or Cd^{2+} using the pH adjusted protocol.[317] The early screening effect between Zn^{2+} and carboxylate anions reduced the negative charge around the NC surface, triggering the intra-NC assembly. The subsequent bridging effect between nearby NCs resulted in stable inter-NC spherical assemblies via NC crosslinking. Such solid-spherical assemblies displayed an enhanced PL quantum yield compared to pristine NCs due to reduced nonradiative relaxation and the improved charge-transfer interaction.[318] Recently, Chandra et al. reported the fabrication of highly luminescent Au NC frameworks (GNCFs) by coordinating divalent cations with carboxylate anions present on the NC surface.[319] [Au@SG] NCs were prepared by heating the presynthesized Au-thiolates at 70 °C for 24 h. Surprisingly, the addition of Sn^{2+} ions into the above prepared NCs has shown a seven-fold enhancement in their PL due to the coordination-assisted assembly. Interaction of negatively charged carboxylate group of SG with divalent Sn^{2+} cations resulted in the formation of GNCFs via inter-NC crosslinking, which was confirmed by observing 3D spherical colloidal structures in STEM and ET (**Figure 14**). A similar strategy was used to demonstrate the assembled frameworks from various NCs.[320–328] Among them, a few found interesting applications.

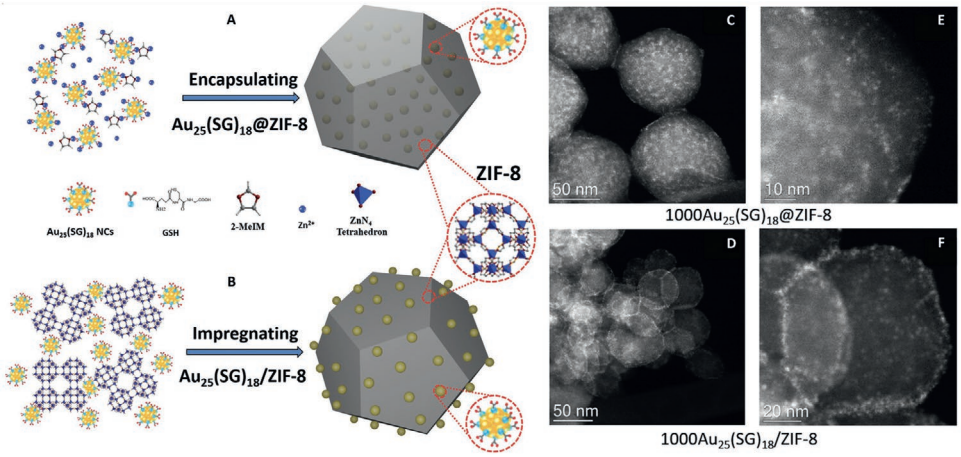

Figure 13. Schematic illustration of the synthesis processes for A) encapsulated $[Au_{25}(SG)_{18}]$@ZIF-8 and B) impregnated $[Au_{25}(SG)_{18}]$/ZIF-8. C–F) STEM images of C,E) $[Au_{25}(SG)_{18}]$@ZIF-8, and D,F) $[Au_{25}(SG)_{18}]$/ZIF-8. Reproduced with permission.[315] Copyright 2018, Wiley-VCH.

For example, the assembled superstructures fabricated from $[Au_{14}(MPA)_7(His)_5]$[320] and $[Au_{14}(MPA)_{10}(Phe)_4]^{3+}$[321] (MPA = mercaptopropionic acid; His = L-histidine; Phe = L-phenyl alanine) NCs have been successfully used to demonstrate the gas storage (details are provided in Section 4).

NC-based MOFs were also achieved by using the bridging ligands instead of metal coordination. The ability to control the length and the denticity of linkers could help to tune the assemblies. For example, Huang et al. demonstrated the formation of 3D Ag(I) chalcogenide NC-based MOFs using the bipyridine bridges.[329] Ligand exchange reaction of $[Ag_{12}(S^tBu)_6(CF_3COO)_6(CH_3CN)_6]\cdot CH_3CN$ NCs (S^tBu = *tert*-butylthiol; CF_3COOH = trifluoroacetic acid) using 4,4′-bipyridine (bpy) resulted in the replacement of CH_3CN with linearly coordinated bipyridine (**Figure 15**). Subsequent coordination of bipyridine linker with adjacent Ag_{12} nodes produced light-emitting porous $[Ag_{12}(S^tBu)_8(CF_3COO)_4(bpy)_4]_n$ (Ag_{12}bpy)-MOF. Surprisingly, the single-emissive tetragonal (Ag_{12}bpy) NCs were transformed into a dual-emissive trigonal (Ag_{12}bpy-2) crystals ($[Ag_{12}(S^tBu)_6(CF_3COO)_6(bpy)_3]_n$) when the crystallization medium changed.[330] The temperature-dependent dual emission occurred due to the Ag core compression originated from the argentophilic interaction. Bridging chemistry has been further extended to demonstrate self-assembly of Ag_{10},[331,332] Ag_{12},[333–335] $Ag_{12}Ag_8$,[336] $Ag_{14}Cl$ and $Ag_{15}Cl$,[337] Ag_{14},[338] and Cd_6Ag_4,[339] NCs using diverse organic bridges. Later, Chen et al. demonstrated 3D superatom inorganic porous framework assembly from $[Au_1Ag_{22}(S\text{-}ADM)_{12}]^{3+}$ NCs (S-ADM = 1-adamantanethiol) using hexafluoroantimonate (SbF_6^-) linker instead of the conventional organic bridges described above.[340] Here, SbF_6^- can act as a counter ion, protecting ligand, and a bridging ligand. $[Au_1Ag_{22}(S\text{-}ADM)_{12}]^{3+}$ NC consists of Au_1Ag_{12} bimetallic core and a chiral shell composed of $Ag_{10}(S\text{-}ADM)_{12}$. The chiral shell has two types of Ag atoms ($Ag_{\mu 2}$ and $Ag_{\mu 3}$), in which $Ag_{\mu 2}$ and $Ag_{\mu 3}$

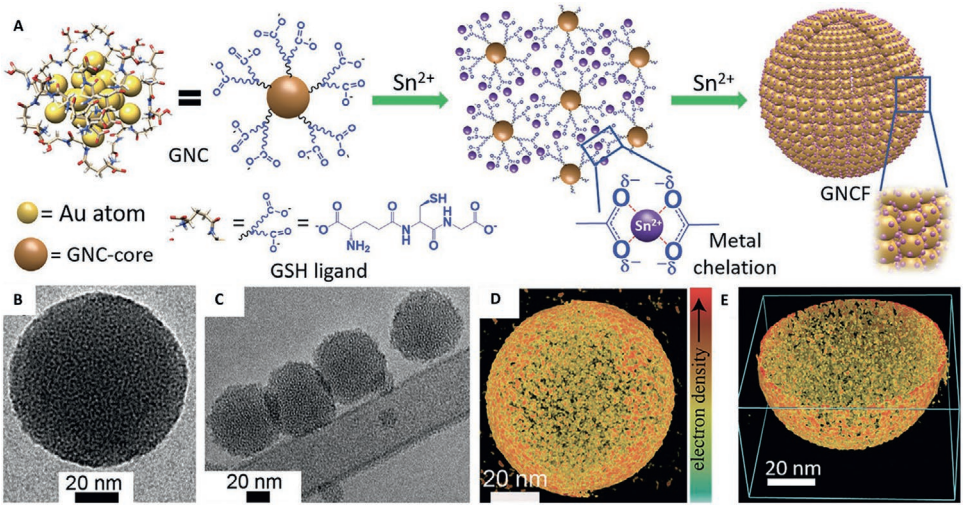

Figure 14. A) Representation of a luminescent [Au@SG] NC, the possible interactions between the metal ions and COO^- groups of the ligand over NCs through chelation, and the schematic illustration for the formation of GNCFs. B) HR-TEM micrograph of GNCF-100 dispersed in water, C) cryo-TEM micrograph of GNCF-100, D) ET reconstruction of a GNCF-100, and E) its cross-sectional view. Reproduced with permission.[319] Copyright 2019, Wiley-VCH.

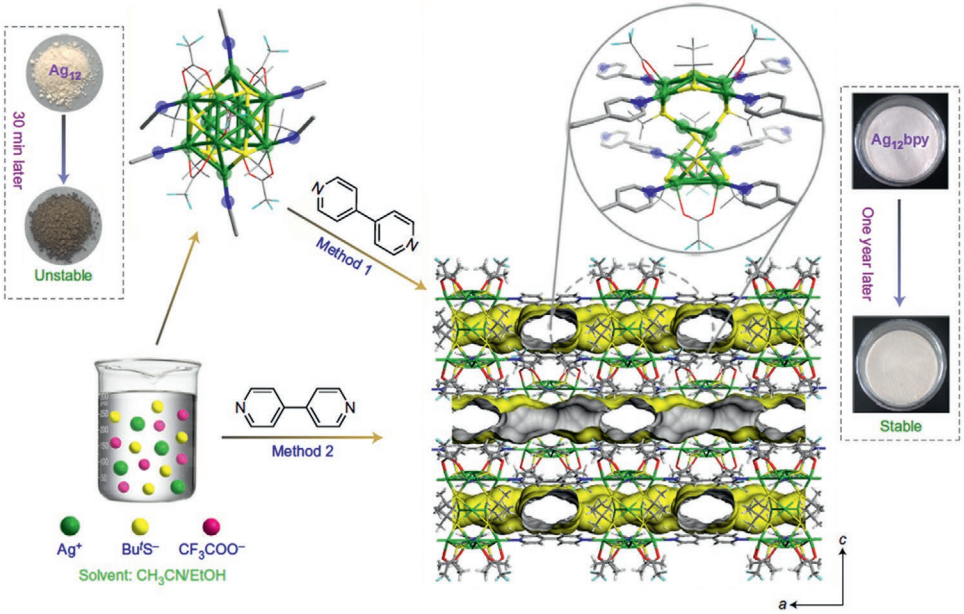

Figure 15. Schematic representation of the ligand-exchange strategy used to obtain Ag_{12}bpy crystals (Method 1, giving low yield) and one-pot synthesis (Method 2, for gram quantity production) under identical conditions. Interconnected channels of Ag_{12}bpy are viewed along with the *a* and *b* axes, where the yellow surface represents the pore surface. Insets: Photographs showing the changes of Ag_{12} and Ag_{12}bpy crystals under ambient conditions. Reproduced with permission.[329] Copyright 2017, Springer Nature.

were connected to two and three thiolate groups, respectively. Based on the number of counter anions, two assembled porous superstructures were produced with different types of structural units. The first unit shows a tetrahedral structure consists of four SbF_6^- ions, which were linked to four $Ag_{\mu3}$ atoms of $[Au_1Ag_{22}(S\text{-}ADM)_{12}]^{3+}$ NC through an $Ag_{\mu3}$—F bond. Such an assembled structure consists of both clockwise and anticlockwise optical isomers. At the same time, the excess addition of SbF_6^- ions forms the second structural unit, where six SbF_6^- ions were linked to NC via six Ag—F bonds (three $Ag_{\mu2}$—F and three $Ag_{\mu3}$—F bonds). This assembly has only either the clockwise or anticlockwise isomers. Therefore, they showed CPL.

2.3.3. Temperature-Controlled Assembly

The temperature has a vital role in NCs self-assembly, especially those protected with long-alkyl chain ligands. In general, the careful elevation of temperature helps to facilitate or hinder some intermolecular interactions. To establish the self-assembly in long-chain hydrophobic ligands protected NCs, sufficient thermal energy is required to cross their thermodynamic barrier. The annealing of NCs at high temperatures could help to increase the mobility of the alkyl chains. Subsequent interligand interactions, especially the van der Waals interactions, drive the long-range self-assembly. Details are provided in Section 2.1.3.[232–236]

2.4. Miscellaneous Examples

2.4.1. Covalently Linked NCs

Synthetic chemistry approaches also allow selective functionalization and formation of covalently linked NC dimers and trimers. For example, Lahtinen et al. demonstrated the formation of covalently bound multimers from $[Au_{102}(p\text{-}MBA)_{44}]$ and $[Au_{\approx250}(p\text{-}MBA)_n]$ NCs when the biphenyl-4,4′-dithiol (BPDT) was incorporated via the ligand exchange reaction.[341] The TEM micrographs obtained from different bands, separated using gel electrophoresis showed monomers, dimers, and trimers. Musnier et al. studied the influence of anisotropic surface charge distributions on the absorption and self-assembly of $[Au_{25}(MHA)_{18}]$ NCs by incorporating dithiol (bidentate hexa(ethelene glycol) dithiol; HDT) on their surface.[342] Interestingly, NCs bound with the maximum number of HDT were found to form a dendritic network structure via the self-assembly driven by oligomerization. During such assembly, optical absorption features of NCs were enhanced and red-shifted. However, a noticeable enhancement in their PL resulted from the assembly was not observed. A similar strategy has been used to assemble diverse NCs including $[Au_{25}(SBu)_{18}]^-$, $[Au_{25}(PET)_{18}]^-$, $[Au_{250}(p\text{-}MBA)_n]$, and $[Ag_{25}(2,4\text{-}DMBT)_{18}]$ NCs.[343–345] Though covalent modification offers routes for NCs oligomers, a long-range colloidal assembly using this approach has not been demonstrated.

2.4.2. Atom Transfer Reaction

One of the important properties of NCs is their chemical reactivity and sensitivity for the removal or addition of atoms (i.e., atom exchange). It has been shown that inter-NC reactions between two different types of NCs using atom exchange reactions can lead to selective doping, alloy NCs or offer routes for new NC compositions.[346] The inter-NC reactions have been reported for $[Au_{25}(PET)_{18}]^-$ NC with various NCs such as $[Ag_{44}(FTP)_{30}]$ (FTP = 4-fluorothiophenol), $[Ag_{25}(2,4\text{-}DMBT)_{18}]$, $[Ag_{51}(BDT)_{19}(TPP)_3]$, $[Ag_{29}(BDT)_{12}(TPP)_4]^{3-}$, and

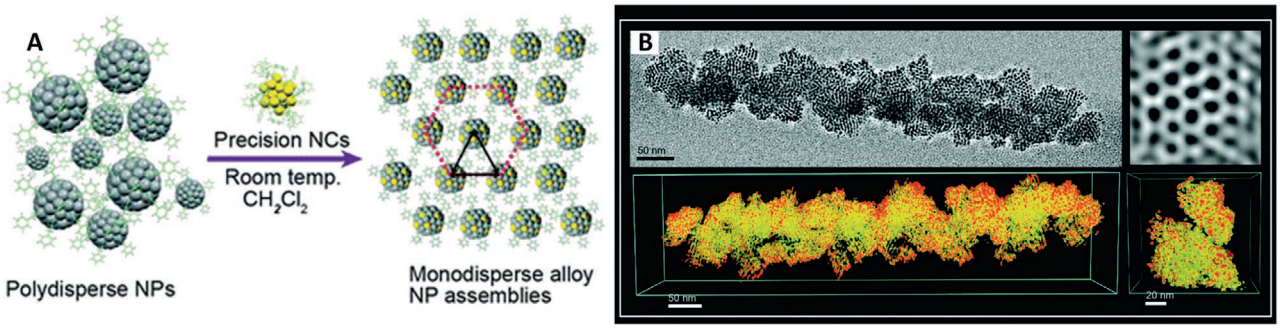

Figure 16. A) Schematic representation of atom transfer reaction between polydisperse Ag@PET NPs and $[Au_{25}(PET)_{18}]^-$ NCs. B) TEM micrograph, corresponding ET 3D reconstruction, and inverse fast Fourier transform image of Ag@PET NPs superlattice assembly (hcp) formed by atom transfer reaction. Reproduced with permission.[352] Copyright 2020, The Royal Society of Chemistry.

$[Ir_9(PET)_6]$.[347–351] Very recently, Bose et al. demonstrated an atom transfer reaction between Au NCs and polydispersed Ag NPs as a facile route for monodisperse alloy NPs and their self-assembled superstructures.[352] The authors used $[Au_{25}(PET)_{18}]^-$ NCs and polydispersed Ag@PET NPs. A systematic analysis using time-dependent electrospray ionization mass spectrometry (ESI-MS) suggested an atom transfer reaction between the Au NCs and Ag NPs, through transient $[Au_{25-x}Ag_x(PET)_n]$ alloy NC intermediates. More importantly, the reaction was specific to the nature of ligands. The alloy NP formation was supported using energy disperse X-ray spectroscopic (EDS) analysis and absorption spectroscopy by monitoring the change in surface plasmon resonance band. The resulting monodisperse alloy NPs spontaneously assembled into 2D layered assemblies and 3D spherical superstructures. ET reconstruction suggests layered structures with hexagonally close-packed (hcp) arrangement of NPs (**Figure 16**). This work suggests numerous possibilities to explore atom transfer reaction mediated colloidal-level reactions and assemblies using various NCs for functional materials.

3. Enhanced Optical and Mechanical Properties

NCs are emerging nanomaterials with exciting photophysical properties. Some of these NCs show excellent PL with relatively better photostability. PL quantum yield of NCs is lower compared to semiconductor quantum dots or organic dyes. However, one could improve the PL of NCs by ligand engineering,[353] encapsulation of NCs inside protein pockets,[354,355] self-assembly,[319] doping,[356–358] and AIE.[28,359–361] AIE has been further investigated in the self-assembled superstructures originated from different NCs, and their potential applications have been reviewed.[362] For example, Wu et al. have shown improved PL from the assembled $[Cu_{14}(DT)_{10}]$ NCs.[236] Though the isolated NC was nonemissive, the self-assembled nanoribbons have shown bright emission with an improved quantum yield of up to 6.5%. The restricted movements of DT ligands and improved cuprophilic interactions resulted in the formation of highly ordered assembly with maximum rigidity and compactness. Such compact structures helped to improve the radiative energy transfer channel via ligand-to-metal charge transfer (LMCT) and/or ligand-to-metal–metal charge transfer (LMMCT) process. To demonstrate the significance of compact assembly in AIE, NCs were loosely assembled into nanosheets by controlling a lower annealing temperature for a longer time. The PL quantum yield of nanosheets was lowered to 3.6% owing to the increased movement of DT ligands and reduced cuprophlilic interactions. More remarkably, the self-assembly strategy allowed to tune the regularity of NCs in the assemblies, which could produce polymorphic assemblies with different emission colors owing to the mechanochromic PL (**Figure 17**A–C). For example, the mechanical grinding of self-assembled nanoribbons fabricated from $[Cu_{14}(DT)_{10}]$ NCs has shown a reduced quantum yield (3.8%) with a bathochromic shift in their PL.[236] The color change is attributed to the decreased average $Cu^1\cdots Cu^1$ distance in the nanoribbon caused by the grinding treatment. The creation of metal defects in the assembled nanostructures can also enhance their PL. For example, Wu et al. showed that the addition of ethanol into $[Cu_{14}(DT)_{10}]$ NC solution accelerates the self-assembly by altering the coordination environment of metal with increased Cu^1 defects on the surface.[240] The assembled ultrathin nanosheet shows bright-yellow PL with an improved quantum yield of up to 15.4%. The metal defect-rich nanosheets possess an increased Cu^1 to Cu^0 ratio, which significantly facilitates the radiative relaxation of excitons by influencing the LMMCT process. More interestingly, the self-assembly could help to delay the PL of NCs. For example, the self-assembled nanofibers fabricated from $(NH_4)_9[Ag_9(o\text{-MBA})_9]$ NCs via hydrogen bonding method showed an enhanced AIE together with a transition from fluorescence to phosphorescence owing to their structural rearrangement within nanofibers.[223] AIE has been further extended to different assembled NCs, including $[Au_{25}(p\text{-MBA})_{18}]^-$,[262] [Au@SG-PAH],[273,318,319] $[Au_3\{(R \text{ or } S)\text{-Tol-BINAP}\}_3Cl]$,[246] and $(NH_4)_9[Ag_9(p\text{-MBA})_9]$,[224]. Details are provided in **Table 1**.

The periodic self-organization of NCs allows amplification of their optical and mechanical properties. For example, Musnier et al. reported the enhanced optical absorption from $[Au_{25}(MHA)_{18}]$ NCs while increasing the concentration of externally added HDT molecules during the formation of [Au@MHA-HDT] network.[342] The UV–vis absorption spectrum of $[Au_{25}(MHA)_{18}]$ shows a major hump ≈670 nm (highest occupied molecular orbital (HOMO)-lowest unoccupied molecular orbital (LUMO)) with two shoulder peaks ≈440 and

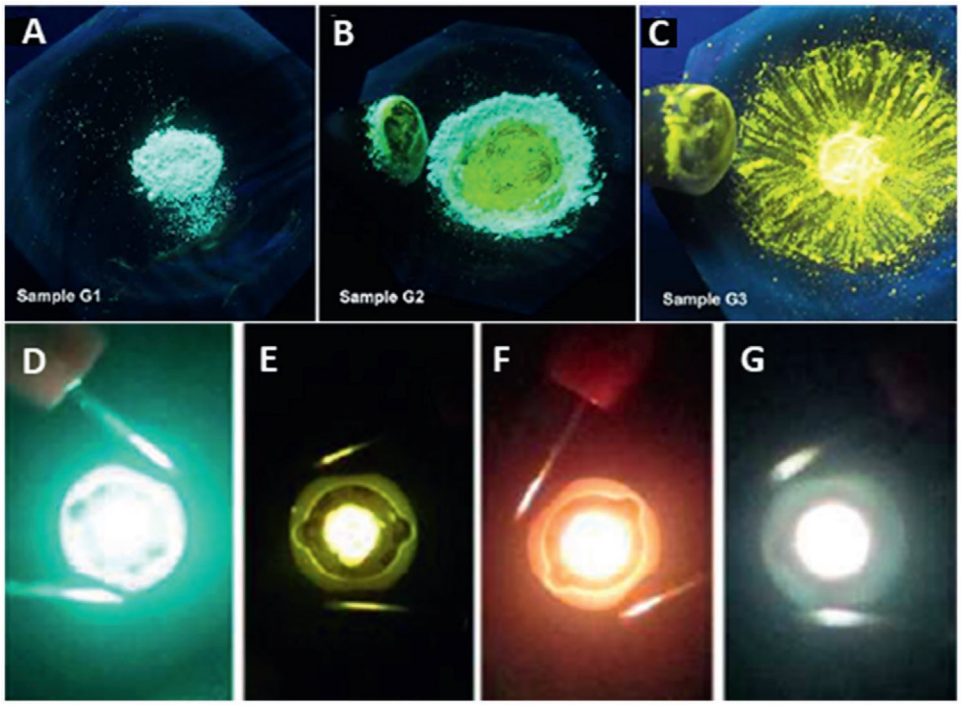

Figure 17. A–C) Photographs demonstrate the mechanochromic PL of assembled $[Cu_{14}(DT)_{10}]$ NCs. D–G) Photographs of LED fabricated from different NC-assemblies: D) $[Cu_{14}(DT)_{10}]$ nanoribbon, E) $[Cu_{14}(DT)_{10}]$ nanosheet, F) [Au@NC] sheet, and G) WLED fabricated by mixing $[Cu_{14}(DT)_{10}]$ ribbon, $[Cu_{14}(DT)_{10}]$ sheet, and [Au@NC] sheet. Reproduced with permission.[236] Copyright 2015, American Chemical Society.

770 nm. However, the replacement of MHA with HDT resulted in the disappearance and enhancement of the shoulder peaks ≈440 and 770 nm, respectively. The additional bands were formed ≈610 and 985 nm along with the red-shifted HOMO–LUMO band (690 nm). The enhanced optical features observed from the assembled NCs is attributed to the surface charge anisotropy created on NC during the ligand replacement. In another example, Shi et al. reported an enhanced CPL from the assembled chiral $[Au_3\{(R)\text{-Tol-BINAP}\}_3Cl]$ and $[Au_3\{(S)\text{-Tol-BINAP}\}_3Cl]$ NCs.[246] The self-assembled nanocubes showed enhanced circular dichroism (CD) with a significant CPL signal compared to pristine NCs. The restricted intramolecular rotation of inward *p*-tolyl rings could populate the excited state radiative decay pathway by quenching their nonradiative relaxation channels. As a result, PL and CPL are generated through the ^{3}LMCT or ^{3}LMMCT processes. Recently, Sugi et al. studied the enhanced mechanical properties of single-crystal solids self-assembled from dithiol-protected Ag_{29} polymorphs (Ag_{29} C and Ag_{29} T), monothiol-protected Ag_{46} (Ag_{46} T), and cocrystals of Ag_{40}/Ag_{46} ($Ag_{40/46}$ M).[245] Interestingly, the assembled solid fabricated from dithiol protected Ag_{29} showed higher Young's modulus (E_r) and hardness (H) compared to single-crystal solids from monothiol protected Ag_{46} having the trend Ag_{29} T > Ag_{29} C > $Ag_{40/46}$ M > Ag_{46} T. Higher E_r and H values for Ag_{29} T crystals is due to the inter-NC interactions, the presence of two pairs of H···H interactions, and a pair of C—H···π interactions between BDT ligands. While comparing Ag_{46} T and $Ag_{40/46}$ M systems, $Ag_{40/46}$ M holds supramolecular interactions between the primary DMBT ligands, similar to Ag_{29} T systems, which provide higher E_r and H values. These unusual mechanical properties of assembled solids are comparable to the mechanical properties of zeolitic imidazolate frameworks.

4. Applications of Assembled NCs

4.1. Device Fabrication

Self-assembled NCs have been used to construct multicolor light-emitting diodes (LEDs), in which NC assembly act as a color conversion layer. For example, Wu et al. successfully demonstrated the fabrication of LEDs from the assembled $[Cu_{14}(DT)_{10}]$ NCs using a 365 nm GaN LED chip as the light source.[236] The authors have also fabricated the white light-emitting diodes (WLEDs) by using a combination of $[Cu_{14}(DT)_{10}]$ ribbons, $[Cu_{14}(DT)_{10}]$ sheets, and [Au@NC] sheets (Figure 17D–G). Later, multicolored LEDs were fabricated from NC assembly. For this, different approaches were introduced to generate multicolored PL from the assembled NCs. For example, Ai et al. were able to tune the PL from the assembled Cu NCs by modulating the inter-NC distances in the assembly.[238] To regulate the inter-NC distances, the experimental variables such as solvents, ligands, duration of assembly, and temperature were adjusted. Aromatic thiols with different electron-donating functionalities were also used to synthesize Cu NCs to address the color-tunable emissive assemblies.[237] The successive doping of Au^1 into Cu NCs was helped to enhance the PL quantum yield up to 23.5%.[239] By changing the percentage of doping, one could control the PL intensity. Later, the electrophoretic deposition of a mixture of assembled nanosheets separately fabricated from Au and

Table 1. Synopses of all the methods used to demonstrate the self-assembly of NCs. The properties and applications of assembled NCs are mentioned.

Interactions	NCs	Applications and properties	Refs.
Hydrogen bonding interaction	$[Au_{102}(p\text{-MBA})_{44}]$ and $[Na_4Ag_{44}(p\text{-MBA})_{30}]$		[120,217–219,225,226]
	$[Au_{250}(p\text{-MBA})_n]$		[225]
	$[Au_{22}(SG)_{18}]$	Bioimaging	[221]
	$(NH_4)_9[Ag_9(o\text{-MBA})_9]$ and $(NH_4)_9[Ag_9(p\text{-MBA})_9]$	AIE and delayed PL	[223,224]
Electrostatic interaction	$[Na_4Ag_{44}(p\text{-MBA})_{30}]$ and $[Au_{102}(p\text{-MBA})_{44}]$		[218,219]
	[Au@SG]-Si NPs or C-dots	Sensing and intracellular temp. detection	[227,228]
	$[Ag_{26}Au(2\text{-EBT})_{18}(TPP)_6]^+[Ag_{24}Au(2\text{-EBT})_{18}]^-$ (DNIC)		[229]
	$[Cs_3Ag_{29}(BDT)_{12}(DMF)_x]^0$	Enhanced PL	[230]
van der Waals interaction	$[Au_{15}(DT)_{15}]$		[232,234]
	$[Cu_{12}(DT)_8Ac_4]$	Electrocatalysis	[233]
	$[Co_{14}(DT)_9]$ and $[Co_9S_8]$	Electrocatalysis	[235]
	$[Cu_{14}(DT)_{10}]$	LED fabrication, AIE, and mechanochromic PL	[236,240]
	$[Au_{246}(p\text{-MBT})_{80}]$		[242]
C—H···π/π···π interaction	$[Ag_{29}(BDT)_{12}(TPP)_4]^{3-}$	Enhanced PL	[124,244]
	$[Au_3\{(S \text{ or } R)\text{-Tol-BINAP}\}_3Cl]$	AIE and CPL	[246]
	$[Au_{103}S_2(S\text{-NAP})_{41}]$		[249]
	$[Au_{144}(PMT)_{60}]$		[121]
	$[Au_4Ag_{13}(DPPM)_3(2,5\text{-DMBT})_9]$	Enhanced PL	[251]
	$[Au_{52}Cu_{72}(p\text{-MBT})_{55}]^+Cl^-$		[253]
	$[Au_{11}(TPP)_7Cl_3]$ and $[Au_{11}(p\text{-Cl-TPP})_7Cl_3]$		[252]
	$[Au_{21}(S\text{-}C_6H_{11})_{12}(DPPM)_2]^+[Cl]^-$ and $[Au_{21}(S\text{-}C_6H_{11})_{12}(DPPM)_2]^+[AgCl_2]^-$	Electron transport	[254]
	$[Ag_{29}(BDT)_{12}(TPP)_4]^{3-}$, $[Ag_{46}(2,5\text{-DMBT})_{24}(TPP)_8]$, and $[Ag_{40/46}(2,4\text{-DMBT})_{24}(TPP)_8]$	Enhanced mechanical stability	[245]
	$[Ag_{30}(C_2B_{10}H_9S_3)_8(DPPM)_6]$	Chirality	[248]
Metallophilic interaction	$[Au_{25}(p\text{-MBA})_{18}]^-$	AIE	[262]
	$[Cu_{14}(DT)_{10}]$	LED fabrication	[236]
	$[Ag_9(o\text{-MBA})_9]$	LED fabrication	[264]
	$[Au_{25}(SBu)_{18}]^0$		[257]
	$[Au_{25}(S\text{-}C_nH_{2n+1})_{18}]^0$ (n = 3,4,5) and $[Au_{25}(PET)_{18}]^-$		[258]
	$[Au_{24}Hg(SBu)_{18}]^0$ and $[Au_{24}Cd(SBu)_{18}]^0$		[259]
	$[Au_4Pt_2(SR)_8]^0$		[260]
	$[(AuAg)_{34}]$		[261]
	[Cu@MMI]	Bioimaging and AIE	[364]
Amphiphilic interaction	$[Au_{25}(MHA)_{18}@x\text{CTA}]$	Enhanced stability	[270]
Polymer-templated	[Au@SG-PAH]	Bioimaging, drug delivery, and AIE	[273,275]
	[Au@S-PNIPAm-PEG]	Bioimaging	[276]
	[Au@SG]-PAMAM [Au_5@PAMAM]	Bioimaging, intracellular GSH sensing, and AIE	[277]
	[Cu@S-p(MEO_2MA-co-AcSEMA)]	Metal ion sensing	[278]
	$(NH_4)_6[Ag_6(MNA)_6$-PEI]	Metal ion sensing and AIE	[274]
	[PtNC/MA-F127]-pH-ADT	Cancer therapy	[280]
	[AuNC-PNF]	Temperature sensing and bioimaging	[281]
	$[Pt_1Ag_{28}(S\text{-ADM})_{18}(PPh_3)_4]^{2+}$-ACD	Delivery, bioimaging, phototherpay, and AIE	[282]
	[Au@SG-SpCas9]	Protein delivery	[279]
DNA-templated	[CuNC]	Bioimaging	[285]
	[AuNC]	Bioimaging and therapy	[289]
Macrocycle-templated	$[Au_{22}(FGGC)_{18}]$-CB[7] and $[Au_{22}(FGGC)_{18}]$-CB[8]	Enhanced PL and bioimaging	[295]

Table 1. Continued.

Interactions	NCs	Applications and properties	Refs.
	$[Ag_{29}(BDT)_{12}(TPP)_4][(DB18C6Na)_3]$	Enhanced PL	[296]
	$[Au_{25}(SR)_{18}]^-$ and $[Ag_{25}(SR)_{18}]^-$		[297]
	[Cu@S-βCD]-(AD-AD)	Bioimaging and AIE	[299]
	$[Ag_{29}(LA\text{-}P5)_{12}(TPP)_2]$	Enhanced PL	[298]
Light-induced	$[Au_{25}(PET)_{18-x}(SP)_x]^-$		[311]
	$[Au_{25}(C_3\text{-}AMT)_{18}]^-$		[313]
	$[Cu_{13}(C_nAMT)_{10}Ac_2]$ (n = 4, 6, and 8)	Electrocatalysis	[314]
Coordination-assisted	$[Au_{25}(SG)_{18}]$@ZIF-8 and $[Au_{25}(SG)_{18}]$/ZIF-8	Catalysis	[315]
	[UiO-66@Au_{25}@UiO-66]	Photocatalysis	[316]
	[Au@SG]	Bioimaging, AIE, and LED	[318,319]
	$[Au_{14}(MPA)_7(His)_5]$, $[Au_{14}(MPA)_{10}(Phe)_4]^{3+}$, and $[Au_{14}(MPA)_{10}(Cys)_4]$	Gas sensing	[320,321,327]
	[Au@MPA]	Metal ion sensing and AIE	[324]
	$[Au_{14}(MPA)_6(Trp)_4]$	Chiral sensing	[326]
	[Au@MPA]	Separation of geometrical isomers	[328]
	$[Au_{14}(MPA)_6(Tyr)_4]$	Cancer therapy	[323]
	[Au@SG]	Device fabrication, protein delivery, and cancer diagnosis	[318,322,325]
	$[(Ag_{12}(S^tBu)_8(CF_3COO)_4(bpy)_4)]_n$ and $[Ag_{12}(S^tBu)_8(CF_3COO)_4(bpy\text{-}NH_2)_4]_n$	Gas sensing	[329,363]
	$[Ag_{12}(S^tBu)_6(CF_3COO)_6(NH_2\text{-}bpz)_3$	Molecular sensing	[335]
	$\{[Ag_{27}S_2(S^tBu)_{14}(CF_3COO)_8(TPyP\text{-}H_2)](CF_3COO)\}_n$	Catalysis	[365]
	$[Ag_{12}(S^tBu)_6(CF_3COO)_3(TPyP)]_n$	Photocatalysis	[334]
	$[Au_1Ag_{22}(S\text{-}ADM)_{12}]^{3+}$	CPL	[340]
Temperature-controlled	$[Au_{15}(DT)_{15}]$		[232,234]
	$[Cu_{12}(DT)_8Ac_4]$	Electrocatalysis	[233]
	$[Co_{14}(DT)_9]$	Electrocatalysis	[235]
	$[Cu_{14}(DT)_{10}]$	LED fabrication, AIE, and mechanochromic PL	[236,240]
Miscellaneous examples			
i) Covalently linked NCs	$[Au_{25}(MHA)_{18}]$-HDT	Enhanced optical absorption	[342]
ii) Atom transfer reaction	$[Au_{25}(PET)_{18}]$-Ag@PET NPs		[352]

Cu NCs has been used to generate the white-light emission.[241] Huang et al. fabricated WLED from solid-state emitting Zn-coordinated NC assemblies ([Zn–Au@SG]).[318] The careful physical blending of green-emitting carbon nanodots and yellow-orange emitting NC assembly could generate multicolor nanophosphors. The combination of the above-prepared nanophosphors with blue emissive LEDs facilitated the preparation of WLED. Furthermore, the self-assembled $(NH_4)_9[Ag_9(p\text{-}MBA)_9]$ or $(NH_4)_9[Ag_9(o\text{-}MBA)_9]$ NCs were utilized to produce white-light emission by incorporating commercially available phosphors.[224,264] The above-discussed NC-assemblies have been successfully used to fabricate the color conversion layers in LEDs.

4.2. Molecular and Metal Ion Sensing

The assembled NCs have been efficiently used to fabricate molecular sensors. For example, Wang et al. reported the rapid and cyclic detection of explosives such as nitrobenzene (NB) using a polymer hybrid membrane fabricated from $[Ag_{12}(S^tBu)_6(CF_3COO)_6(NH_2\text{-}bpz)_3]_n$-MOF ($NH_2$-$Ag_{12}$bpz).[335] To demonstrate the sensing, NH_2-Ag_{12}bpz was initially synthesized by connecting Ag_{12} NCs with (1,4-bis(pyrid-4-yl)benzenenamine (NH_2-bpz) linker. Further modification with methacrylamide functional group was performed by reacting in the presence of methacrylic anhydride (MA). The subsequent crosslinking of MA-Ag_{12}bpz with acrylate monomers (butyl methacrylate or triethylene glycol dimethacrylate) through a convenient photopolymerization resulted in a hybrid Ag_{12}bpz-polymer membrane. Notably, the addition of butyl methacrylate and triethylene glycol dimethacrylate monomer resulted in a rigid and flexible polymer membrane, respectively. The physical and chemical properties of the Ag_{12}bpz polymer membrane was significantly altered compared to the pristine NCs, which is evident from their improved chemical stability and PL quantum yield. The interaction of NB with polymer membrane caused a reasonable quenching in their PL due to the efficient electron transfer. The limit of detection (LOD) of NB using the polymer membrane

was calculated to be 3.19 ppb. In another example, Kuppan and Maitra developed an assembled [Au@MPA] (MPA = 3-mercaptopropionic acid) NC-based fluorescence sensor to detect Zn^{2+} ions in drinking water.[324] The tunable PL of [Au@MPA] NCs in the presence of varying concertation of Zn^{2+}, due to the in situ formation of coordination-assisted assembly is the basic concept of such devices. They could detect Zn^{2+} ion with a detection limit of 30×10^{-6} and 9×10^{-9} M by visual and fluorometric methods, respectively. A similar strategy has been further employed to detect Al^{3+} using $(NH_4)_6[Ag_6(MNA)_6]$ NCs assembled within PEI template.[274] The self-assembled luminescent NCs have been further employed for the selective detection of biomolecules. For example, Xue et al. used the dual-emissive spherical assemblies made up of [Au@SG] NCs and silicon NPs for the ratiometric detection of protamine and trypsin.[227] Strong adsorption of positively charged protamine on the NC surface could inhibit the electrostatic attractions in the self-assembly as well as the AIE. However, the addition of trypsin helped to dissociate the protamine/[Au@SG] NCs complex by hydrolyzing the protamine, which eventually brings back the self-assembly and AIE. In another example, Benavides et al. demonstrated the selective detection of Hg^{2+} using the assembled [Cu@S-p(MEO_2MA-*co*-AcSEMA)] NCs fabricated inside the multithiolated polymer.[278] The inherent PL from assembled NCs was quenched selectively in the presence of Hg^{2+}. Such chemistry has been further extended for the detection of Hg^{2+} present in human urine. Also, Au_5 NCs prepared inside PAMAM dendrimer (poly-Au_5) were used for the selective detection of intracellular endogenous GSH.[277] The electrostatic affinity between carboxylic groups of GSH (present in cells) and amine groups in poly-Au_5 resulted in the self-assembly of NCs within the cells. The enhanced PL originated from the self-assembly has been used to probe the intracellular endogenous GSH. Basu et al. successfully demonstrated the chiral recognition of D- and L-Trp (Trp = tryptophan) using the assembled enantiomeric $[Au_{14}(MPA)_6$(D/L-Trp)$_4]$ NCs fabricated by the Zn^{2+} coordination.[326] Interestingly, the addition of D/L-Trp into the similar enantiomeric NC assembly could quench PL. On the other hand, the extent of PL quenching reduced when D/L-Trp was injected into the counter enantiomeric NC assembly. Such assembly has been further used for the discrimination of geometrical isomers.[328]

4.3. Gas Sensing and Storage

The self-assembled NCs are found to be excellent materials for gas sensing and storage. For example, Huang et al. developed Ag NC-based MOF sensors for the selective detection of a variety of sensitive gas molecules.[329] The assembled porous (Ag_{12}bpy)-MOF has shown precisely the OFF and ON switchable PL in the presence of molecular oxygen ($^3O_2$) and volatile organic compounds, respectively. More interestingly, the authors were able to harvest multicolor PL from (Ag_{12}bpy)-MOF, depending on the polarity of organic compounds detected. Further, the ligand engineering of same NC using 3-amino-4,4′-bipyridine (bpy-NH_2) resulted in the formation of $[Ag_{12}(S^tBu)_8(CF_3COO)_4$(bpy-$NH_2)_4]_n$ (Ag_{12}bpy-NH_2)-MOF.[363] Introduction of amino groups into the bpy-linkers resulted in dual emissive (fluorescent-blue and phosphorescent-yellow) MOF under vacuum. (Ag_{12}bpy-NH_2)-MOF showed a prolonged lifetime owing to the enhanced triplet excitons resulted from strong spin–orbit coupling and increased rate of the intersystem crossing. Later, (Ag_{12}bpy-NH_2)-MOF has been used for the ultrasensitive ratiometric sensing of $^3O_2$. The interaction of (Ag_{12}bpy-NH_2)-MOF with $^3O_2$ quenched their yellow emission and left the blue emission of the ligand. On the other hand, such interactions in (Ag_{12}bpy)-MOF completely destroyed their green PL (**Figure 18**). By using such MOF, authors could detect $^3O_2$ with LOD 0.1 ppm, and 0.3 s response time, which is visualized by the naked eye. Furthermore, different substituents such as $-CH_3$ and mixed $-NH_2$ and $-CH_3$ groups were employed for the detection of $^3O_2$ at different concentration ranges. Basu et al. demonstrated the reversible storage of hydrogen and oxygen gas using the Zn-coordinated self-assembled superstructures fabricated from luminescent Au_{14} NCs protected with MPA and amino acids.[320] The reversible hydrogen storage was achieved using the 3D assembled crystalline framework designed from $[Au_{14}(MPA)_7(His)_5]$ NCs. The hydrogen storage capacity has been determined to be 0.244×10^{-3} M g^{-1} of the assembled framework at 20 °C and under 20 bar pressure. The enhanced PL from the assembled framework could indicate the hydrogen adsorption and desorption process. A similar strategy was further employed for the recyclable storage of oxygen and carbon dioxide gases using 2D nanosheets of $[Au_{14}(MPA)_{10}(Phe)_4]^{3+}$ NCs[321] and crystalline 3D assembly of $[Au_{14}(MPA)_{10}(Cys)_4]$ NCs (Cys = cysteine),[327] respectively. The storage capacity of oxygen and carbon dioxide gas under ambient conditions is restricted to $\approx 0.266 \times 10^{-3}$ and 1.79×10^{-3} M g^{-1}, respectively.

4.4. Delivery, Bioimaging, and Therapeutics

The self-assembled NCs have been further used for delivery, bioimaging, and therapeutic applications. For example, the assembled GNC–DNA complexes fabricated inside the cancer cells have shown an enhanced intracellular PL compared to the normal cells kept in similar experimental conditions. Such assembled materials are excellent biomarkers for targeted nanoscale imaging and cancer therapy. More interestingly, the in situ self-assembly of NCs using a tumor-suppressing double-stranded phosphatase and tensin homolog (PTEN) gene (GNC–PTEN) showed an enhanced inhibition of tumor growth in a tumor affected mice (**Figure 19**).[289] In another study, the temperature-sensitive dual emission originated from the carbon dot–NCs assembly has been used to monitor the intracellular temperature in the range from 20 to 80 °C owing to their high reproducibility, stability, and biocompatibility.[228] Similarly, the in situ fabricated gold NC-embedded peptide nanofibers (AuNC-PNF) has been used for cellular imaging and temperature sensing.[281] The stable PL (QY = 21.3%) and better biocompatibility of AuNC-PNF helped to demonstrate the concept of fluorescent thermometers. Further, the assembled [Au@SG] NCs fabricated using the cationic polymer template were successfully used for cancer cell imaging and drug delivery.[273] The cellular uptake of self-assembled NCs was found to be higher than that of individual NCs in human monocytic cells. To

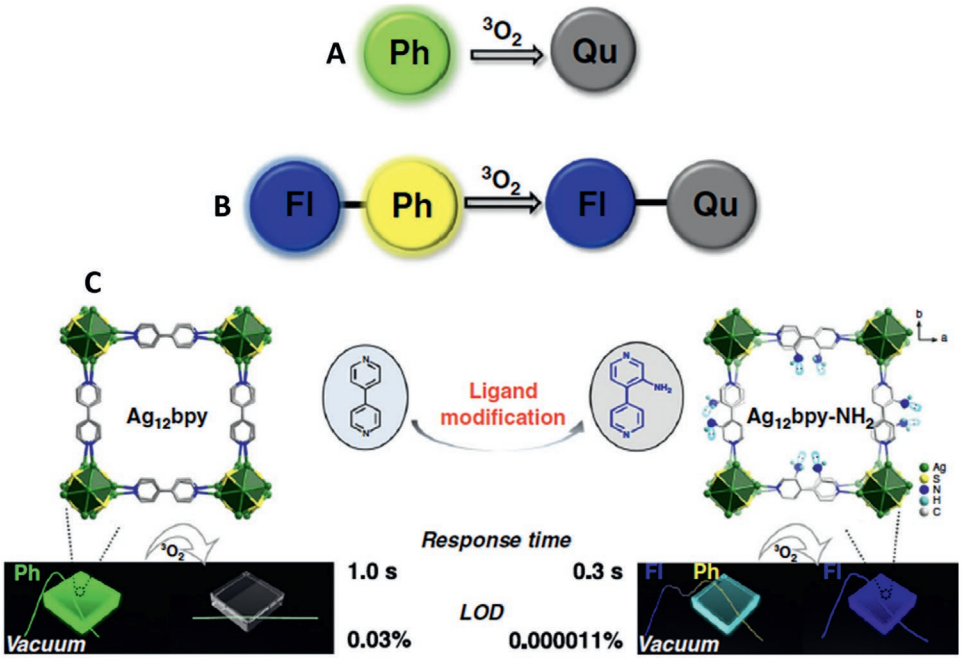

Figure 18. Schematic of $^3O_2$ sensing based on A) a single Ph emission and B) dual Fl–Ph emissions (Fl = fluorescence, Ph = phosphorescence, and Qu = quenched). Each colored circle represents an emissive center. C) Schematic of Ag_{12}bpy crystals emitting a single green color under vacuum that is quenched by $^3O_2$ with a response time of ≈1.0 s, and an LOD of 0.03%; the isostructural Ag_{12}bpy-NH_2 crystal modified with $-NH_2$ groups on the bpy linkers emits nearly a different cyan color that is composed of a blue Fl and a yellow Ph component under a certain vacuum, but only emits blue Fl under $^3O_2$. Note: the color emitted by Ag_{12}bpy-NH_2 is variable under different vacuum conditions. When using Ag_{12}bpy-NH_2 as a ratiometric oxygen sensor, the response time decreased to 0.3 s, and the LOD dropped to 0.000011%. Reproduced with permission.[363] Copyright 2020, Springer Nature.

address the drug delivery, the peptides or antibodies were initially loaded into the NC assembly using a one-pot method. The enhanced PL from peptide/antibody loaded assembled-NCs has been efficiently used to monitor the drug delivery. The fluorescence microscopy and flow cytometry data showed better intracellular colocalization of peptides or antibodies compared to free biomolecules. In another study, a tumor-targeted pH-sensitive platinum (Pt) NC assembly was designed by incorporating NCs with a pH-sensitive polypeptide via hydrophobic force, followed by surface functionalization with targeting peptide.[280] The efficient delivery of Pt ions into the subcellular compartments was achieved using such assembled NCs. The intracellular acidic pH helps to disassemble them into individual NCs and release Pt ion for the efficient treatment of chemoresistant hepatocellular carcinoma. Similarly, pH-controlled release of SpCas9 protein and gene therapy using the assembled [Au@SG]-SpCas9 composite was demonstrated.[279] Very recently, Yang et al. reported the targeted delivery, cancer cell imaging, photothermal/photodynamic therapies using $[Pt_1Ag_{28}]$ NC-assembly fabricated inside the amphiphilic chitosan micelles.[282] Further, the folic acid conjugated-assembled $[Au_{22}(SG)_{18}]$ NCs have been used to demonstrate the efficient internalization of NCs inside the

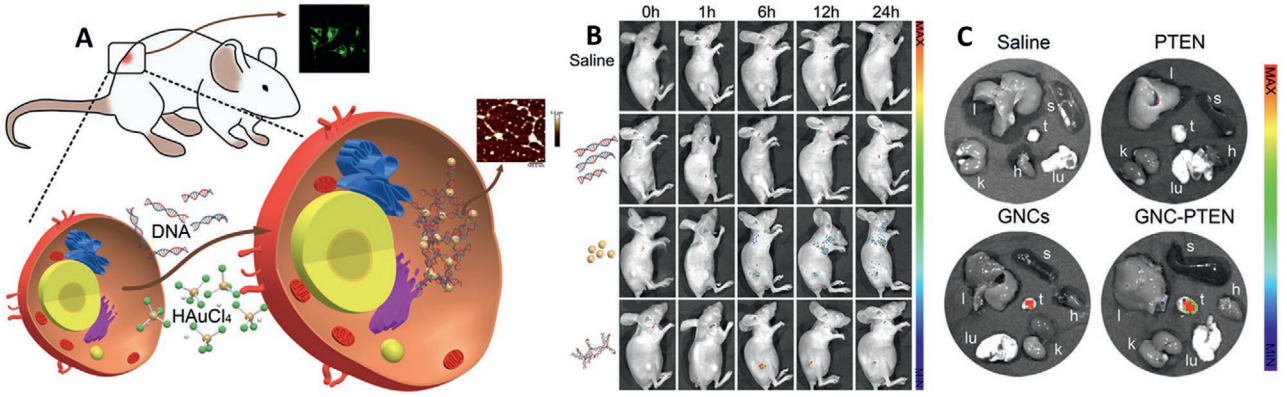

Figure 19. A) Schematic diagram of in situ self-assembled GNC–DNA complexes in cancer cells. B) Dynamic biodistribution of normal saline, PTEN, GNC, and GNC–PTEN complexes in mice using fluorescent imaging. C) Twenty-four hours after injection, animals were killed, and tumor (t, tumor), major organs (l, liver; k, kidney; s, spleen; lu, lung; h, heart) were collected for ex vivo imaging. Reproduced with permission.[289] Copyright 2020, PNAS.

cancer cells via macropinocytosis pathway, which is analogous to the endocytosis mechanism exploited by pathogens during the attack of host cells.[221] The $[Au_{22}(FGGC)_{18}]$/CB[7] NCs were also used for bioimaging applications.[295] The red emission of NCs, successfully internalized in human lung adenocarcinoma cells (A549) could help to track the cytoplasm under 515 nm excitation. Several NC-assemblies have been studied for biomedical applications.[299,322,323,325,364] Among them, Zn^{2+} coordinated $[Au_{14}(MPA)_6(Tyr)_4]$ (Tyr = tyrosine) NC-assembly showed mitochondrial enhanced anticancer activities,[323] Gd^{3+} coordinated [Au@SG] NC assembly for its application for multimodal tumor diagnosis,[325] and Ca^{2+} coordinated [Au@SG] NC assembly used for cytosolic protein delivery.[322]

4.5. Catalysis

NCs are excellent candidates for certain catalytic reactions, especially for the reduction of CO_2, oxidation of CO, and hydrogenation of alkynes.[35,39,41,48] However, fabrication of assembled-NCs without losing the optical integrity of individual NCs and their subsequent performance in catalysis are still in its infancy. Wu et al. successfully demonstrated the catalytic efficiency of assembled nanoribbons fabricated from $[Cu_{12}(DT)_8Ac_4]$ NCs.[233] The electrocatalytic oxygen reduction reaction (ORR) efficiencies of assembled nanowires and nanoribbons were compared with the parent NCs as the cathode catalysts. The catalytic activity and durability of assembled NCs are found to be better than individual NCs. A similar trend was observed in the self-assembled nanoribbons fabricated from $[Cu_{13}(AMT)_{10}Ac_2]$ NCs.[314] In another example, Wu et al. demonstrated the electrocatalytic oxygen evolution reaction (OER) efficiency of $[Co_9S_8]$ self-assembled nanosheets fabricated by the sulfurization of preassembled $[Co_{14}(DT)_9]$ NCs in the presence of excess DT at 400 °C under N_2 atm.[235] Later, Cao et al. demonstrated the photocatalytic degradation (oxidation) of mustard gas simulant (2-chloroethyl ethyl sulfide, CEES) using $[Ag_{12}(S^tBu)_6(CF_3COO)_3(TPyP)]_n$, ($Ag_{12}$TPyP)-MOF (TPyP = tetrapyridyl porphyrin).[334] The well-defined porous structure and the strong affinity between NCs and CEES in (Ag_{12}TPyP)-MOF resulted in improved uptake of CEES (74.2 mg g^{-1}). The combined photosensitizing efficiency of both porphyrin and NCs could produce a sufficient amount of singlet oxygen ($^1O_2$), which helped to accelerate the degradation of CEES into nontoxic oxidation product CEESO (**Figure 20**). Similarly, Zhu et al. used the sandwiched [UiO-66@Au_{25}@UiO-66]-MOF as a heterogeneous catalyst for the selective conversion of sulfide to sulfoxide. The $^1O_2$ produced by the photosensitization of [UiO-66@Au_{25}@UiO-66]-MOF triggered the photocatalytic transformation.[316] Very recently, the catalytic activity of $\{[Ag_{27}S_2(S^tBu)_{14}(CF_3COO)_8(TPyP\text{-}H_2)](CF_3COO)\}_n$, 2D Ag_{27}-MOF has been successfully demonstrated by the chemical fixation of CO_2 via the cycloaddition reaction with both terminal and internal propargylamines.[365]

Summary of different methods used to demonstrate the assembly of NCs are given in Table 1.

5. Conclusions and Future Perspectives

Atomically precise noble metal nanoclusters act as a link between molecular-level organometallic complexes and colloidal-level plasmonic nanoparticles. Systematic studies on various aspects of nanocluster fabrication, optical properties, enhanced photoluminescence, and catalytic activity have been efficiently used to enrich different aspects of materials science.

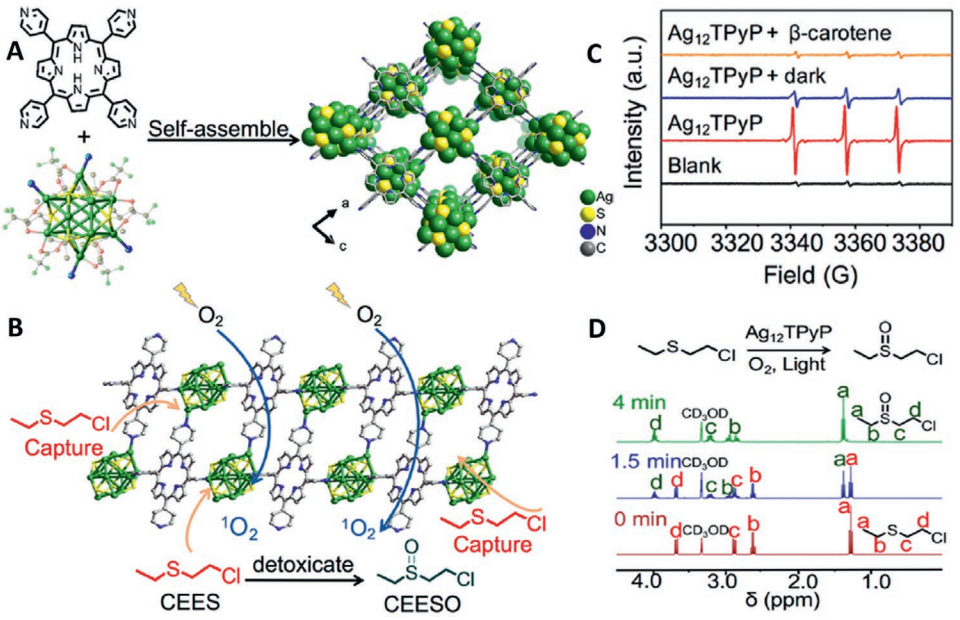

Figure 20. A) Schematic representation for the synthesis of Ag_{12}TPyP. B) Capture and photodetoxification of CEES molecule by (Ag_{12}TPyP). C) Electron paramagnetic resonance (EPR) spectra of Ag_{12}TPyP under visible-light irradiation or in the dark shows the formation of $^1O_2$ by the photosensitized mechanism. D) ^1H NMR spectra of CEES during the photooxidation reaction by (Ag_{12}TPyP) shows the efficient conversion of CEES to nontoxic CEESO. Reproduced with permission.[334] Copyright 2019, American Chemical Society.

With the introduction of new and improved protocols for the synthesis, surface functionalization, and subsequent purification, nanoclusters have been used in various research areas. The applications of nanoclusters in solar energy harvesting, light-emitting devices, molecular recognition, bioimaging, and biosensing have been explored. Later, the surface coverage of nanoclusters with several functional molecules was addressed using the organic transformation toolbox. The well-defined structure, covalently bound functional groups, optoelectronic properties, and inherent structural complexities of nanoclusters make them excellent building blocks for fabricating a wide range of functional 3D periodic superstructures via the colloidal self-assembly process. This review has presented details on how the nanocluster-building blocks have been used efficiently to construct the hierarchical superstructures. The different aspects of self-assembly driven by the nanocluster-surface forces such as hydrogen bonding, electrostatic interactions, van der Waals interactions, dipolar interactions, $C-H\cdots\pi/\pi\cdots\pi$ interactions, amphiphilicity, metal chelation, metal–metal interactions, light-triggered dipole-induced attractions, and external templates were discussed in great detail. The reduced free energy of the system during the self-organization was found to be the inspiring hands for the overall process. Among different methods described, the assembly of nanoclusters via external stimuli such as light or metal coordination is fascinating due to their multiple-switchability or enhanced photoluminescence. Despite the recent progress in the assembled superstructures, there are several limitations in nanocluster self-assembly. For example, hydrogen bonding assemblies have so far been demonstrated using only a few selected ligands. Such assemblies will face substantial challenges when more than one type of hydrogen bonding motifs or competing interactions are available. Electrostatic assemblies often lead to irreversible aggregates. Notably, a wide range of crystal structures was reported only for organic solvent-soluble nanoclusters. Due to the lack of well-established crystal structure, the self-assembly of water-soluble nanoclusters faces limitations in understanding the molecular level details and structure–property correlation. However, the assembled superstructures could bring new photophysical properties such as aggregation-induced emission, enhanced circularly polarized luminescence, amplified optical absorption, and better mechanical strength. These properties have been effectively utilized to demonstrate molecular and metal ion sensing, gas sensing and storage, bioimaging and therapeutics, catalysis, and device fabrications. So far, the reported structures in the literature are static and equilibrium nanocluster self-assemblies. Recent efforts, however, have shown that proper ligand engineering allows reversible nanocluster self-assemblies. The molecule-like nature of nanoclusters offers an excellent opportunity to explore the concepts of dissipative and out-of-equilibrium self-assembly in colloidal systems. More importantly, the recent progress on the fabrication of monodisperse nanoparticles using the algorithm programmed automated techniques are highly admirable. Such techniques are demanded to formulate the precise nanoclusters tethered with desired functional moieties by solving the unknown errors using the computed programs. Further, the latest development on programable self-assembly of nanoparticles using i) the custom-made DNA origami tiles, ii) the atom transfer reactions between nanoclusters and plasmonic nanoparticles, iii) controlled assembly via oligomerization, and iv) gold(I)thiolate-induced self-organization at their embryonic state, are the most advanced techniques to potentially paving the way for new generation metamaterials from atomically precise nanoclusters. These new hybrid materials are expected to cover a spectrum of enhanced optoelectronic properties, which are useful for addressing many unsolved problems, particularly in catalysis and biophysics.

Acknowledgements

J.V.R. and E.S.S. contributed equally to this work. E.S.S. thanks the Science and Engineering Research Board (SERB) for a Ramanujan fellowship. T.P. thanks the Department of Science and Technology, Government of India, for constantly supporting his research program on nanomaterials. N. thanks the Academy of Finland's Photonics Research and Innovation (PREIN) flagship platform. J.V.R. thanks SERB for supporting the research fellowship. P.M. and K.M.L. thank the Council of Scientific and Industrial Research (CSIR/UGC) for their junior research fellowships. Dr. N. Kalaiselvi (Director) and Dr. P. Murugan, CSIR-CECRI, are acknowledged for their support. This work was supported by SERB (SB/S2/RJN-005/2017).

Conflict of Interest

The authors declare no conflict of interest.

Keywords

colloidal superstructures, enhanced optical properties, hierarchical structural complexity, nanoscale driving forces, precision nanoclusters, self-assembly

Received: September 14, 2020
Revised: November 7, 2020
Published online: January 25, 2021

[1] G. Schmid, *Chem. Rev.* **1992**, *92*, 1709.
[2] G. Schmid, M. Bäumle, M. Geerkens, I. Heim, C. Osemann, T. Sawitowski, *Chem. Soc. Rev.* **1999**, *28*, 179.
[3] H. Häkkinen, *Chem. Soc. Rev.* **2008**, *37*, 1847.
[4] R. L. Whetten, J. T. Khoury, M. M. Alvarez, S. Murthy, I. Vezmar, Z. L. Wang, P. W. Stephens, C. L. Cleveland, W. D. Luedtke, U. Landman, *Adv. Mater.* **1996**, *8*, 428.
[5] J. F. Parker, C. A. Fields-Zinna, R. W. Murray, *Acc. Chem. Res.* **2010**, *43*, 1289.
[6] R. Jin, C. Zeng, M. Zhou, Y. Chen, *Chem. Rev.* **2016**, *116*, 10346.
[7] Q. Yao, T. Chen, X. Yuan, J. Xie, *Acc. Chem. Res.* **2018**, *51*, 1338.
[8] P. Chakraborty, A. Nag, A. Chakraborty, T. Pradeep, *Acc. Chem. Res.* **2019**, *52*, 2.
[9] R. Jin, *Nanoscale* **2015**, *7*, 1549.
[10] I. Chakraborty, T. Pradeep, *Chem. Rev.* **2017**, *117*, 8208.
[11] H. Qian, M. Zhu, Z. Wu, R. Jin, *Acc. Chem. Res.* **2012**, *45*, 1470.
[12] M. Walter, J. Akola, O. Lopez-Acevedo, P. D. Jadzinsky, G. Calero, C. J. Ackerson, R. L. Whetten, H. Grönbeck, H. Häkkinen, *Proc. Natl. Acad. Sci. USA* **2008**, *105*, 9157.
[13] Y. Negishi, K. Nobusada, T. Tsukuda, *J. Am. Chem. Soc.* **2005**, *127*, 5261.

[14] R. S. Ingram, M. J. Hostetler, R. W. Murray, T. G. Schaaff, J. T. Khoury, R. L. Whetten, T. P. Bigioni, D. K. Guthrie, P. N. First, *J. Am. Chem. Soc.* **1997**, *119*, 9279.
[15] T. G. Schaaff, R. L. Whetten, *J. Phys. Chem. B* **2000**, *104*, 2630.
[16] T. G. Schaaff, M. N. Shafigullin, J. T. Khoury, I. Vezmar, R. L. Whetten, *J. Phys. Chem. B* **2001**, *105*, 8785.
[17] C. M. Aikens, *J. Phys. Chem. Lett.* **2010**, *2*, 99.
[18] V. L. Jimenez, D. G. Georganopoulou, R. J. White, A. S. Harper, A. J. Mills, D. Lee, R. W. Murray, *Langmuir* **2004**, *20*, 6864.
[19] E. S. Shibu, M. A. H. Muhammed, T. Tsukuda, T. Pradeep, *J. Phys. Chem. C* **2008**, *112*, 12168.
[20] A. W. Castleman, S. N. Khanna, *J. Phys. Chem. C* **2009**, *113*, 2664.
[21] J. U. Reveles, S. N. Khanna, P. J. Roach, A. W. Castleman, *Proc. Natl. Acad. Sci. USA* **2006**, *103*, 18405.
[22] Y. Negishi, Y. Takasugi, S. Sato, H. Yao, K. Kimura, T. Tsukuda, *J. Am. Chem. Soc.* **2004**, *126*, 6518.
[23] Y. Negishi, N. K. Chaki, Y. Shichibu, R. L. Whetten, T. Tsukuda, *J. Am. Chem. Soc.* **2007**, *129*, 11322.
[24] S. Kumar, M. D. Bolan, T. P. Bigioni, *J. Am. Chem. Soc.* **2010**, *132*, 13141.
[25] H. Qian, M. Y. Sfeir, R. Jin, *J. Phys. Chem. C* **2010**, *114*, 19935.
[26] T. P. Bigioni, R. L. Whetten, Ö. Dag, *J. Phys. Chem. B* **2000**, *104*, 6983.
[27] S. A. Miller, J. M. Womick, J. F. Parker, R. W. Murray, A. M. Moran, *J. Phys. Chem. C* **2009**, *113*, 9440.
[28] Z. Luo, X. Yuan, Y. Yu, Q. Zhang, D. T. Leong, J. Y. Lee, J. Xie, *J. Am. Chem. Soc.* **2012**, *134*, 16662.
[29] M. S. Devadas, J. Kim, E. Sinn, D. Lee, T. Goodson, G. Ramakrishna, *J. Phys. Chem. C* **2010**, *114*, 22417.
[30] E. S. Shibu, T. Pradeep, *Int. J. Nanosci.* **2009**, *8*, 223.
[31] S. Link, A. Beeby, S. FitzGerald, M. A. El-Sayed, T. G. Schaaff, R. L. Whetten, *J. Phys. Chem. B* **2002**, *106*, 3410.
[32] H. C. Weissker, H. B. Escobar, V. D. Thanthirige, K. Kwak, D. Lee, G. Ramakrishna, R. L. Whetten, X. Lopez-Lozano, *Nat. Commun.* **2014**, *5*, 3785.
[33] M. Zhu, C. M. Aikens, M. P. Hendrich, R. Gupta, H. Qian, G. C. Schatz, R. Jin, *J. Am. Chem. Soc.* **2009**, *131*, 2490.
[34] A. Akbari-Sharbaf, M. Hesari, M. S. Workentin, G. Fanchini, *J. Chem. Phys.* **2013**, *138*, 024305.
[35] J. Fang, B. Zhang, Q. Yao, Y. Yang, J. Xie, N. Yan, *Coord. Chem. Rev.* **2016**, *322*, 1.
[36] A. Shivhare, D. M. Chevrier, R. W. Purves, R. W. J. Scott, *J. Phys. Chem. C* **2013**, *117*, 20007.
[37] H. Tsunoyama, N. Ichikuni, H. Sakurai, T. Tsukuda, *J. Am. Chem. Soc.* **2009**, *131*, 7086.
[38] Y. Zhu, H. Qian, R. Jin, *J. Mater. Chem.* **2011**, *21*, 6793.
[39] S. Yamazoe, K. Koyasu, T. Tsukuda, *Acc. Chem. Res.* **2014**, *47*, 816.
[40] E. S. Andreiadis, M. R. Vitale, N. Mézailles, X. L. Goff, P. L. Floch, P. Y. Toullec, V. Michelet, *Dalton Trans.* **2010**, *39*, 10608.
[41] G. Li, R. Jin, *Acc. Chem. Res.* **2013**, *46*, 1749.
[42] Y. Zhu, H. Qian, M. Zhu, R. Jin, *Adv. Mater.* **2010**, *22*, 1915.
[43] G. Li, H. Abroshan, C. Liu, S. Zhuo, Z. Li, Y. Xie, H. J. Kim, N. L. Rosi, R. Jin, *ACS Nano* **2016**, *10*, 7998.
[44] D. R. Kauffman, D. Alfonso, C. Matranga, H. Qian, R. Jin, *J. Am. Chem. Soc.* **2012**, *134*, 10237.
[45] X. Du, R. Jin, *ACS Nano* **2019**, *13*, 7383.
[46] X. Nie, H. Qian, Q. Ge, H. Xu, R. Jin, *ACS Nano* **2012**, *6*, 6014.
[47] X.-K. Wan, J.-Q. Wang, Z.-A. Nan, Q.-M. Wang, *Sci. Adv.* **2017**, *3*, e1701823.
[48] L. Liu, A. Corma, *Chem. Rev.* **2018**, *118*, 4981.
[49] C. Sun, N. Mammen, S. Kaappa, P. Yuan, G. Deng, C. Zhao, J. Yan, S. Malola, K. Honkala, H. Häkkinen, B. K. Teo, N. Zheng, *ACS Nano* **2019**, *13*, 5975.
[50] C. Liu, C. Yan, J. Lin, C. Yu, J. Huang, G. Li, *J. Mater. Chem. A* **2015**, *3*, 20167.
[51] A. Mathew, P. R. Sajanlal, T. Pradeep, *Angew. Chem., Int. Ed.* **2012**, *51*, 9596.
[52] T.-H. Chen, W.-L. Tseng, *Small* **2012**, *8*, 1912.
[53] D. Hu, Z. Sheng, P. Gong, P. Zhang, L. Cai, *Analyst* **2010**, *135*, 1411.
[54] Y. Yue, T.-Y. Liu, H.-W. Li, Z. Liu, Y. Wu, *Nanoscale* **2012**, *4*, 2251.
[55] X. Yuan, Z. Luo, Y. Yu, Q. Yao, J. Xie, *Chem. - Asian J.* **2013**, *8*, 858.
[56] M. A. H. Muhammed, P. K. Verma, S. K. Pal, R. C. A. Kumar, S. Paul, R. V. Omkumar, T. Pradeep, *Chem. - Eur. J.* **2009**, *15*, 10110.
[57] X.-R. Song, N. Goswami, H.-H. Yang, J. Xie, *Analyst* **2016**, *141*, 3126.
[58] M. A. H. Muhammed, P. K. Verma, S. K. Pal, A. Retnakumari, M. Koyakutty, S. Nair, T. Pradeep, *Chem. - Eur. J.* **2010**, *16*, 10103.
[59] C.-A. J. Lin, T.-Y. Yang, C.-H. Lee, S. H. Huang, R. A. Sperling, M. Zanella, J. K. Li, J.-L. Shen, H.-H. Wang, H.-I. Yeh, W. J. Parak, W. H. Chang, *ACS Nano* **2009**, *3*, 395.
[60] K. Basu, K. Gayen, T. Mitra, A. Baral, S. S. Roy, A. Banerjee, *ChemNanoMat* **2017**, *3*, 808.
[61] X. Wu, X. He, K. Wang, C. Xie, B. Zhou, Z. Qing, *Nanoscale* **2010**, *2*, 2244.
[62] Y. Yu, S. Y. New, J. Xie, X. Su, Y. N. Tan, *Chem. Commun.* **2014**, *50*, 13805.
[63] Y. Wang, J. Chen, J. Irudayaraj, *ACS Nano* **2011**, *5*, 9718.
[64] X.-D. Zhang, J. Chen, Z. Luo, D. Wu, X. Shen, S.-S. Song, Y.-M. Sun, P.-X. Liu, J. Zhao, S. Huo, S. Fan, F. Fan, X.-J. Liang, J. Xie, *Adv. Healthcare Mater.* **2014**, *3*, 133.
[65] N. Goswami, K. Zheng, J. Xie, *Nanoscale* **2014**, *6*, 13328.
[66] E. S. Shibu, S. Sugino, K. Ono, H. Saito, A. Nishioka, S. Yamamura, M. Sawada, Y. Nosaka, V. Biju, *Angew. Chem., Int. Ed.* **2013**, *52*, 10559.
[67] H.-H. Wang, C.-A. J. Lin, C.-H. Lee, Y.-C. Lin, Y.-M. Tseng, C.-L. Hsieh, C.-H. Chen, C.-H. Tsai, C.-T. Hsieh, J.-L. Shen, W.-H. Chan, W. H. Chang, H.-I. Yeh, *ACS Nano* **2011**, *5*, 4337.
[68] X.-D. Zhang, Z. Luo, J. Chen, H. Wang, S.-S. Song, X. Shen, W. Long, Y.-M. Sun, S. Fan, K. Zheng, D. T. Leong, J. Xie, *Small* **2015**, *11*, 1683.
[69] D. C. Lim, B. Y. Seo, S. Nho, D. H. Kim, E. M. Hong, J. Y. Lee, S.-Y. Park, C.-L. Lee, Y. D. Kim, S. Cho, *Adv. Energy Mater.* **2015**, *5*, 1500393.
[70] M. A. Abbas, P. V. Kamat, J. H. Bang, *ACS Energy Lett.* **2018**, *3*, 840.
[71] Y.-S. Chen, H. Choi, P. V. Kamat, *J. Am. Chem. Soc.* **2013**, *135*, 8822.
[72] M. A. Abbas, S. J. Yoon, H. Kim, J. Lee, P. V. Kamat, J. H. Bang, *ACS Appl. Mater. Interfaces* **2019**, *11*, 12492.
[73] R. Bauld, M. Hesari, M. S. Workentin, G. Fanchini, *Nanoscale* **2014**, *6*, 7570.
[74] T.-W. Koh, A. M. Hiszpanski, M. Sezen, A. Naim, T. Galfsky, A. Trivedi, Y.-L. Loo, V. Menon, B. P. Rand, *Nanoscale* **2015**, *7*, 9140.
[75] Y.-C. Chao, K.-P. Cheng, C.-Y. Lin, Y.-L. Chang, Y.-Y. Ko, T.-Y. Hou, C.-Y. Huang, W. H. Chang, C.-A. J. Lin, *Sci. Rep.* **2018**, *8*, 8860.
[76] X.-K. Wan, Z.-W. Lin, Q.-M. Wang, *J. Am. Chem. Soc.* **2012**, *134*, 14750.
[77] X.-K. Wan, S.-F. Yuan, Z.-W. Lin, Q.-M. Wang, *Angew. Chem., Int. Ed.* **2014**, *53*, 2923.
[78] J. Chen, Q.-F. Zhang, P. G. Williard, L.-S. Wang, *Inorg. Chem.* **2014**, *53*, 3932.
[79] J. Chen, Q.-F. Zhang, T. A. Bonaccorso, P. G. Williard, L.-S. Wang, *J. Am. Chem. Soc.* **2014**, *136*, 92.
[80] A. Das, T. Li, K. Nobusada, Q. Zeng, N. L. Rosi, R. Jin, *J. Am. Chem. Soc.* **2012**, *134*, 20286.
[81] Y. Shichibu, Y. Negishi, T. Watanabe, N. K. Chaki, H. Kawaguchi, T. Tsukuda, *J. Phys. Chem. C* **2007**, *111*, 7845.
[82] H. Qian, W. T. Eckenhoff, M. E. Bier, T. Pintauer, R. Jin, *Inorg. Chem.* **2011**, *50*, 10735.
[83] R. Jin, C. Liu, S. Zhao, A. Das, H. Xing, C. Gayathri, Y. Xing, N. L. Rosi, R. R. Gil, R. Jin, *ACS Nano* **2015**, *9*, 8530.

[84] B. K. Teo, X. Shi, H. Zhang, *J. Am. Chem. Soc.* **1992**, *114*, 2743.
[85] W. Kurashige, M. Yamaguchi, K. Nobusada, Y. Negishi, *J. Phys. Chem. Lett.* **2012**, *3*, 2649.
[86] W. Kurashige, S. Yamazoe, K. Kanehira, T. Tsukuda, Y. Negishi, *J. Phys. Chem. Lett.* **2013**, *4*, 3181.
[87] I. Chakraborty, W. Kurashige, K. Kanehira, L. Gell, H. Häkkinen, Y. Negishi, T. Pradeep, *J. Phys. Chem. Lett.* **2013**, *4*, 3351.
[88] W. Kurashige, K. Munakata, K. Nobusada, Y. Negishi, *Chem. Commun.* **2013**, *49*, 5447.
[89] I. Chakraborty, T. Pradeep, *Nanoscale* **2014**, *6*, 14190.
[90] T. U. B. Rao, B. Nataraju, T. Pradeep, *J. Am. Chem. Soc.* **2010**, *132*, 16304.
[91] T. U. B. Rao, T. Pradeep, *Angew. Chem., Int. Ed.* **2010**, *49*, 3925.
[92] E. S. Shibu, B. Radha, P. K. Verma, P. Bhyrappa, G. U. Kulkarni, S. K. Pal, T. Pradeep, *ACS Appl. Mater. Interfaces* **2009**, *1*, 2199.
[93] T. Udayabhaskararao, T. Pradeep, *J. Phys. Chem. Lett.* **2013**, *4*, 1553.
[94] Y. Yu, X. Chen, Q. Yao, Y. Yu, N. Yan, J. Xie, *Chem. Mater.* **2013**, *25*, 946.
[95] X. Yuan, B. Zhang, Z. Luo, Q. Yao, D. T. Leong, N. Yan, J. Xie, *Angew. Chem., Int. Ed.* **2014**, *53*, 4623.
[96] M. Zhu, E. Lanni, N. Garg, M. E. Bier, R. Jin, *J. Am. Chem. Soc.* **2008**, *130*, 1138.
[97] Z. Wu, J. Suhan, R. Jin, *J. Mater. Chem.* **2009**, *19*, 622.
[98] Y. Shichibu, Y. Negishi, H. Tsunoyama, M. Kanehara, T. Teranishi, T. Tsukuda, *Small* **2007**, *3*, 835.
[99] Y. Shichibu, K. Konishi, *Small* **2010**, *6*, 1216.
[100] R. Jin, H. Qian, Z. Wu, Y. Zhu, M. Zhu, A. Mohanty, N. Garg, *J. Phys. Chem. Lett.* **2010**, *1*, 2903.
[101] H. Qian, Y. Zhu, R. Jin, *ACS Nano* **2009**, *3*, 3795.
[102] X. Yuan, Y. Yu, Q. Yao, Q. Zhang, J. Xie, *J. Phys. Chem. Lett.* **2012**, *3*, 2310.
[103] K. Kimura, N. Sugimoto, S. Sato, H. Yao, Y. Negishi, T. Tsukuda, *J. Phys. Chem. C* **2009**, *113*, 14076.
[104] Y. Niihori, M. Matsuzaki, C. Uchida, Y. Negishi, *Nanoscale* **2014**, *6*, 7889.
[105] S. Knoppe, J. Boudon, I. Dolamic, A. Dass, T. Bürgi, *Anal. Chem.* **2011**, *83*, 5056.
[106] A. Ghosh, J. Hassinen, P. Pulkkinen, H. Tenhu, R. H. A. Ras, T. Pradeep, *Anal. Chem.* **2014**, *86*, 12185.
[107] Y. Niihori, M. Matsuzaki, T. Pradeep, Y. Negishi, *J. Am. Chem. Soc.* **2013**, *135*, 4946.
[108] H. Tsunoyama, Y. Negishi, T. Tsukuda, *J. Am. Chem. Soc.* **2006**, *128*, 6036.
[109] S. Chen, S. Wang, J. Zhong, Y. Song, J. Zhang, H. Sheng, Y. Pei, M. Zhu, *Angew. Chem., Int. Ed.* **2015**, *54*, 3145.
[110] A. Das, C. Liu, H. Y. Byun, K. Nobusada, S. Zhao, N. Rosi, R. Jin, *Angew. Chem., Int. Ed.* **2015**, *54*, 3140.
[111] C. Zeng, C. Liu, Y. Chen, N. L. Rosi, R. Jin, *J. Am. Chem. Soc.* **2014**, *136*, 11922.
[112] A. Das, T. Li, K. Nobusada, C. Zeng, N. L. Rosi, R. Jin, *J. Am. Chem. Soc.* **2013**, *135*, 18264.
[113] D. Crasto, G. Barcaro, M. Stener, L. Sementa, A. Fortunelli, A. Dass, *J. Am. Chem. Soc.* **2014**, *136*, 14933.
[114] M. W. Heaven, A. Dass, P. S. White, K. M. Holt, R. W. Murray, *J. Am. Chem. Soc.* **2008**, *130*, 3754.
[115] M. Zhu, C. M. Aikens, F. J. Hollander, G. C. Schatz, R. Jin, *J. Am. Chem. Soc.* **2008**, *130*, 5883.
[116] C. Zeng, T. Li, A. Das, N. L. Rosi, R. Jin, *J. Am. Chem. Soc.* **2013**, *135*, 10011.
[117] D. Crasto, S. Malola, G. Brosofsky, A. Dass, H. Häkkinen, *J. Am. Chem. Soc.* **2014**, *136*, 5000.
[118] C. Zeng, H. Qian, T. Li, G. Li, N. L. Rosi, B. Yoon, R. N. Barnett, R. L. Whetten, U. Landman, R. Jin, *Angew. Chem., Int. Ed.* **2012**, *51*, 13114.
[119] H. Qian, W. T. Eckenhoff, Y. Zhu, T. Pintauer, R. Jin, *J. Am. Chem. Soc.* **2010**, *132*, 8280.
[120] P. D. Jadzinsky, G. Calero, C. J. Ackerson, D. A. Bushnell, R. D. Kornberg, *Science* **2007**, *318*, 430.
[121] N. Yan, N. Xia, L. Liao, M. Zhu, F. Jin, R. Jin, Z. Wu, *Sci. Adv.* **2018**, *4*, eaat7259.
[122] K. M. Jensen, P. Juhas, M. A. Tofanelli, C. L. Heinecke, G. Vaughan, C. J. Ackerson, S. J. L. Billinge, *Nat. Commun.* **2016**, *7*, 11859.
[123] C. P. Joshi, M. S. Bootharaju, M. J. Alhilaly, O. M. Bakr, *J. Am. Chem. Soc.* **2015**, *137*, 11578.
[124] L. G. AbdulHalim, M. S. Bootharaju, Q. Tang, S. D. Gobbo, R. G. AbdulHalim, M. Eddaoudi, D. Jiang, O. M. Bakr, *J. Am. Chem. Soc.* **2015**, *137*, 11970.
[125] H. Yang, Y. Wang, H. Huang, L. Gell, L. Lehtovaara, S. Malola, H. Häkkinen, N. Zheng, *Nat. Commun.* **2013**, *4*, 2422.
[126] A. Dass, *J. Am. Chem. Soc.* **2009**, *131*, 11666.
[127] J. Guo, S. Kumar, M. Bolan, A. Desireddy, T. P. Bigioni, W. P. Griffith, *Anal. Chem.* **2012**, *84*, 5304.
[128] K. M. Harkness, D. E. Cliffel, J. A. McLean, *Analyst* **2010**, *135*, 868.
[129] R. Tsunoyama, H. Tsunoyama, P. Pannopard, J. Limtrakul, T. Tsukuda, *J. Phys. Chem. C* **2010**, *114*, 16004.
[130] T. Udayabhaskararao, M. S. Bootharaju, T. Pradeep, *Nanoscale* **2013**, *5*, 9404.
[131] H. Qian, R. Jin, *Chem. Commun.* **2011**, *47*, 11462.
[132] H. Qian, Y. Zhu, R. Jin, *J. Am. Chem. Soc.* **2010**, *132*, 4583.
[133] K. M. Harkness, Y. Tang, A. Dass, J. Pan, N. Kothalawala, V. J. Reddy, D. E. Cliffel, B. Demeler, F. Stellacci, O. M. Bakr, J. A. McLean, *Nanoscale* **2012**, *4*, 4269.
[134] C. Yao, Y. Lin, J. Yuan, L. Liao, M. Zhu, L. Weng, J. Yang, Z. Wu, *J. Am. Chem. Soc.* **2015**, *137*, 15350.
[135] J. Yan, H. Su, H. Yang, S. Malola, S. Lin, H. Häkkinen, N. Zheng, *J. Am. Chem. Soc.* **2015**, *137*, 11880.
[136] M. S. Bootharaju, L. Sinatra, O. M. Bakr, *Nanoscale* **2016**, *8*, 17333.
[137] S. Tian, L. Liao, J. Yuan, C. Yao, J. Chen, J. Yang, Z. Wu, *Chem. Commun.* **2016**, *52*, 9873.
[138] H. Qian, D. Jiang, G. Li, C. Gayathri, A. Das, R. R. Gil, R. Jin, *J. Am. Chem. Soc.* **2012**, *134*, 16159.
[139] Z. Wang, Z. Zhu, C. Zhao, Q. Yao, X. Li, H. Liu, F. Du, X. Yuan, J. Xie, *Chem. - Asian J.* **2019**, *14*, 765.
[140] K. Kwak, W. Choi, Q. Tang, M. Kim, Y. Lee, D. Jiang, D. Lee, *Nat. Commun.* **2017**, *8*, 14723.
[141] T. Udayabhaskararao, Y. Sun, N. Goswami, S. K. Pal, K. Balasubramanian, T. Pradeep, *Angew. Chem., Int. Ed.* **2012**, *51*, 2155.
[142] C. Kumara, A. Dass, *Nanoscale* **2012**, *4*, 4084.
[143] S. Wang, Y. Song, S. Jin, X. Liu, J. Zhang, Y. Pei, X. Meng, M. Chen, P. Li, M. Zhu, *J. Am. Chem. Soc.* **2015**, *137*, 4018.
[144] Y. Negishi, K. Igarashi, K. Munakata, W. Ohgake, K. Nobusada, *Chem. Commun.* **2012**, *48*, 660.
[145] Y. Negishi, T. Iwai, M. Ide, *Chem. Commun.* **2010**, *46*, 4713.
[146] S. Yang, S. Wang, S. Jin, S. Chen, H. Sheng, M. Zhu, *Nanoscale* **2015**, *7*, 10005.
[147] H. Yang, Y. Wang, J. Lei, L. Shi, X. Wu, V. Mäkinen, S. Lin, Z. Tang, J. He, H. Häkkinen, L. Zheng, N. Zheng, *J. Am. Chem. Soc.* **2013**, *135*, 9568.
[148] S. Wang, S. Jin, S. Yang, S. Chen, Y. Song, J. Zhang, M. Zhu, *Sci. Adv.* **2015**, *1*, e1500441.
[149] N. Yan, L. Liao, J. Yuan, Y. Lin, L. Weng, J. Yang, Z. Wu, *Chem. Mater.* **2016**, *28*, 8240.
[150] C. Kumara, A. Dass, *Nanoscale* **2011**, *3*, 3064.
[151] S. R. Biltek, S. Mandal, A. Sen, A. C. Reber, A. F. Pedicini, S. N. Khanna, *J. Am. Chem. Soc.* **2013**, *135*, 26.
[152] J. Yan, H. Su, H. Yang, C. Hu, S. Malola, S. Lin, B. K. Teo, H. Häkkinen, N. Zheng, *J. Am. Chem. Soc.* **2016**, *138*, 12751.
[153] J.-L. Zeng, Z.-J. Guan, Y. Du, Z.-A. Nan, Y.-M. Lin, Q.-M. Wang, *J. Am. Chem. Soc.* **2016**, *138*, 7848.
[154] S. L. Christensen, M. A. MacDonald, A. Chatt, P. Zhang, H. Qian, R. Jin, *J. Phys. Chem. C* **2012**, *116*, 26932.

[155] C. Yao, J. Chen, M.-B. Li, L. Liu, J. Yang, Z. Wu, *Nano Lett.* **2015**, *15*, 1281.
[156] Y. Wang, H. Su, C. Xu, G. Li, L. Gell, S. Lin, Z. Tang, H. Häkkinen, N. Zheng, *J. Am. Chem. Soc.* **2015**, *137*, 4324.
[157] K. R. Krishnadas, A. Baksi, A. Ghosh, G. Natarajan, A. Som, T. Pradeep, *Acc. Chem. Res.* **2017**, *50*, 1988.
[158] Q. Yao, Y. Feng, V. Fung, Y. Yu, D. Jiang, J. Yang, J. Xie, *Nat. Commun.* **2017**, *8*, 1555.
[159] B. Zhang, G. Salassa, T. Bürgi, *Chem. Commun.* **2016**, *52*, 9205.
[160] M. A. H. Muhammed, A. K. Shaw, S. K. Pal, T. Pradeep, *J. Phys. Chem. C* **2008**, *112*, 14324.
[161] M. S. Devadas, K. Kwak, J.-W. Park, J.-H. Choi, C.-H. Jun, E. Sinn, G. Ramakrishna, D. Lee, *J. Phys. Chem. C* **2010**, *1*, 1497.
[162] C. Gautier, R. Taras, S. Gladiali, T. Bürgi, *Chirality* **2008**, *20*, 486.
[163] S. Knoppe, T. Bürgi, *Acc. Chem. Res.* **2014**, *47*, 1318.
[164] J. J. Pelayo, R. L. Whetten, I. L. Garzón, *J. Phys. Chem. C* **2015**, *119*, 28666.
[165] O. Lopez-Acevedo, H. Tsunoyama, T. Tsukuda, H. Häkkinen, C. M. Aikens, *J. Am. Chem. Soc.* **2010**, *132*, 8210.
[166] Y. Zhu, H. Wang, K. Wan, J. Guo, C. He, Y. Yu, L. Zhao, Y. Zhang, J. Lv, L. Shi, R. Jin, X. Zhang, X. Shi, Z. Tang, *Angew. Chem., Int. Ed.* **2018**, *57*, 9059.
[167] I. E. Santizo, F. Hidalgo, L. A. Pérez, C. Noguez, I. L. Garzón, *J. Phys. Chem. C* **2008**, *112*, 17533.
[168] I. Dolamic, S. Knoppe, A. Dass, T. Bürgi, *Nat. Commun.* **2012**, *3*, 798.
[169] S. Knoppe, I. Dolamic, A. Dass, T. Bürgi, *Angew. Chem., Int. Ed.* **2012**, *51*, 7589.
[170] I. Dolamic, B. Varnholt, T. Bürgi, *Nat. Commun.* **2015**, *6*, 7117.
[171] C. Zeng, R. Jin, *Chem. - Asian J.* **2017**, *12*, 1839.
[172] H. Yao, *J. Phys. Chem. Lett.* **2012**, *3*, 1701.
[173] Y. Negishi, H. Tsunoyama, M. Suzuki, N. Kawamura, M. M. Matsushita, K. Maruyama, T. Sugawara, T. Yokoyama, T. Tsukuda, *J. Am. Chem. Soc.* **2006**, *128*, 12034.
[174] K. J. M. Bishop, C. E. Wilmer, S. Soh, B. A. Grzybowski, *Small* **2009**, *5*, 1600.
[175] B. L. V. Prasad, C. M. Sorensen, K. J. Klabunde, *Chem. Soc. Rev.* **2008**, *37*, 1871.
[176] L. Wang, L. Xu, H. Kuang, C. Xu, N. A. Kotov, *Acc. Chem. Res.* **2012**, *45*, 1916.
[177] T. P. Bigioni, X.-M. Lin, T. T. Nguyen, E. I. Corwin, T. A. Witten, H. M. Jaeger, *Nat. Mater.* **2006**, *5*, 265.
[178] M. R. Jones, N. C. Seeman, C. A. Mirkin, *Science* **2015**, *347*, 1260901.
[179] Z. Nie, A. Petukhova, E. Kumacheva, *Nat. Nanotechnol.* **2010**, *5*, 15.
[180] J. Henzie, M. Grünwald, A. Widmer-Cooper, P. L. Geissler, P. Yang, *Nat. Mater.* **2012**, *11*, 131.
[181] B. Pietrobon, M. McEachran, V. Kitaev, *ACS Nano* **2009**, *3*, 21.
[182] D. Nykypanchuk, M. M. Maye, D. van der Lelie, O. Gang, *Nature* **2008**, *451*, 549.
[183] Y. Min, M. Akbulut, K. Kristiansen, Y. Golan, J. Israelachvili, *Nat. Mater.* **2008**, *7*, 527.
[184] Y. Yang, S. Liu, K. Kimura, *Angew. Chem., Int. Ed.* **2006**, *45*, 5662.
[185] D. Manna, T. Udayabhaskararao, H. Zhao, R. Klajn, *Angew. Chem., Int. Ed.* **2015**, *54*, 12394.
[186] Y. H. Lee, W. Shi, H. K. Lee, R. Jiang, I. Y. Phang, Y. Cui, L. Isa, Y. Yang, J. Wang, S. Li, X. Y. Ling, *Nat. Commun.* **2015**, *6*, 6990.
[187] M. B. Ross, J. C. Ku, V. M. Vaccarezz, G. C. Schatz, C. A. Mirkin, *Nat. Nanotechnol.* **2015**, *10*, 453.
[188] L. Xu, W. Ma, L. Wang, C. Xu, H. Kuang, N. A. Kotov, *Chem. Soc. Rev.* **2013**, *42*, 3114.
[189] K. J. Si, Y. Chen, Q. Shi, W. Cheng, *Adv. Sci.* **2018**, *5*, 1700179.
[190] R. Klajn, K. J. M. Bishop, B. A. Grzybowski, *Proc. Natl. Acad. Sci. USA* **2007**, *104*, 10305.
[191] F. Gao, Q. Lu, S. Komarneni, *Chem. Mater.* **2005**, *17*, 856.
[192] S. Wang, H. Yao, S. Sato, K. Kimura, *J. Am. Chem. Soc.* **2004**, *126*, 7438.
[193] E. S. Shibu, M. A. H. Muhammed, K. Kimura, T. Pradeep, *Nano Res.* **2009**, *2*, 220.
[194] N. Nishida, E. S. Shibu, H. Yao, T. Oonishi, K. Kimura, T. Pradeep, *Adv. Mater.* **2008**, *20*, 4719.
[195] A. M. Kalsin, M. Fialkowski, M. Paszewski, S. K. Smoukov, K. J. M. Bishop, B. A. Grzybowski, *Science* **2006**, *312*, 420.
[196] M. A. Kostiainen, P. Hiekkataipale, A. Laiho, V. Lemieux, J. Seitsonen, J. Ruokolainen, P. Ceci, *Nat. Nanotechnol.* **2013**, *8*, 52.
[197] S. Srivastava, A. Verma, B. L. Frankamp, V. M. Rotello, *Adv. Mater.* **2005**, *17*, 617.
[198] N. N. Kariuki, J. Luo, S. A. Hassan, I. I. S. Lim, L. Wang, C. J. Zhong, *Chem. Mater.* **2006**, *18*, 123.
[199] M. P. Pileni, *J. Mater. Chem.* **2011**, *21*, 16748.
[200] K. Kimura, T. Pradeep, *Phys. Chem. Chem. Phys.* **2011**, *13*, 19214.
[201] C.-C. Chang, H.-L. Wu, C.-H. Kuo, M. H. Huang, *Chem. Mater.* **2008**, *20*, 7570.
[202] R. T. M. Jakobs, J. v. Herrikhuyzen, J. C. Gielen, P. C. M. Christianen, S. C. J. Meskers, A. P. H. J. Schenning, *J. Mater. Chem.* **2008**, *18*, 3438.
[203] S. A. Harfenist, Z. L. Wang, M. M. Alvarez, I. Vezmar, R. L. Whetten, *J. Phys. Chem.* **1996**, *100*, 13904.
[204] Y. Ofir, B. Samanta, V. M. Rotello, *Chem. Soc. Rev.* **2008**, *37*, 1814.
[205] B. Derjaguin, *Prog. Surf. Sci.* **1993**, *43*, 1.
[206] B. Derjaguin, L. D. Landau, *Prog. Surf. Sci.* **1993**, *43*, 30.
[207] E. J. W. Verwey, J. T. G. Overbeek, *Theory of the Stability of Lyophobic Colloids: The Interaction of Sol Particles Having an Electric Double Layer*, Elsevier, Amsterdam **1948**.
[208] Y. Liang, N. Hilal, P. Langston, V. Starov, *Adv. Colloid Interface Sci.* **2007**, *134–135*, 151.
[209] B. W. Ninham, *Adv. Colloid Interface Sci.* **1999**, *83*, 1.
[210] Y. S. Lee, *Self-Assembly and Nanotechnology: A Force Balance Approach*, Wiley, Hoboken, NJ **2008**.
[211] Y. Xia, T. D. Nguyen, M. Yang, B. Lee, A. Santos, P. Podsiadlo, Z. Tang, S. C. Glotzer, N. A. Kotov, *Nat. Nanotechnol.* **2011**, *6*, 580.
[212] C. Pigliacelli, D. Maiolo, Nonappa, J. S. Haataja, H. Amenitsch, C. Michelet, P. S. Moreno, I. Tirotta, P. Metrangolo, F. B. Bombelli, *Angew. Chem., Int. Ed.* **2017**, *56*, 16186.
[213] S. Wintzheimer, T. Granath, M. Oppmann, T. Kister, T. Thai, T. Kraus, N. Vogel, K. Mandel, *ACS Nano* **2018**, *12*, 5093.
[214] C. Pigliacelli, K. B. Sanjeeva, Nonappa, A. Pizzi, A. Gori, F. B. Bombelli, P. Metrangolo, *ACS Nano* **2019**, *13*, 2158.
[215] Nonappa, J. S. Haataja, J. V. I. Timonen, S. Malola, P. Engelhardt, N. Houbenov, M. Lahtinen, H. Häkkinen, O. Ikkala, *Angew. Chem., Int. Ed.* **2017**, *56*, 6473.
[216] V. Liljeström, A. Ora, J. Hassinen, H. T. Rekola, Nonappa, M. Heilala, V. Hynninen, J. J. Joensuu, R. H. A. Ras, P. Törmä, O. Ikkala, M. A. Kostiainen, *Nat. Commun.* **2017**, *8*, 671.
[217] B. Yoon, W. D. Luedtke, R. N. Barnett, J. Gao, A. Desireddy, B. E. Conn, T. Bigioni, U. Landman, *Nat. Mater.* **2014**, *13*, 807.
[218] Q. Yao, Y. Yu, X. Yuan, Y. Yu, D. Zhao, J. Xie, J. Y. Lee, *Angew. Chem., Int. Ed.* **2015**, *54*, 184.
[219] Nonappa, T. Lahtinen, J. S. Haataja, T.-R. Tero, H. Häkkinen, O. Ikkala, *Angew. Chem., Int. Ed.* **2016**, *55*, 16035.
[220] Nonappa, O. Ikkala, *Adv. Funct. Mater.* **2018**, *28*, 1704328.
[221] C. Zhang, A. Zhang, W. Hou, T. Li, K. Wang, Q. Zhang, J. M. de la Fuente, W. Jin, D. Cui, *ACS Nano* **2018**, *12*, 4408.
[222] C. Zhang, C. Li, Y. Liu, J. Zhang, C. Bao, S. Liang, Q. Wang, Y. Yang, H. Fu, K. Wang, D. Cui, *Adv. Funct. Mater.* **2015**, *25*, 1314.

[223] Z. Xie, P. Sun, Z. Wang, H. Li, L. Yu, D. Sun, M. Chen, Y. Bi, X. Xin, J. Hao, *Angew. Chem., Int. Ed.* **2020**, *59*, 9922.
[224] P. Sun, Z. Wang, D. Sun, H. Bai, Z. Zhu, Y. Bi, T. Zhao, X. Xin, *J. Colloid Interface Sci.* **2020**, *567*, 235.
[225] A. Chakraborty, A. C. Fernandez, A. Som, B. Mondal, G. Natarajan, G. Paramasivam, T. Lahtinen, H. Häkkinen, Nonappa, T. Pradeep, *Angew. Chem., Int. Ed.* **2018**, *57*, 6522.
[226] A. Som, I. Chakraborty, T. A. Maark, S. Bhat, T. Pradeep, *Adv. Mater.* **2016**, *28*, 2827.
[227] F. Xue, F. Qu, W. Han, L. Xia, J. You, *Anal. Chim. Acta* **2019**, *1046*, 170.
[228] Y. Jia, X. Zhang, C. Yin, X. Zhang, J. Zhang, X. Wang, J. Xin, *Anal. Methods* **2019**, *11*, 3974.
[229] L. He, Z. Gan, N. Xia, L. Liao, Z. Wu, *Angew. Chem., Int. Ed.* **2019**, *58*, 9897.
[230] X. Wei, X. Kang, Q. Yuan, C. Qin, S. Jin, S. Wang, M. Zhu, *Chem. Mater.* **2019**, *31*, 4945.
[231] E. Hadjittofis, S. C. Das, G. G. Z. Zhang, J. Y. Y. Heng, *Developing Solid Oral Dosage Forms*, Elsevier, Academic Press, Boston, MA **2017**.
[232] Z. Wu, C. Dong, Y. Li, H. Hao, H. Zhang, Z. Lu, B. Yang, *Angew. Chem., Int. Ed.* **2013**, *52*, 9952.
[233] Z. Wu, Y. Li, J. Liu, Z. Lu, H. Zhang, B. Yang, *Angew. Chem., Int. Ed.* **2014**, *53*, 12196.
[234] Z. Wu, J. Liu, Y. Li, Z. Cheng, T. Li, H. Zhang, Z. Lu, B. Yang, *ACS Nano* **2015**, *9*, 6315.
[235] Z. Wu, H. Zou, T. Li, Z. Cheng, H. Liu, Y. Liu, H. Zhang, B. Yang, *Chem. Commun.* **2017**, *53*, 416.
[236] Z. Wu, J. Liu, Y. Gao, H. Liu, T. Li, H. Zou, Z. Wang, K. Zhang, Y. Wang, H. Zhang, B. Yang, *J. Am. Chem. Soc.* **2015**, *137*, 12906.
[237] L. Ai, W. Jiang, Z. Liu, J. Liu, Y. Gao, H. Zou, Z. Wu, Z. Wang, Y. Liu, H. Zhang, B. Yang, *Nanoscale* **2017**, *9*, 12618.
[238] L. Ai, Z. Liu, D. Zhou, J. Liu, H. Zou, Z. Wu, Y. Liu, H. Zhang, B. Yang, *Nanoscale* **2017**, *9*, 18845.
[239] J. Liu, Z. Wu, Y. Tian, Y. Li, L. Ai, T. Li, H. Zou, Y. Liu, X. Zhang, H. Zhang, B. Yang, *ACS Appl. Mater. Interfaces* **2017**, *9*, 24899.
[240] Z. Wu, H. Liu, T. Li, J. Liu, J. Yin, O. F. Mohammed, O. M. Bakr, Y. Liu, B. Yang, H. Zhang, *J. Am. Chem. Soc.* **2017**, *139*, 4318.
[241] J. Liu, Z. Wu, T. Li, D. Zhou, K. Zhang, Y. Sheng, J. Cui, H. Zhang, B. Yang, *Nanoscale* **2016**, *8*, 395.
[242] C. Zeng, Y. Chen, K. Kirschbaum, K. J. Lambright, R. Jin, *Science* **2016**, *354*, 1580.
[243] S. Tsuzuki, *Annu. Rep. Prog. Chem., Sect. C: Phys. Chem.* **2012**, *108*, 69.
[244] A. Nag, P. Chakraborty, M. Bodiuzzaman, T. Ahuja, S. Antharjanam, T. Pradeep, *Nanoscale* **2018**, *10*, 9851.
[245] K. S. Sugi, P. Bandyopadhyay, M. Bodiuzzaman, A. Nag, M. Hridya, W. A. Dar, P. Ghosh, T. Pradeep, *Chem. Mater.* **2020**, *32*, 7973.
[246] L. Shi, L. Zhu, J. Guo, L. Zhang, Y. Shi, Y. Zhang, K. Hou, Y. Zheng, Y. Zhu, J. Lv, S. Liu, Z. Tang, *Angew. Chem., Int. Ed.* **2017**, *56*, 15397.
[247] Y. Yanagimoto, Y. Negishi, H. Fujihara, T. Tsukuda, *J. Phys. Chem. B* **2006**, *110*, 11611.
[248] J.-H. Huang, Z.-Y. Wang, S.-Q. Zang, T. C. W. Mak, *ACS Cent. Sci.* **2020**, *6*, 1971.
[249] T. Higaki, C. Liu, M. Zhou, T.-Y. Luo, N. L. Rosi, R. Jin, *J. Am. Chem. Soc.* **2017**, *139*, 9994.
[250] G. Li, C. Zeng, R. Jin, *J. Am. Chem. Soc.* **2014**, *136*, 3673.
[251] T. Chen, S. Yang, J. Chai, Y. Song, J. Fan, B. Rao, H. Sheng, H. Yu, M. Zhu, *Sci. Adv.* **2017**, *3*, e1700956.
[252] C. Qin, Q. Yuan, P. Li, S. Wang, S. Chen, M. Zhu, *RSC Adv.* **2020**, *10*, 11493.
[253] Y. Song, Y. Li, H. Li, F. Ke, J. Xiang, C. Zhou, P. Li, M. Zhu, R. Jin, *Nat. Commun.* **2020**, *11*, 478.
[254] Q. Li, J. C. Russell, T.-Y. Luo, X. Roy, N. L. Rosi, Y. Zhu, R. Jin, *Nat. Commun.* **2018**, *9*, 3871.
[255] S. Sculfort, P. Braunstein, *Chem. Soc. Rev.* **2011**, *40*, 2741.
[256] H. Schmidbaur, A. Schier, *Chem. Soc. Rev.* **2012**, *41*, 370.
[257] M. D. Nardi, S. Antonello, D. Jiang, F. Pan, K. Rissanen, M. Ruzzi, A. Venzo, A. Zoleo, F. Maran, *ACS Nano* **2014**, *8*, 8505.
[258] S. Antonello, T. Dainese, F. Pan, K. Rissanen, F. Maran, *J. Am. Chem. Soc.* **2017**, *139*, 4168.
[259] W. Fei, S. Antonello, T. Dainese, A. Dolmella, M. Lahtinen, K. Rissanen, A. Venzo, F. Maran, *J. Am. Chem. Soc.* **2019**, *141*, 16033.
[260] S. Hossain, Y. Imai, Y. Motohashi, Z. Chen, D. Suzuki, T. Suzuki, Y. Kataoka, M. Hirata, T. Ono, W. Kurashige, T. Kawawaki, T. Yamamoto, Y. Negishi, *Mater. Horiz.* **2020**, *7*, 796.
[261] P. Yuan, R. Zhang, E. Selenius, P. Ruan, Y. Yao, Y. Zhou, S. Malola, H. Häkkinen, B. K. Teo, Y. Cao, N. Zheng, *Nat. Commun.* **2020**, *11*, 2229.
[262] Z. Wu, Y. Du, J. Liu, Q. Yao, T. Chen, Y. Cao, H. Zhang, J. Xie, *Angew. Chem., Int. Ed.* **2019**, *58*, 8139.
[263] Z. Luo, V. Nachammai, B. Zhang, N. Yan, D. T. Leong, D. Jiang, J. Xie, *J. Am. Chem. Soc.* **2014**, *136*, 10577.
[264] P. Sun, Z. Wang, Y. Bi, D. Sun, T. Zhao, F. Zhao, W. Wang, X. Xin, *ACS Appl. Nano Mater.* **2020**, *3*, 2038.
[265] B. Kronberg, K. Holmberg, B. Lindman, *Surface Chemistry of Surfactants and Polymers*, Wiley, Chichester, UK **2014**.
[266] J. He, X. Huang, Y.-C. Li, Y. Liu, T. Babu, M. A. Aronova, S. Wang, Z. Lu, X. Chen, Z. Nie, *J. Am. Chem. Soc.* **2013**, *135*, 7974.
[267] A. C. Kamps, B. L. Sanchez-Gaytan, R. J. Hickey, N. Clarke, M. Fryd, S.-J. Park, *Langmuir* **2010**, *26*, 14345.
[268] Z. Nie, D. Fava, E. Kumacheva, S. Zou, G. C. Walker, M. Rubinstein, *Nat. Mater.* **2007**, *6*, 609.
[269] H.-Y. Lee, S. H. R. Shin, A. M. Drews, A. M. Chirsan, S. A. Lewis, K. J. M. Bishop, *ACS Nano* **2014**, *8*, 9979.
[270] Q. Yao, X. Yuan, Y. Yu, Y. Yu, J. Xie, J. Y. Lee, *J. Am. Chem. Soc.* **2015**, *137*, 2128.
[271] M. Grzelczak, J. Vermant, E. M. Furst, L. M. Liz-Marzán, *ACS Nano* **2010**, *4*, 3591.
[272] Z. Wu, Q. Yao, S. Zang, J. Xie, *ACS Mater. Lett.* **2019**, *1*, 237.
[273] A. Yahia-Ammar, D. Sierra, F. Mérola, N. Hildebrandt, X. L. Guével, *ACS Nano* **2016**, *10*, 2591.
[274] J. Shen, Z. Wang, D. Sun, C. Xia, S. Yuan, P. Sun, X. Xin, *ACS Appl. Mater. Interfaces* **2018**, *10*, 3955.
[275] Y. B. Yin, C. L. Coonrod, K. N. Heck, F. Lejarza, M. S. Wong, *ACS Appl. Mater. Interfaces* **2019**, *11*, 17491.
[276] M. Hembury, N. Beztsinna, H. Asadi, J. B. van den Dikkenberg, J. D. Meeldijk, W. E. Hennink, T. Vermonden, *Biomacromolecules* **2018**, *19*, 2841.
[277] L. Yang, H. Wang, D. Li, L. Li, X. Lou, H. Liu, *Chem. Mater.* **2018**, *30*, 5507.
[278] J. Benavides, I. Quijada-Garrido, O. García, *Nanoscale* **2020**, *12*, 944.
[279] E. Ju, T. Li, S. Ramos da Silva, S.-J. Gao, *ACS Appl. Mater. Interfaces* **2019**, *11*, 34717.
[280] H. Xia, F. Li, X. Hu, W. Park, S. Wang, Y. Jang, Y. Du, S. Baik, S. Cho, T. Kang, D.-H. Kim, D. Ling, K. M. Hui, T. Hyeon, *ACS Cent. Sci.* **2016**, *2*, 802.
[281] W. Zhang, D. Lin, H. Wang, J. Li, G. U. Nienhaus, Z. Su, G. Wei, L. Shang, *Bioconjugate Chem.* **2017**, *28*, 2224.
[282] Y. Yang, S. Wang, Y. Zhou, X. Wang, X. Liu, A. Xie, Y. Shen, M. Zhu, *Colloids Surf., B* **2020**, *196*, 111346.
[283] C. A. Mirkin, R. L. Letsinger, R. C. Mucic, J. J. Storhoff, *Nature* **1996**, *382*, 607.
[284] W. Cheng, M. J. Campolongo, J. J. Cha, S. J. Tan, C. C. Umbach, D. A. Muller, D. Luo, *Nat. Mater.* **2009**, *8*, 519.

[285] X. Ouyang, M. Wang, L. Guo, C. Cui, T. Liu, Y. Ren, Y. Zhao, Z. Ge, X. Guo, G. Xie, J. Li, C. Fan, L. Wang, *Angew. Chem., Int. Ed.* **2020**, *59*, 11836.
[286] X. Ouyang, Y.-N. Chang, K.-W. Yang, W.-M. Wang, J.-J. Bai, J.-W. Wang, Y.-J. Zhang, S.-Y. Wang, B.-B. Xie, L.-L. Wang, *Chem. Commun.* **2017**, *53*, 8878.
[287] Z. Qing, X. He, D. He, K. Wang, F. Xu, T. Qing, X. Yang, *Angew. Chem., Int. Ed.* **2013**, *52*, 9719.
[288] A. Rotaru, S. Dutta, E. Jentzsch, K. Gothelf, A. Mokhir, *Angew. Chem., Int. Ed.* **2010**, *49*, 5665.
[289] M. Wang, Y. Chen, W. Cai, H. Feng, T. Du, W. Liu, H. Jiang, A. Pasquarelli, Y. Weizmann, X. Wang, *Proc. Natl. Acad. Sci. USA* **2020**, *117*, 308.
[290] J.-M. Lehn, *Chem. Soc. Rev.* **2007**, *36*, 151.
[291] E. S. Shibu, T. Pradeep, *Chem. Mater.* **2011**, *23*, 989.
[292] A. Mathew, G. Natarajan, L. Lehtovaara, H. Häkkinen, R. M. Kumar, V. Subramanian, A. Jaleel, T. Pradeep, *ACS Nano* **2014**, *8*, 139.
[293] A. Nag, P. Chakraborty, G. Paramasivam, M. Bodiuzzaman, G. Natarajan, T. Pradeep, *J. Am. Chem. Soc.* **2018**, *140*, 13590.
[294] P. Chakraborty, A. Nag, G. Paramasivam, G. Natarajan, T. Pradeep, *ACS Nano* **2018**, *12*, 2415.
[295] T. Jiang, G. Qu, J. Wang, X. Ma, H. Tian, *Chem. Sci.* **2020**, *11*, 3531.
[296] P. Chakraborty, A. Nag, K. S. Sugi, T. Ahuja, B. Varghese, T. Pradeep, *ACS Mater. Lett.* **2019**, *1*, 534.
[297] P. Chakraborty, A. Nag, B. Mondal, E. Khatun, G. Paramasivam, T. Pradeep, *J. Phys. Chem. C* **2020**, *124*, 14891.
[298] M. A. H. Muhammed, L. K. Cruz, A.-H. Emwas, A. M. El-Zohry, B. Moosa, O. F. Mohammed, N. M. Khashab, *Angew. Chem., Int. Ed.* **2019**, *58*, 15665.
[299] Y. Huang, J. Ji, J. Zhang, F. Wang, J. Lei, *Chem. Commun.* **2020**, *56*, 313.
[300] P. K. Kundu, D. Samanta, R. Leizrowice, B. Margulis, H. Zhao, M. Börner, T. Udayabhaskararao, D. Manna, R. Klajn, *Nat. Chem.* **2015**, *7*, 646.
[301] X. Mei, S. Yang, D. Chen, N. Li, H. Li, Q. Xu, J. Ge, J. Lu, *Chem. Commun.* **2012**, *48*, 10010.
[302] M. Suda, M. Nakagawa, T. Iyoda, Y. Einaga, *J. Am. Chem. Soc.* **2007**, *129*, 5538.
[303] M. Taguchi, K. Yamada, K. Suzuki, O. Sato, Y. Einaga, *Chem. Mater.* **2005**, *17*, 4554.
[304] B. I. Ipe, S. Mahima, K. G. Thomas, *J. Am. Chem. Soc.* **2003**, *125*, 7174.
[305] R. Klajn, *Chem. Soc. Rev.* **2014**, *43*, 148.
[306] H. Lee, W. Wu, J. K. Oh, L. Mueller, G. Sherwood, L. Peteanu, T. Kowalewski, K. Matyjaszewski, *Angew. Chem., Int. Ed.* **2007**, *46*, 2453.
[307] N. S. Bell, M. Piech, *Langmuir* **2006**, *22*, 1420.
[308] K. M. Yeo, C. J. Gao, K.-H. Ahn, I. S. Lee, *Chem. Commun.* **2008**, *38*, 4622.
[309] R. Klajn, J. F. Stoddart, B. A. Grzybowski, *Chem. Soc. Rev.* **2010**, *39*, 2203.
[310] R. Klajn, P. J. Wesson, K. J. M. Bishop, B. A. Grzybowski, *Angew. Chem., Int. Ed.* **2009**, *48*, 7035.
[311] T. Udayabhaskararao, P. K. Kundu, J. Ahrens, R. Klajn, *ChemPhysChem* **2016**, *17*, 1805.
[312] Y. Negishi, U. Kamimura, M. Ide, M. Hirayama, *Nanoscale* **2012**, *4*, 4263.
[313] J. V. Rival, Nonappa, E. S. Shibu, *ACS Appl. Mater. Interfaces* **2020**, *12*, 14569.
[314] L. Ai, Y. Li, Z. Wu, J. Liu, Y. Gao, Y. Liu, Z. Lu, H. Zhang, B. Yang, *J. Phys. Chem. C* **2016**, *120*, 24427.
[315] Y. Luo, S. Fan, W. Yu, Z. Wu, D. A. Cullen, C. Liang, J. Shi, C. Su, *Adv. Mater.* **2018**, *30*, 1704576.
[316] Y. Zhu, X. Qiu, S. Zhao, J. Guo, X. Zhang, W. Zhao, Y. Shi, Z. Tang, *Nano Res.* **2020**, *13*, 1928.
[317] Q. Yao, Z. Luo, X. Yuan, Y. Yu, C. Zhang, J. Xie, J. Y. Lee, *Sci. Rep.* **2014**, *4*, 3848.
[318] H.-Y. Huang, K.-B. Cai, M. J. Talite, W.-C. Chou, P.-W. Chen, C.-T. Yuan, *Sci. Rep.* **2019**, *9*, 4053.
[319] S. Chandra, Nonappa, G. Beaune, A. Som, S. Zhou, J. Lahtinen, H. Jiang, J. V. I. Timonen, O. Ikkala, R. H. A. Ras, *Adv. Opt. Mater.* **2019**, *7*, 1900620.
[320] S. Basu, A. Paul, A. Chattopadhyay, *J. Mater. Chem. A* **2016**, *4*, 1218.
[321] M. Paul, S. Basu, A. Chattopadhyay, *Langmuir* **2020**, *36*, 754.
[322] L. Wang, C. Zhang, T. Li, M. Duan, F. Xia, X. Li, C. Song, S. Pan, B. Liu, D. Cui, *Nanoscale* **2019**, *11*, 22237.
[323] S. Basu, U. Goswami, A. Paul, A. Chattopadhyay, *J. Mater. Chem. B* **2018**, *6*, 1650.
[324] B. Kuppan, U. Maitra, *Nanoscale* **2017**, *9*, 15494.
[325] W. Hou, F. Xia, G. Alfranca, H. Yan, X. Zhi, Y. Liu, C. Peng, C. Zhang, J. M. de la Fuente, D. Cui, *Biomaterials* **2017**, *120*, 103.
[326] S. Basu, A. Paul, A. Chattopadhyay, *Chem. - Eur. J.* **2017**, *23*, 9137.
[327] S. Basu, S. Bhandari, U. N. Pan, A. Paul, A. Chattopadhyay, *J. Mater. Chem. C* **2018**, *6*, 8205.
[328] S. Basu, A. Hajra, C. Gayen, A. Paul, *ChemPhysChem* **2020**, *21*, 809.
[329] R.-W. Huang, Y.-S. Wei, X.-Y. Dong, X.-H. Wu, C.-X. Du, S.-Q. Zang, T. C. W. Mak, *Nat. Chem.* **2017**, *9*, 689.
[330] R.-W. Huang, X.-Y. Dong, B.-J. Yan, X.-S. Du, D.-H. Wei, S.-Q. Zang, T. C. W. Mak, *Angew. Chem., Int. Ed.* **2018**, *57*, 8560.
[331] X.-Y. Dong, H.-L. Huang, J.-Y. Wang, H.-Y. Li, S.-Q. Zang, *Chem. Mater.* **2018**, *30*, 2160.
[332] S.-H. Lu, Y. Li, S.-X. Yang, R.-D. Zhao, Z.-X. Lu, X.-L. Liu, Y. Qin, L.-Y. Zheng, Q.-E. Cao, *Inorg. Chem.* **2019**, *58*, 11793.
[333] Z. Wei, X.-H. Wu, P. Luo, J.-Y. Wang, K. Li, S.-Q. Zang, *Chem. - Eur. J.* **2019**, *25*, 2750.
[334] M. Cao, R. Pang, Q.-Y. Wang, Z. Han, Z.-Y. Wang, X.-Y. Dong, S.-F. Li, S.-Q. Zang, T. C. W. Mak, *J. Am. Chem. Soc.* **2019**, *141*, 14505.
[335] Y.-M. Wang, J.-W. Zhang, Q.-Y. Wang, H.-Y. Li, X.-Y. Dong, S. Wang, S.-Q. Zang, *Chem. Commun.* **2019**, *55*, 14677.
[336] X.-H. Wu, P. Luo, Z. Wei, Y.-Y. Li, R.-W. Huang, X.-Y. Dong, K. Li, S.-Q. Zang, B. Z. Tang, *Adv. Sci.* **2019**, *6*, 1801304.
[337] M. J. Alhilaly, R.-W. Huang, R. Naphade, B. Alamer, M. N. Hedhili, A.-H. Emwas, P. Maity, J. Yin, A. Shkurenko, O. F. Mohammed, M. Eddaoudi, O. M. Bakr, *J. Am. Chem. Soc.* **2019**, *141*, 9585.
[338] Z.-Y. Wang, M.-Q. Wang, Y.-L. Li, P. Luo, T.-T. Jia, R.-W. Huang, S.-Q. Zang, T. C. W. Mak, *J. Am. Chem. Soc.* **2018**, *140*, 1069.
[339] Z.-K. Wang, M.-M. Sheng, S.-S. Qin, H.-T. Shi, M. Strømme, Q.-F. Zhang, C. Xu, *Inorg. Chem.* **2020**, *59*, 2121.
[340] S. Chen, W. Du, C. Qin, D. Liu, L. Tang, Y. Liu, S. Wang, M. Zhu, *Angew. Chem., Int. Ed.* **2020**, *59*, 7542.
[341] T. Lahtinen, E. Hulkko, K. Sokołowska, T.-R. Tero, V. Saarnio, J. Lindgren, M. Pettersson, H. Häkkinen, L. Lehtovaara, *Nanoscale* **2016**, *8*, 18665.
[342] B. Musnier, K. D. Wegner, C. Comby-Zerbino, V. Trouillet, M. Jourdan, I. Häusler, R. Antoine, J.-L. Coll, U. Resch-Genger, X. Le Guével, *Nanoscale* **2019**, *11*, 12092.
[343] A. Sels, G. Salassa, F. Cousin, L.-T. Lee, T. Bürgi, *Nanoscale* **2018**, *10*, 12754.
[344] K. Sokolowska, E. Hulkko, L. Lehtovaara, T. Lahtinen, *J. Phys. Chem. C* **2018**, *122*, 12524.
[345] M. Bodiuzzaman, A. Nag, N. R. Pradeep, A. Chakraborty, R. Bag, G. Paramasivam, G. Natarajan, G. Sekar, S. Ghosh, T. Pradeep, *Chem. Commun.* **2019**, *55*, 5025.
[346] K. R. Krishnadas, A. Baksi, A. Ghosh, G. Natarajan, T. Pradeep, *Nat. Commun.* **2016**, *7*, 13447.
[347] K. R. Krishnadas, A. Ghosh, A. Baksi, I. Chakraborty, G. Natarajan, T. Pradeep, *J. Am. Chem. Soc.* **2015**, *138*, 140.

[348] A. Ghosh, D. Ghosh, E. Khatun, P. Chakraborty, T. Pradeep, *Nanoscale* **2017**, *9*, 1068.
[349] E. Khatun, P. Chakraborty, B. R. Jacob, G. Paramasivam, M. Bodiuzzaman, W. A. Dar, T. Pradeep, *Chem. Mater.* **2019**, *32*, 611.
[350] S. Bhat, A. Baksi, S. K. Mudedla, G. Natarajan, V. Subramanian, T. Pradeep, *J. Phys. Chem. Lett.* **2017**, *8*, 2787.
[351] R. Kazan, U. Müller, T. Bürgi, *Nanoscale* **2019**, *11*, 2938.
[352] P. Bose, P. Chakraborty, J. S. Mohanty, Nonappa, A. R. Chowdhuri, E. Khatun, T. Ahuja, A. Mahendranath, T. Pradeep, *Nanoscale* **2020**, *12*, 22116.
[353] E. Khatun, A. Ghosh, P. Chakraborty, P. Singh, M. Bodiuzzaman, P. Ganesan, G. Nataranjan, J. Ghosh, S. K. Pal, T. Pradeep, *Nanoscale* **2018**, *10*, 20033.
[354] J. Xie, Y. Zheng, J. Y. Ying, *J. Am. Chem. Soc.* **2009**, *131*, 888.
[355] J. S. Mohanty, A. Baksi, H. Lee, T. Pradeep, *RSC Adv.* **2015**, *5*, 48039.
[356] G. Soldan, M. A. Aljuhani, M. S. Bootharaju, L. G. AbdulHalim, M. R. Parida, A.-H. Emwas, O. F. Mohammed, O. M. Bakr, *Angew. Chem., Int. Ed.* **2016**, *55*, 5749.
[357] S. Wang, X. Meng, A. Das, T. Li, Y. Song, T. Cao, X. Zhu, M. Zhu, R. Jin, *Angew. Chem., Int. Ed.* **2014**, *53*, 2376.
[358] M. van der Linden, A. J. van Bunningen, L. Amidani, M. Bransen, H. Elnaggar, P. Glatzel, A. Meijerink, F. M. F. de Groot, *ACS Nano* **2018**, *12*, 12751.
[359] X. Jia, J. Li, E. Wang, *Small* **2013**, *9*, 3873.
[360] N. Goswami, Q. Yao, Z. Luo, J. Li, T. Chen, J. Xie, *J. Phys. Chem. Lett.* **2016**, *7*, 962.
[361] X. Dou, X. Yuan, Y. Yu, Z. Luo, Q. Yao, D. T. Leong, J. Xie, *Nanoscale* **2014**, *6*, 157.
[362] Nonappa, *Beilstein J. Nanotechnol.* **2020**, *11*, 533.
[363] X.-Y. Dong, Y. Si, J.-S. Yang, C. Zhang, Z. Han, P. Luo, Z.-Y. Wang, S.-Q. Zang, T. C. W. Mak, *Nat. Commun.* **2020**, *11*, 3678.
[364] K. T. Prakash, N. Singh, V. Venkatesh, *Chem. Commun.* **2019**, *55*, 322.
[365] M. Zhao, S. Huang, Q. Fu, W. Li, R. Guo, Q. Yao, F. Wang, P. Cui, C.-H. Tung, D. Sun, *Angew. Chem., Int. Ed.* **2020**, *59*, 20031.

Jose V. Rival is a Ph.D. student of Dr. E. S. Shibu in the Division of Electrochemical Power Sources, CSIR-CECRI, India. He received his M.Sc. degree from the University of Calicut, Kerala, India, in 2017. His research mainly focuses on the photoswitchable self-assembly of nanoclusters and functional nanomaterials.

Paloli Mymoona is a Ph.D. student of Dr. E. S. Shibu in the Division of Electrochemical Power Sources, CSIR-CECRI, India. She received her M.Sc. degree from Mahatma Gandhi University, Kerala, India, in 2012. Her research mainly focuses on the effective modifications and applications of nanomaterials through click reaction.

Kavalloor Murali Lakshmi is a Ph.D. student of Dr. E. S. Shibu in the Division of Electrochemical Power Sources, CSIR-CECRI, India. She received her M.Sc. degree from Mahatma Gandhi University, Kerala, India, in 2017. Her research mainly focuses on multimodal nanosystems for bioimaging and light-mediated therapy.

Nonappa is an associate professor at the Faculty of Engineering and Natural Sciences, Tampere University, Finland. He received his Ph.D. degree (2008) from the Indian Institute of Science, Bangalore, India. He carried out his postdoctoral research at the University of Jyväskylä and Aalto University, Finland. His research interests include precision nanomaterials, colloidal self-assembly, and soft matter cryogenic electron tomography.

Thalappil Pradeep received his Ph.D. degree from the Indian Institute of Science in 1986. After postdoctoral training at the Lawrence Berkeley Laboratory, University of California, Berkeley, and Purdue University, Indiana, he moved to the Indian Institute of Technology Madras in 1993. He has been recognized as an institute professor (since 2015) and as the Deepak Parekh Institute Chair professor (since 2017). His research interests include molecular and nanoscale materials, water purification, and instrumentation. He took part in the commercialization of technologies for drinking water purification.

Edakkattuparambil Sidharth Shibu received his Ph.D. degree from the Indian Institute of Technology Madras in 2010. He completed his postdoctoral research from AIST, Japan (JSPS fellow) and the University of Bordeaux, France (Madam Marie Curie fellow). He moved to CSIR-Central Electrochemical Research Institute (CECRI) as an assistant professor (AcSIR) and Ramanujan fellow (SERB) in 2017. His research interests include light-induced colloidal self-assembly of nanoclusters and fabrication of multimodal photoactive nanoprobes for bioimaging and light-mediated therapy.